

AMERICAN UNIVERSITY OF BEIRUT

RECTENNAS FOR WIDE RANGE RF POWER HARVESTING

by
MAHMOUD MOHAMMAD ABDALLAH

A thesis
submitted in partial fulfillment of the requirements
for the degree of Master of Engineering
to the Department of Electrical and Computer Engineering
of the Faculty of Engineering and Architecture
at the American University of Beirut

Beirut, Lebanon
December 2015

AMERICAN UNIVERSITY OF BEIRUT

RECTENNAS FOR WIDE RANGE RF POWER HARVESTING

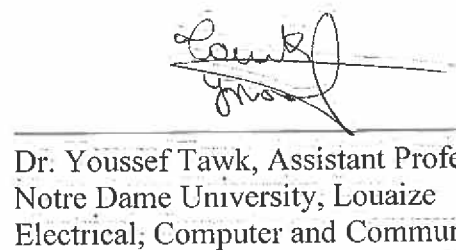
by

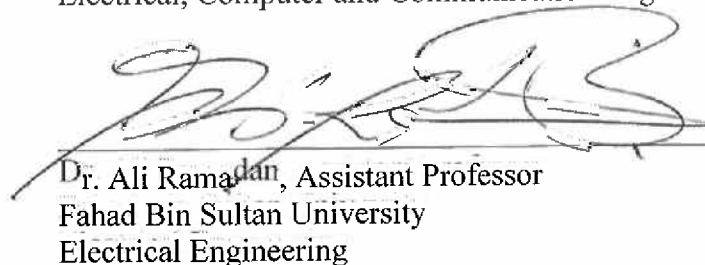
MAHMOUD ABDALLAH

Approved by:


Dr. Joseph Costantine, Assistant Professor
Electrical and Computer Engineering
Advisor


Dr. Karim Kabalan, Professor
Electrical and Computer Engineering
Member of Committee


Dr. Youssef Tawk, Assistant Professor
Notre Dame University, Louaize
Electrical, Computer and Communication Engineering
Member of Committee


Dr. Ali Ramadan, Assistant Professor
Fahad Bin Sultan University
Electrical Engineering
Member of Committee

Date of thesis defense: December 17, 2015

AMERICAN UNIVERSITY OF BEIRUT

THESIS, DISSERTATION, PROJECT RELEASE FORM

Student Name: Abdallah Mahmoud Mohammad
Last First Middle

Master's Thesis Master's Project Doctoral Dissertation

I authorize the American University of Beirut to: (a) reproduce hard or electronic copies of my thesis, dissertation, or project; (b) include such copies in the archives and digital repositories of the University; and (c) make freely available such copies to third parties for research or educational purposes.

I authorize the American University of Beirut, **three years after the date of submitting my thesis, dissertation, or project**, to: (a) reproduce hard or electronic copies of it; (b) include such copies in the archives and digital repositories of the University; and (c) make freely available such copies to third parties for research or educational purposes.

Mahmoud Abdallah February 12, 2016

Signature

Date

ACKNOWLEDGMENTS

I would like to thank my advisor Dr. Joseph Costantine for his continuous and valuable support throughout this research. His guidance was the key element in the accomplishment of this work.

Also, I would like to express full appreciation to my thesis committee members: Dr. Ali Ramadan, Dr. Youssef Tawk and Dr. Karim Kabalan for their help and motivation.

Special thanks to the University Research Board (URB) and the Munib and Angela Masri Institute of Energy and Natural Resources at the American University of Beirut (AUB) for providing financial support throughout this research.

Last but not least, my deepest gratitude goes to my family members who were patient enough to supply me continuously with unlimited love and confidence.

AN ABSTRACT OF THE THESIS OF

Mahmoud Mohammad Abdallah for Master of Engineering
Major: ECE

Title: Rectennas for Wide Range RF Power Harvesting

Wireless communication applications fill up our ambient environment with electromagnetic waves (EM) carrying energy at different frequencies. The RF energy harvesting process relies on these EM waves in order to rectify them into DC power. This process can be directed towards the charging of battery dependent devices such as mobile devices or distant sensor networks. Such technique is the basis of what is now known as wireless charging from RF energy and constitutes a great advantage for any mobile or distant device.

Many factors affect the design process of any RF harvesting circuit. The appropriate high-frequency impedance matching and the transmission line effects must be taken into account during the design stage in addition to the nonlinear effects of the incorporated rectifying diodes. The Schottky rectifying diodes are mainly capable of efficiently converting the RF energy into DC under specific conditions of the received power. At very low power levels, the forward voltage effect limits the conversion efficiency of the overall circuit. On the other hand, as the received power increases the diode enters into breakdown which causes the generated DC power to saturate and hence the efficiency to drop exponentially.

In this thesis, the aim is to design a new RF circuit with enhanced operable power range over which rectification can be efficiently performed. The objective is to find a solution to the breakdown problem that is inherent in the nature of diodes. The investigation process is based on understanding the inadequacy of using the well-known PN junction diode at microwave frequencies, deciphering RF rectification, and incorporating all the gathered information to design the new rectifying system that is able to cater for a wider range of power levels at a practical frequency of operation.

Various rectifying circuits and rectenna systems are developed, tested and compared. These systems are able to harvest and rectify the RF signal at an acceptable efficiency for a wide power range. The measured designs have the ability to delay the breakdown of the incorporated diodes and hence achieve an enhancement in the power range over which efficient harvesting of energy can take place.

CONTENTS

ACKNOWLEDGMENTS	v
ABSTRACT	vi
LIST OF ILLUSTRATIONS	xi
LIST OF TABLES	xvi
Chapter	
I. INTRODUCTION	1
II. AVAILABLE KNOWLEDGE ON RF HARVESTING	5
A. Objectives	5
B. Surveyed Rectifiers	5
1. Rectifiers with $PCE \geq 50\%$	5
2. Rectifiers with $PCE < 50\%$	15
C. Summary	29
III. CHARACTERISTICS OF RF SCHOTTKY DIODES	30
A. Objectives	30
B. The PN Junction	30
C. Schottky Diodes: Physical and Electrical Characteristics	33
D. Summary	38
IV. THEORETICAL ANALYSIS OF RECTIFICATION	39
A. Objectives	39

B. Assumptions	39
C. Study Cases	41
1. Scenario I: $V_p < V_{br}$	41
2. Scenario II: $V_p \geq V_{br}$	48
D. Effects of the Diode Parameters	56
E. Effect of the Load Resistance.....	58
F. Summary	59
V. EFFICIENT RF HARVESTING OVER WIDER POWER RANGE.....	61
A. Objectives.....	61
B. Method I – Controlling the Flow of Input RF Power.....	61
C. Method II – Splitting of the Input RF Power	67
D. Summary	69
VI. A 2.1GHZ RECTIFIER WITH ENHANCED OPERABLE POWER RANGE.....	71
A. Objectives.....	71
B. ADS Simulations and Results	71
1. Single Diode Rectifier	71
2. Design of the Wilkinson Power Divider.....	75
3. The Complete Rectifier	76
C. Fabrication and Measurement	79
D. Summary	85
VII. A 2.4GHZ RECTIFIER WITH ENHANCED OPERABLE POWER RANGE.....	87
A. Objectives.....	87
B. Rectifier Design.....	87

C. ADS Simulations and Results	88
1. Unequal Split Wilkinson Power Divider	88
2. The Complete Rectifier	91
D. Fabrication and Measurement	93
E. Debugging the Circuit	94
1. Assumption of halved series resistance	94
2. Other error sources	96
F. Summary	97
VIII. A 1.84GHZ RECTIFIER WITH ENHANCED OPERABLE POWER RANGE	98
A. Objectives	98
B. The Rectifier's Modified Design.....	98
C. ADS Simulations and Results	99
1. Single Diode Rectifier	99
2. The Complete Rectifier	102
D. Fabrication and Measurement	106
E. Summary	111
IX. 1.84GHZ RECTENNA FOR RF POWER HARVESTING... 112	
A. Objectives	112
B. Antenna Design	112
C. Summary	116
X. CONCLUSIONS AND FUTURE WORK..... 117	
A. Achieved Research Results	117
B. Future Work	119
1. Output DC Load	119
2. Rectifier Design.....	119

3. Prediction and Theoretical Analysis of Performance	120
REFERENCES	121

LIST OF ILLUSTRATIONS

Figure 1. Designed and fabricated CP rectenna operating at 5.8GHz [2]	7
Figure 2. Class-F rectifiers. (a) 900MHz rectifier (b) 5.8GHz rectifier [4].....	8
Figure 3. Dual-diode 2.45GHz rectifier [5]	9
Figure 4. 35GHz rectenna proposed in [7]	12
Figure 5. Schematic of the designed 5.5GHz rectenna [9]	15
Figure 6. RF harvesting device with a folded dipole reception antenna [10].....	16
Figure 7. Novel Yagi-Uda antenna designed for the RF harvester [13]	18
Figure 8. (a) 2x2 circular dipole array (b) 3x3 circular dipole array [14]	19
Figure 9. Fabricated 1.575GHz RF harvester [16]	20
Figure 10. Full-wave rectifier based on the modified Greinacher topology [17]	22
Figure 11. Four square spiral antennas on a single FR4 substrate [18]	24
Figure 12. Fabricated 2.45GHz rectenna array [19]	26
Figure 13. Schematic of the layered 2.45GHz rectenna [21].....	28
Figure 14. Diffusion current across the interface of a PN junction	31
Figure 15. Formation of the depletion layer across the PN interface	31
Figure 16. External voltage V_A applied to bias the PN junction	32
Figure 17. Formation of diffusion capacitance upon forward biasing the junction.....	33
Figure 18. Physical construction of a typical Schottky diode [22].....	35
Figure 19. Electrical model of a typical Schottky diode [22].....	35
Figure 20. Current-voltage characteristics of two commercial Schottky diodes.....	37
Figure 21. Shunt Schottky diode connected in reverse.....	39
Figure 22. Assumed current-voltage characteristics of the Schottky diode	40

Figure 23. Diode model when $V_p < V_{br}$	41
Figure 24. Time points for the case of $V_p < V_{br}$	41
Figure 25. Diode voltage and current waveforms for $V_p < V_{br}$	43
Figure 26. Equivalent circuit of the rectifier after adding R_L	45
Figure 27. DC power generated by the diode for $V_p < V_{br}$	46
Figure 28. RF power consumed by the diode for $V_p < V_{br}$	47
Figure 29. Generated RF power at the second harmonic for $V_p < V_{br}$	47
Figure 30. Generated RF power at the third harmonic for $V_p < V_{br}$	48
Figure 31. Diode equivalent model during breakdown	49
Figure 32. Time points for the case of $V_p \geq V_{br}$	49
Figure 33. Diode voltage and current waveforms for the case of $V_p \geq V_{br}$	51
Figure 34. Generated DC power for the case of $V_p \geq V_{br}$	53
Figure 35. RF power consumed by the diode for the case of $V_p \geq V_{br}$	54
Figure 36. RF power generated at the second harmonic for the case of $V_p \geq V_{br}$	55
Figure 37. RF generated power at the third harmonic for the case of $V_p > V_{br}$	56
Figure 38. Breakdown effect on the generated second and third harmonic powers	56
Figure 39. DC power generated by the Skyworks diodes.....	57
Figure 40. Effect of R_L over the output DC voltage	58
Figure 41. Block diagram of the rectenna proposed in method I	62
Figure 42. Controlling the RF power flow based on method I.....	63
Figure 43. Schematic of the rectifier proposed in method I	64
Figure 44. Input reflection coefficient of the rectifier in method I.....	65
Figure 45. PCE curve of the rectifier in method I	65
Figure 46. Block diagram of a single diode typical RF rectifier	67

Figure 47. Typical PCE curve for a single diode rectifier	68
Figure 48. Splitting of input RF power between two identical rectifiers	69
Figure 49. ADS schematic of the single diode 2.1GHz rectifier	72
Figure 50. S_{11} of the 2.1GHz single diode rectifier	74
Figure 51. PCE of the 2.1GHz single diode rectifier	74
Figure 52. Diode voltage and current waveforms for the rectifier in figure 49	75
Figure 53. Design of an equal split Wilkinson power divider	76
Figure 54. S-parameters of the 2.1GHz Wilkinson power divider	76
Figure 55. Layout of the complete proposed 2.1GHz rectifier	77
Figure 56. Reflection coefficient of the complete 2.1GHz rectifier at -15dBm	77
Figure 57. PCE of the complete 2.1GHz rectifier	78
Figure 58. Achieved enhancement over the efficient rectification power range	78
Figure 59. Simulated output DC voltage from the proposed 2.1GHz rectifier	79
Figure 60. Fabricated 2.1GHz rectifier	80
Figure 61. Measurement setup for characterizing the 2.1GHz rectifier	81
Figure 62. DC voltage (2.91V) measured from the rectifier at 20dBm input power	82
Figure 63. Lighting an LED using the output DC voltage by the 2.1GHz rectifier	82
Figure 64. Reduction of the output DC voltage due to the connection of the LED	83
Figure 65. Reflection coefficient of the 2.1GHz rectifier at -15dBm	84
Figure 66. Measured output DC voltage of the 2.1GHz rectifier	84
Figure 67. Measured PCE of the 2.1GHz rectifier	85
Figure 68. Schematic of an unequal split Wilkinson divider	88
Figure 69. Splitting of input power (P_1) between ports 2 and 3	89
Figure 70. Characteristic impedances of the upper and lower lines	90

Figure 71. Isolation resistance as a function of (K).....	90
Figure 72. Output resistance as a function of (K).....	91
Figure 73. Layout of the designed 2.4GHz rectifier.....	91
Figure 74. DC power generated over a 50Ω load for 20Ω and 10Ω series resistances ..	92
Figure 75. Fabricated 2.4GHz rectifier with unequal split Wilkinson divider.....	93
Figure 76. Simulated versus measured output DC voltage.....	93
Figure 77. Simulated versus measured PCE.....	94
Figure 78. Simulated forward current through single and parallel SMS-7630 diodes ...	95
Figure 79. Measured forward current through single and parallel SMS-7630 diodes....	96
Figure 80. Schematic of the single diode 1.84GHz rectifier	99
Figure 81. Input reflection coefficient of the single diode 1.84GHz rectifier	102
Figure 82. PCE of the 1.84GHz single diode rectifier.....	102
Figure 83. Layout of the 1.84GHz complete rectifier.....	103
Figure 84. Simulated S_{11} of the 1.84GHz complete rectifier.....	103
Figure 85. Simulated PCE of the complete rectifier at 1.84GHz	104
Figure 86. Simulated output DC voltage of the 1.84GHz complete rectifier	104
Figure 87. Simulated improvement in efficient power range at 1.84GHz.....	105
Figure 88. Simulated PCE of the 1.84 and 2.1GHz rectifiers.....	106
Figure 89. Fabricated 1.84GHz rectifier.....	106
Figure 90. Measured output DC of 515mV at 0dBm input power for a 600Ω load.....	107
Figure 91. Measured input reflection coefficient of the 1.84GHz circuit.....	108
Figure 92. Measured output DC voltage of the 1.84GHz rectifier	108
Figure 93. Measured and simulated PCE of the 1.84GHz rectifier	109
Figure 94. Comparison between the measured PCE curves for the three rectifiers	110

Figure 95. Measured DC voltage from the 1.84GHz rectifier for 9840 Ω load	110
Figure 96. (a) Top layer of antenna-1 (b) Bottom layer of antenna-1	112
Figure 97. Simulated and measured S-parameters of antenna-1	113
Figure 98. Realized gain of antenna-1 at 1.84GHz.....	113
Figure 99. (a) Top layer of antenna-2 (b) Bottom layer of antenna-2	114
Figure 100. Simulated and measured S-parameters of antenna-2	114
Figure 101. Realized gain of antenna-2 at 1.84GHz.....	115
Figure 102. Improved realized gain of antenna-1 after inserting the ground plane.....	116
Figure 103. Improved realized gain of antenna-2 after inserting the ground plane.....	116

LIST OF TABLES

Table 1. Common Parameters of Schottky Diodes [22]	35
Table 2. Operating regions for the case of $V_p < V_{br}$	42
Table 3. Operating regions for the case of $V_p \geq V_{br}$	50
Table 4. Properties of the compared Skyworks diodes.....	57
Table 5. Dimensions and component values of the 2.1GHz single diode rectifier.....	72
Table 6. Dimensions and component values of the 1.84GHz single diode rectifier.....	100
Table 7. Summary of the measured specifications of the three fabricated rectifiers....	118

CHAPTER I

INTRODUCTION

Wireless communication applications such as WiFi, GSM, 3G, etc... fill our surroundings with radio waves generated at different frequencies. Wireless power harvesting is a technology that aims to utilize ambient RF energy for purposes such as the development of battery-less wireless sensor nodes for remote health monitoring, surveillance and environmental tracking. The main element in an RF-harvesting device is called the “rectenna”. This concept was first introduced by William C. Brown [1] in 1964 and is the product of integrating an antenna with an RF rectifier.

The main component of a rectifier is an RF diode which is a non-linear element. When fed by RF power at a fundamental frequency (f_0), it generates higher order harmonics ($2f_0, 3f_0$, etc...) as well as DC power. This is why the term “Power Conversion Efficiency” (PCE) is used to compare different RF rectifiers. PCE is the ratio of the output DC power generated by the diode to the input RF power.

The properties of RF diodes cause their PCE to vary with input RF power. For instance, at low power levels, a rectifier might have a good PCE. However, increasing the input power causes the PCE to degrade. In contrast, with other diodes the PCE might require an increase in the input power for it to become acceptable. These behaviors are mainly attributed to the nonlinear properties of diodes.

The purpose of this study is to find a method that overcomes the negative effects that one particular property of commercial Schottky diodes, known as the breakdown potential, has over the PCE.

However, before going into the details of the subject, a brief historical review is necessary. Initially, transmission of power using radio waves was demonstrated by Heinrich Hertz who proved that electromagnetic energy can propagate in free space. Later on, Nikola Tesla studied the possibility of transmitting low-frequency electrical power between two points that were not connected by wires. Using 150KHz oscillators working at 150MV, Tesla managed to light two bulbs from radiated electromagnetic energy [1].

Wireless power transmission using microwaves started in 1958, with sponsors including Raytheon Company, NASA's Marshall Space Flight Center, NASA's Lewis Research Center, and the Jet Propulsion Laboratory (JPL). The effort was focused on Solar Power Satellite (SPS) applications. Later however, this technology witnessed larger participation by companies like Boeing, Rockwell International and others [1].

In May 1963, William C. Brown of Raytheon succeeded in demonstrating the first microwave power transmission system, where 100W of DC power was retrieved (at 2.45GHz), and used to drive a DC motor attached to the rotor fan of a helicopter from a magnetron transmitting 400W of continuous wave power. A thermionic diode was used for rectification but proved to be unreliable and short-lived. During the same year, the first rectenna developed at Raytheon was built and tested at Purdue University, where bridge rectifiers, made of four 1N82G point-contact semiconductor diodes, were attached to 28 half-wave dipole antennas to give an output DC power of 7W and a conversion efficiency of 40% at 2.45GHz [1].

In 1975, a 2.45GHz rectenna was developed under the sponsorship of JPL by Raytheon and used GaAs Schottky barrier diodes. It achieved an RF-DC conversion efficiency of 54% with an output DC power of 495W. Two years later, Brown of

Raytheon designed a rectenna that used GaAs-Pt Schottky diodes, an aluminum bar dipole, and transmission lines to achieve the highest ever recorded conversion efficiency of 90.6% for an input power of 8W at 2.45GHz [2].

ARCO power technologies managed to design a rectenna in 1983 which operated at 35GHz with a conversion efficiency of 72%. The shift from 2.45GHz to 35GHz was mainly due to the need for lower sized microwave components for SPS applications [2].

In 1992, Bharj et al. developed the first C-band rectenna which gave a conversion efficiency of 80%. Later, in 1998, McSpadden et al. developed a rectenna that achieved the highest conversion efficiency at 5.8GHz corresponding to 82% [2].

Based on this brief historical study of wireless power harvesting, it is obvious that this technology has witnessed many changes over time. Today, it has reached a state of high-level maturity nominating it to be an invaluable energy resource for present and future use.

The remaining of the thesis is divided into ten chapters as follows. Chapter II carries out a survey to get familiar with the available knowledge on the subject of RF harvesting. It serves as a foundation for any new ideas that can be added to the literature. Chapter III discusses the characteristics of RF Schottky diodes. It introduces their electrical and physical parameters that affect the performance of RF rectifiers. Chapter IV introduces a basic theoretical analysis over a typical rectifier. It allows conclusions to be made about the factors affecting the performance of these circuits. Chapter V discusses some methods that can be used to overcome the breakdown problem of commercial Schottky diodes. Chapters VI, VII, and VIII present detailed information about the designed rectifiers with enhanced operable power range.

Simulations and measurements performed over each circuit are included in each chapter. In chapter IX, a complete rectenna device is introduced and its application to wirelessly transmit RF energy is demonstrated. Finally, chapter X ends with a conclusion that summarizes the results that the research has achieved thus far and gives details about the planned future work.

CHAPTER II

AVAILABLE KNOWLEDGE ON RF HARVESTING

A. Objectives

In this chapter, a survey is carried out over some research papers where RF-DC microwave rectifiers have been designed, simulated, and in some cases fabricated and tested. The aim of the survey is to take a closer look at rectenna elements proposed by different authors specialized in the literature and gain insight about antenna designs, rectifier geometries, matching networks, performance parameters, simulation and measurement techniques, etc...

The papers are divided into two sections based on the PCE results. Those with good efficiency values ($PCE \geq 50\%$) are listed in the first section whereas designs that achieved lower PCE values are listed in the second one. For each paper, a summary is first given stating the objectives of the author(s). A small description then shows the different elements used (antenna, rectifier, filter, transmission lines etc...) and the methodology followed to maximize the performance of the proposed design. In addition, the achieved results in terms of output DC voltage and conversion efficiency are stated. Photos of the final design are also included if available.

B. Surveyed Rectifiers

1. *Rectifiers with $PCE \geq 50\%$*

In [2], the authors designed a 5.8GHz circularly polarized (CP) high-efficiency high-gain rectenna. A (CP) Dual-Rhombic-Loop-Antenna (DRLA) with a gain as high

as 10.7dBi and a VSWR of 2 over a 10% bandwidth was used. A Coplanar Stripline (CPS) Band-Reject Filter (BRF) was employed to suppress the second harmonic generated by the nonlinear diode and prevent its re-radiation. Also, a DC-pass filter was used to minimize the leakage of RF power into the resistive DC load. Circular polarization was chosen for the rectenna to maintain constant output DC power irrespective of its orientation.

The Schottky diode used was an M/A COM MA4E1317 detector with (R_s) of 4 Ω , (C_{j0}) of 0.02pF, built-in potential of 0.7V, and (V_{br}) of 7V. For a load resistance of 250 Ω , the diode's input impedance was calculated to be (172.1-j9.1) Ω at 5.8GHz. A DC-pass capacitor was inserted between the diode and load resistance to tune out the reactive part of the detector's impedance as well as reflect back harmonic frequencies which were trapped between the band-reject and DC-pass filters. This caused the remixing of power at the diode to generate more DC. Because the impedance of the diode was around 172 Ω , the CPS transmission lines, used to connect the various elements of the rectenna together, were designed to have a characteristic impedance of 172 Ω to minimize reflections and hence increase the rectenna's conversion efficiency. The CPS BRF was used to pass the 5.8GHz power from the antenna to the detector while suppressing the second harmonic (11.6GHz) generated by the diode. Based on simulations through the IE3D software, the filter gave an insertion loss of 0.3dB at 5.8GHz, while attenuating the 11.6GHz harmonic by more than 20dB.

The DRLA was fabricated and tests were performed to measure its parameters. The antenna had a measured gain of about 10.7dBi at 5.8GHz with an axial ratio of 0.2 dB when a reflecting plane was placed behind it at an air-filled gap distance of 11mm. The DC-pass capacitor used had a 2.4nF capacitance and blocked the second and third

harmonics with more than 16.8dB attenuation causing less than 2% of the RF power to be leaked into the DC load. The rectenna's performance was also measured and an RF-DC conversion efficiency above 80% was realized when R_L was 250Ω for an optimum distance of 9.5mm between the DC-pass capacitor and the diode. A schematic of the designed rectifier is shown in figure 1.

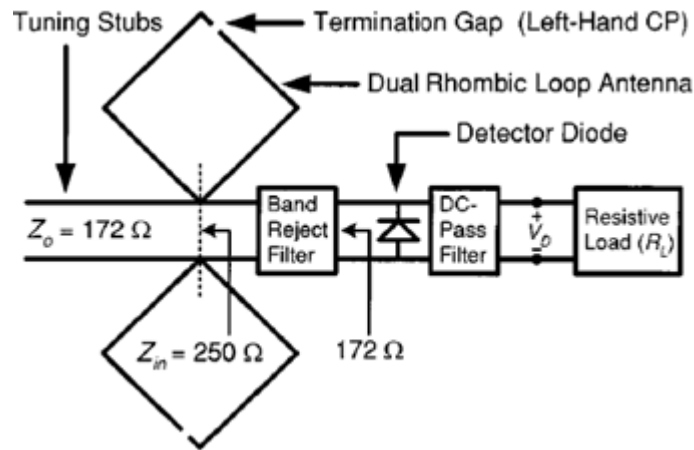


Figure 1. Designed and fabricated CP rectenna operating at 5.8GHz [2]

In [3], the authors focused on the utilization of RF-DC conversion systems in wearable electronic devices for the purpose of healthcare monitoring, mobile computing etc... For this reason, a textile RF rectenna was designed, simulated and fabricated. For the antenna fabrication, pile fabric and jeans were used to model the substrate whereas nylon non-woven fabric with a copper coating was used to model the patch and the ground plane. A full wave bridge rectifier using four Schottky diodes (HSMS-285x) was considered.

The textile patch antenna resonated at 892MHz where the return loss was less than -10dB. A maximum gain of 4.6dB was obtained at 892MHz with a radiation efficiency of 41.4%.

The complete integrated wearable rectenna had a maximum efficiency of 50% at 876MHz for an incident power density of $14\mu\text{Watt}/\text{cm}^2$ and a load of $1\text{K}\Omega$ at a distance of 1m from the transmitter (3dBi monopole antenna). At the maximum conversion efficiency, an output DC voltage of 1.42V was generated.

In [4], the authors presented an analysis for calculating the RF-DC PCE in a Class-F rectifier based on the time domain voltage and current waveforms across the diode. The model provides a calculation routine to determine the threshold input power at which the diode's efficiency (based on its electrical parameters) starts to decrease. Two RF rectifying circuits operating at 900MHz and 5.8GHz were implemented respectively. Photos of the fabricated prototypes are shown in figure 2. The first rectifier (900 MHz) was fabricated using an RO4003C substrate ($\epsilon_r = 3.55$). Harmonics were terminated via $\lambda/8$ and $\lambda/12$ open stubs. HSMS-8202 Schottky diode was used along with a 510Ω load resistance. For an input power range of 1 to 45 mW, a maximum conversion efficiency of 80.4% at 22mW input was obtained. The second rectifier (5.8GHz) was fabricated using the same substrate. Harmonics were also terminated via $\lambda/8$ and $\lambda/12$ open stubs. MA4E1317 Schottky diode was used due to its lower junction capacitance along with a 510Ω load resistance. For an input power range of 1 to 80mW, a maximum conversion efficiency of 79.5% at 58mW input was obtained.

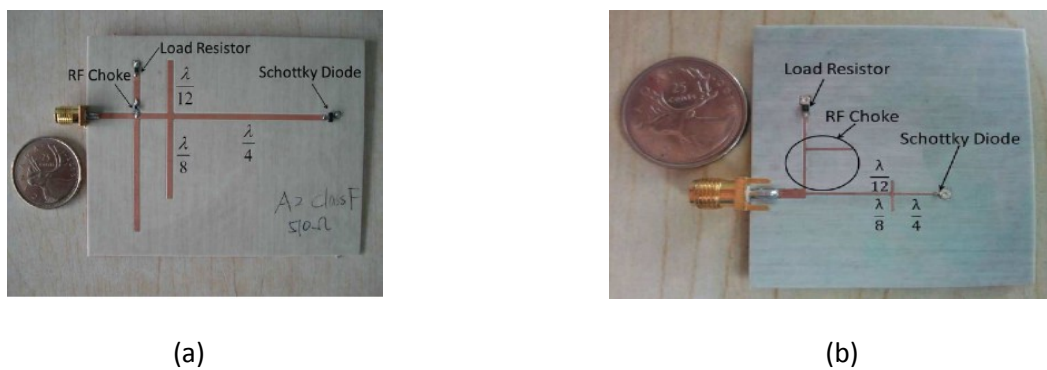


Figure 2. Class-F rectifiers. (a) 900MHz rectifier (b) 5.8GHz rectifier [4]

In [5], the authors aimed at designing a dual-diode microwave rectifier at 2.45GHz for rectenna applications. The design was implemented on two circuits using two different Schottky diodes namely, HSMS-2860 and HSMS-2820, where the latter has a higher breakdown voltage. Both circuits were etched on Arlon 25N substrate. A schematic of the rectifier is shown in figure 3. For circuit 1 using the HSMS-2860 diode, the measured efficiency was 58% at 10mW input power. For an optimum load of 500 Ω , the output DC voltage obtained was 2V. For circuit 2 using HSMS-2820 diode, the measured efficiency was 58.1% at 10mW input power. For a load of 1050 Ω , a 3V output DC voltage was obtained when the input power was 16mW.

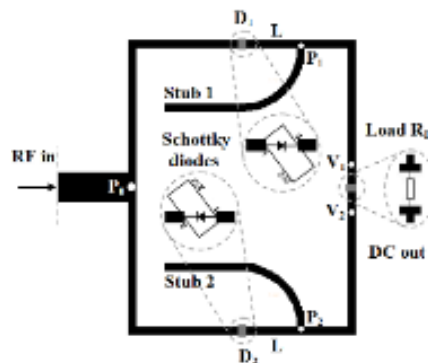


Figure 3. Dual-diode 2.45GHz rectifier [5]

In [6], Kai Chang et al. aimed at designing and simulating a high-efficiency rectenna element operating at 5.8GHz for applications of microwave power transmission. For this reason, closed-form equations were derived to calculate the conversion efficiency and input impedance of the used diode.

The rectenna consisted of a horizontal dipole antenna and CPS which were printed on one side of a 10-mil thick Rogers 5880 Duroid substrate with ($\epsilon_r=2.2$). The CPS gap separation was 2.1mm and printed lines were 1.6mm wide. The simulated characteristic impedance of the CPS was 236 Ω at 5.8GHz. A reflector was placed below

the substrate at an 11.1mm distance with free-space separation. The dipole antenna had a 25.75mm length and an 86Ω input resistance.

The diode input resistance was calculated using the closed-form equation derived and was found to be 236Ω . In order to match the 86Ω input impedance of the antenna to that of the diode (236Ω), a low pass filter was inserted in between. At 5.8GHz, the filter had a simulated return loss below -16dB at the dipole and diode ports. Also, it had an insertion loss of 0.2dB and 4dB at 5.8GHz and 11.6GHz (second harmonic) respectively.

The rectifier diode used was an MA40150-119 component which has a built-in potential of 0.4V and a breakdown voltage of 8.8V. Its zero bias junction capacitance is 0.12pF. The series resistance is around 8Ω . The maximum achievable output DC voltage is about 4V.

An output 47pF capacitor was used to short the RF energy and allow DC power to pass to the resistive load. The distance between the capacitor chip and the diode was chosen in such a way that the capacitive part of the diode's impedance is cancelled. Because the resistance of the used load affects the conversion efficiency, typically a value of $(1.3 \text{ to } 1.4) \times$ input resistance of the diode is chosen. For the designed rectenna, the resistance of the load was taken to be 327Ω .

Testing of the rectenna element through the IE3D waveguide simulator showed that a maximum conversion efficiency of 82% could be achieved (calculated value was 78.3%) for 50mW input power at 5.8GHz and 327Ω load. Simulations showed that good matching conditions existed in the design. Also, it was deduced that the rectenna's PCE remains above 77% over the entire ISM band (5.725 to 5.875)GHz.

In [7], the authors aimed at characterizing a diode at 2.45GHz for the purpose of microwave power transmission applications. For this reason, they devised a method based on a micro strip test mount technique to characterize GaAs packaged Schottky diodes. Using this technique, small signal tests were carried out to find the circuit parameters of the diode, which were then used by a large signal test that determined the power conversion efficiency of the diode as well as its input impedance. The authors also used a nonlinear simulation tool to verify their experimental results at 2.45GHz and to simulate a 35GHz rectenna. Finally, they designed a Frequency Selective Surface (FSS) with the aim of reducing the radiation of second harmonics generated by the diode within the 2.45GHz rectenna.

The small signal test carried out to characterize the 2.45GHz diode showed that it had a series resistance of 0.5Ω , lead inductance of 0.45nH , and parasitic capacitance of 0.3pF . As for the large signal test, which was carried out using 1.2W operating power, it showed that at 2.45GHz, the diode could achieve a maximum conversion efficiency of 85% for a 202Ω DC load resistance. In addition, the input impedance of the diode was found to be $(6+j29)\Omega$.

The 2.45GHz diode was then simulated by computer analysis for an operating power level of 1.2W and a DC load resistance of 200Ω . The maximum achieved conversion efficiency and input impedance of the diode were calculated by the software to be 91% and $(15+j35)\Omega$ respectively. The simulated values were consistent with the measured ones. The differences between both results were due to the effects of the third and higher order harmonics which were not included in the simulation.

The authors then designed and simulated a 35GHz rectenna using a Ka-band mixer diode. The rectenna's optimum diode input impedance, DC load resistance, and

output power were calculated to be 40Ω , 100Ω , and 30mW respectively, for which the maximum power conversion efficiency was simulated to be 50% when the net input power was 60mW . The rectenna used a square patch antenna with a 2.6mm^2 size and 220Ω input impedance. The rectenna, whose schematic is shown in figure 4, was etched on RT/Duroid substrate with a 10-mil thickness and ϵ_r of 2.2. The matching network was realized using a single stub to transform the impedance of the antenna to that of the diode (40Ω). Maximum conversion efficiency measured was 29% at an input power level of 120mW when a 100Ω DC resistive load was used.

Finally, a gridded square array FSS was designed to allow the passage of the fundamental 2.45GHz frequency and reject the second harmonic of 4.9GHz. It achieved about 10dB attenuation at 4.9GHz and caused a reduction by less than 1% to the rectenna's PCE.

In [8], the authors designed, simulated, and fabricated a rectenna for space-to-space microwave power transmission. The rectenna was designed to operate at a high frequency of 35GHz to allow transmission of power over long distances in space while using antennas with reduced sizes. The dipole rectenna was optimized using a computer simulation tool (LIBRA), fabricated, and tested for its conversion efficiency at 10GHz and 35GHz.

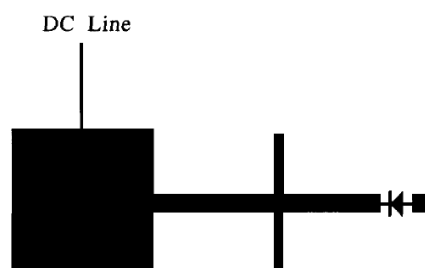


Figure 4. 35GHz rectenna proposed in [7]

It was noted that the conversion efficiency of a Schottky diode is affected by the input RF power. In general, for small input power levels, the efficiency is small since the voltage across the diode junction is below or comparable to its forward biasing voltage. However, as this power increases, efficiency increases and levels-off when higher order harmonics become stronger. As the input power exceeds a critical value of $(V_{br}^2/4R_L)$, the efficiency decreases sharply due to the breakdown effect.

The designed 35GHz rectenna used a microstrip dipole antenna whose length and width were determined to be $0.46\lambda_0$ and $0.02\lambda_0$ respectively. As for the rectifier diode, a GaAs Schottky diode (DMK-6606) was chosen. Its effective impedance was assumed to be 50Ω for an output DC voltage lower than $4.5V$ ($V_{br}/2$) and an operating power level of $100mW$. A low pass filter was inserted between the antenna and diode with a cut-off frequency located between the fundamental and second order harmonic. It was used to pass the fundamental frequency while rejecting higher order harmonics created by the diode. In addition, it was used to match the antenna to the diode. The low pass filter was designed using a software tool (TOUCHSTONE) over a Duroid substrate of 10-mil thickness and 2.2 permittivity. A microstrip line of $0.022\lambda_0$ length was used to connect the diode to the DC pass filter.

After fabrication, the rectenna was tested at 35GHz. The measured maximum efficiency was 39% for a load resistance of 400Ω . It was noted that for load resistances of 100Ω and 400Ω , the maximum conversion efficiency was almost the same. However, while a 12% reflection of incident power (at the diode's input) was measured for a 400Ω load, it was 21% with the 100Ω load. The rectenna was also tested at 10GHz with a 120Ω resistive load, where a maximum conversion efficiency of 60% was achieved.

In [9], the authors proposed a circularly polarized (CP) microstrip patch antenna that could function as a WLAN antenna for data communication in the (5.15~5.35)GHz band as well as a rectenna for microwave power harvesting at 5.5GHz. The proposed antenna had a 14.8mm x 14.8mm x 3mm size which made it suitable to be integrated into moderate to high data rate sensors for applications like infrastructure monitoring. The authors proposed that a Mobile Test Unit (MTU) be used to collect data from the sensors over the WLAN frequency band while delivering microwave energy over 5.5GHz.

The designed antenna was developed using 3.175mm thick Duroid as a substrate with ($\epsilon_r=2.2$) and fed through a coaxial probe. HFSS [45] was used to optimize the antenna characteristics such that wide return loss and circular polarization bandwidths were achieved. The computed and measured return loss bandwidth of the antenna (for which $S_{11} \leq -10\text{dB}$) were found to be 11% and 12% respectively over the (5.15~5.35)GHz band. Hence, it was proven that the antenna could be used for communications within the WLAN band. In addition, the antenna was right-hand circularly polarized over the WLAN band and at 5.5GHz over which wireless power harvesting should take place. The peak gain of the patch was found to be 8dBi at 5.5GHz with a 20dB front-to-back ratio.

A rectenna was fabricated using the designed patch antenna along with a highly efficient M/A COM Schottky diode (MA4E1317). For testing the fabricated rectenna, an output power of 7W was generated by an amplifier that operated within the (5.3~5.9)GHz band and which was connected to a four-element linearly polarized array antenna having a 7.6dBi gain. The diode was connected to the patch antenna through a microstrip line whose width and length were determined in such a way that good

matching exists between the diode (172Ω input impedance) and patch antenna. A 300Ω resistive load was used to measure the output DC voltage produced. At a distance of 35cm from the transmitting antenna, the fabricated rectenna produced 1.74V DC. A maximum conversion efficiency of 57.3% was achieved for an input power density of $2.55\text{mW}/\text{cm}^2$ while keeping in mind that polarization mismatch between both antennas affected the rectification efficiency negatively. A schematic of the designed rectenna is shown in figure 5.

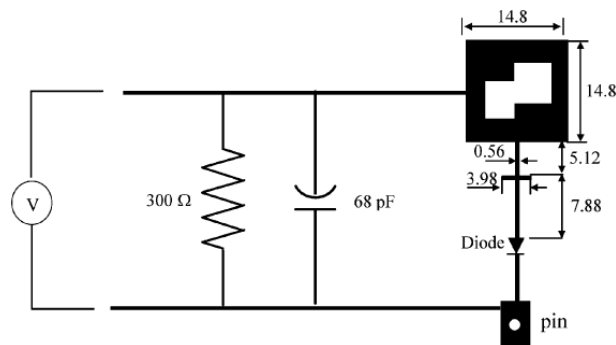


Figure 5. Schematic of the designed 5.5GHz rectenna [9]

2. Rectifiers with PCE < 50%

In [10], the authors presented an RF harvesting system that can be used to rectify low ambient power at 300MHz to supply microcontrollers in autonomous measurement systems. Nonlinear simulation for the harvesting system was carried out using the Harmonic Balance method. For an HSMS-2860 Schottky diode, the non-loaded DC voltage produced was 377mV for an input power of -30dBm. Using the S-parameters simulation, it was found that the return loss at the input of the diode is -3dB at 300MHz (indicating bad matching which negatively affected the rectification efficiency). Maximum PCE of 15.43% at a $3\text{K}\Omega$ load was achieved when a folded

dipole antenna was employed for reception. A photo of the fabricated rectenna is shown in figure 6.



Figure 6. RF harvesting device with a folded dipole reception antenna [10]

In [11], the authors designed a single element circularly polarized CP patch antenna and a 2x2 CP patch antenna array to be fabricated and incorporated in a rectenna system for RF power harvesting at 5.8 GHz. Since any rectenna must include a rectification process, the authors used and compared the performance of two detector types (HSMS286x Schottky diode and LTC5535 RF detectors). The antennas and the detector circuits were first designed and tested separately before being combined into a rectenna system. The single element CP antenna had a return loss of -11dB at 5.8GHz indicating good matching conditions.

In order to improve the RF-DC rectification efficiency of the rectenna, the authors designed a 2x2 CP array antenna with increased gain. The array antenna had a return loss of -12.2dB at 5.8GHz (indicating good matching conditions).

Since Schottky diodes are known for their fast switching and low power consumption, the authors first chose Agilent's HSMS-2862 as the RF-DC detector diode for the rectification process after designing a 5.8GHz input matching circuit for the diode. The authors used for rectification another detector circuit provided by Linear

Technologies as LTC5535 chip which allows RF rectification in a frequency band of 600MHz to 7GHz. The LTC5535 chip combines a Schottky diode together with an output amplifier (with adjustable gain) combined in a small package.

Two rectennas using 2x2 array CP patch antennas were fabricated with one using a Schottky diode for rectification whereas the other using an LTC5535 chip. At a distance of 15cm from the transmitter (signal generator with a horn antenna), for a transmitted power of 16dBm, the rectenna using a Schottky diode provided 72.5mV output DC whereas the one using an LTC5535 chip provided a higher output DC voltage of 428.3mV indicating better performance.

In [12], the authors designed a wideband rectenna to cover a wide range of RF sources (GSM, UMTS, WiFi, Radar, etc...) in the frequency range from 800MHz to 6GHz. This ultra-wide band RF harvesting system can be utilized in wireless sensor networks to minimize the need for dedicated batteries.

The authors used an ultra-wide band spiral antenna with circular polarization. The antenna was matched to the different rectification circuits operating at the various frequency bands by using cascade filters having complementary pass bands. The rectification circuits used HSMS-285A and HSMS-286A Schottky diodes. Finally, the DC outputs of all rectifying circuits were combined via a DC combiner.

In [13], Visser et al. aimed at utilizing the DTV frequency band (470 to 810MHz) to harvest RF energy. For this reason, an RF harvester including a novel Yagi-Uda antenna functioning at the DTV band, along with a matching network and a voltage doubler has been proposed, designed, fabricated, and tested throughout this paper.

The Yagi-Uda antenna designed to function in the DTV band consisted of a wide band strip dipole that was integrated into the antenna. The antenna's measured gain was greater than 4.27dBi while its return loss was less than -10dB over the DTV band.

For the rectifier, an HSMS-285C diode was used to form a 12-stage voltage doubler with the aim of boosting the output DC voltage. To match the rectifier to the 50Ω antenna, a matching network was designed. The network gave a return loss that was less than -10dB within the frequency range (500 to 580)MHz which makes the harvester suitable to be used with DTV channels broadcasting over this range.

The RF harvester (antenna, matching network, voltage doubler) could harvest RF power from the channels lying within the (500 to 580)MHz band with a maximum output voltage of 0.725V being produced at a frequency of 545MHz and an input power level of -15dBm. A schematic of the proposed antenna is shown in figure 7.

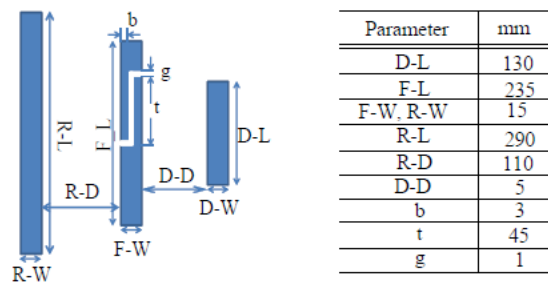


Figure 7. Novel Yagi-Uda antenna designed for the RF harvester [13]

In [14], the authors aimed at designing and implementing a broadband circular dipole rectenna array to harvest RF energy in a wide frequency band from 2.4 to 6.6GHz. For this reason, a circular dipole rectenna (single element) as well as 2x2 and 3x3 array configurations (figure 8) were fabricated and measured. For the rectifier part

of the harvester, the commercial Schottky barrier diode SMS-7621-079LF was used as the RF-DC converter.

For a single element circular dipole antenna, the output voltage was measured to be 47mV at 2.8GHz and a distance of 20cm from a horn antenna transmitting 3dBm of power. However, for the 2x2 rectenna array, the output DC voltage was measured to be around 75mV (approximately doubled) whereas it was about 147mV (approximately tripled) for the 3x3 array. The results show that the more elements the rectenna array consists of, the higher is the output generated DC voltage.

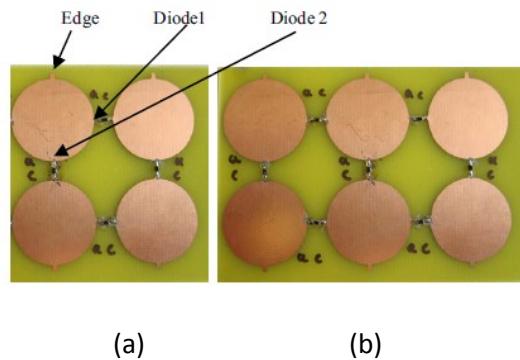


Figure 8. (a) 2x2 circular dipole array (b) 3x3 circular dipole array [14]

In [15], the authors aimed at designing a novel small loop antenna to obtain 1V output DC from -20dBm input power. The objective was to harvest RF power using FM radio waves in the 81.9 to 84.7MHz band. The designed small loop antenna had a gain of about 1.83dBi within the operating band and a return loss lower than -10dB.

To increase the RF-DC conversion efficiency, a matching network made up of lumped (L and C) elements was designed to match the antenna to the rectifier which included of an HSMS-2850 Schottky barrier diode.

After fabricating the harvester prototype, it was tested in a suburb area where FM waves were collected at 81.9MHz (-25dBm) and 84.7MHz (-19dBm) to produce an

output DC voltage of 924mV when a single rectenna circuit was used. For two rectennas connected in series, the output DC voltage generated was measured to be 1.72 V.

In [16], the authors designed and fabricated a 1.575GHz rectenna to be used for RF harvesting. For this reason, an electrically small antenna was designed to match the rectifying circuit (which used an SMS-7630 Schottky diode) at a frequency of 1.575GHz and an input RF power of 0dBm.

A band pass filter was added before the diode to prevent the harmonics and DC power from flowing into the antenna. Similarly, a low pass filter was used after the diode to prevent the higher order harmonics generated from decreasing the DC power fed into the load.

After fabricating the rectenna prototype (figure 9), measurements revealed that the highest rectification efficiency obtained was 34.1% for 0dBm input RF power at 1.545GHz (GPS L1 band). Output DC voltage generated over a load of 1540Ω was found to be 0.73V.

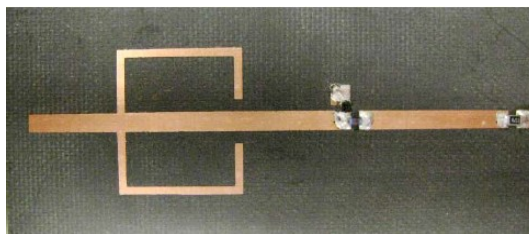


Figure 9. Fabricated 1.575GHz RF harvester [16]

In [17], Volakis et al. worked on testing and comparing the performance of two different rectenna array configurations for the purpose of maximizing RF-DC conversion efficiency in microwave power harvesters. For this purpose, the authors

presented an analytical approach to perform the comparison between both topologies and fabricated two planar rectenna arrays, one for each configuration. Measurements were performed and results were compared with those of the analytical analysis and good agreement was realized.

Because the conversion efficiency of a rectifier changes with input RF power, operating frequency, and diode characteristics, the authors chose a fixed frequency of 2.45GHz, and identical diodes (HSMS-2852) to be implemented in both configurations, hence making the PCE variable only with the input RF power. Based on the analytical analysis, the authors proposed a new parameter called (Rectenna Topology Indicator) or RTI which was defined as the ratio between the output DC power of the RF-combiner topology to that of the DC-combiner topology.

For the rectifier circuit, the authors used a modified version of the single-stage full-wave Greinacher rectifier whose schematic is shown in figure 10. In order to match its impedance to that of the antenna, a matching circuit was designed by using experimental characterization of the rectifier's input impedance at the minimum power level required by the application. After introducing the matching network, simulation showed that the rectifier was well matched to 50Ω (as assumed for the source impedance) in the power range of -25 to -5dBm. Also, the rectifier's PCE was shown to increase monotonically with increasing input power up to -5dBm.

As for the used antenna, the authors designed a Koch type patch antenna with $\lambda_0/2$ inter-element spacing to operate at 2.45GHz. After fabricating the 2x2 array configurations and testing with a 1W transmitter placed at 2.5m away from the rectennas, it was shown that the RF-combiner circuit performs better at bore sight. However, the DC-combiner performs better when rotating away from normal incidence.

In addition, it was deduced that for an increased number of antennas, the DC combiner outperforms the RF-combiner topology. However, for an increased efficiency, the RF-combiner performs better since it harvests more power near the main beam.

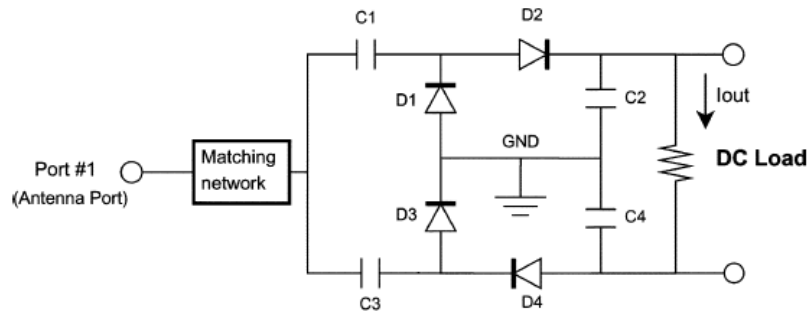


Figure 10. Full-wave rectifier based on the modified Greinacher topology [17]

In [18], the authors focused on the incorporation of multiple energy-harvesting antennas onto one chip with the aim of increasing the (harvested power/area) ratio. For this reason, the authors proposed a design where four antennas were incorporated in a square area that was less than twice that needed by a single antenna. The designed harvester was fabricated and experimentally tested to check its performance.

In general, the authors aimed at investigating the functionality of using multiple combinations of antenna/matching-network/charge-pump within the same physical area for increasing the harvested energy as well as whether these on-chip multiple combinations could be connected to provide DC voltage to a single load.

Because experimenting with Silicon dies tends to be expensive and time consuming, the authors used macro-sized prototypes (fabricated on PCBs) to glean as much information about their design and understand the relative effects on a macro-scale level before scaling down to the micro-world of Silicon chips.

The matching network that was used to match the impedance of each individual antenna to the charge-pump circuit was designed experimentally on the basis of providing maximum output DC voltage from the charge-pump. This was because the input impedance of the charge-pump had a real part of $1\text{K}\Omega$ for which traditional matching networks are difficult to design.

The energy-harvesting antennas used for the prototype were fabricated on an FR4 substrate using (PCB) technology. The substrate had a 1.5mm thickness and ϵ_r of 4.4. The antenna had a square spiral configuration with the inner-most terminal open and the outer-most terminal connected to the matching-network/voltage-doubler combination. The antennas were operated at a frequency of 915MHz and each had three segments of 27.3mm, 54.6mm, and 82mm (refer to figure 11). The width of the metal used was 5mm. The charge-pump used two HSMS-2820 Schottky diodes.

For experimental purposes, three boards were fabricated. Board-1 with a single antenna, board-2 with two antennas, and board-3 with four antennas. The output DC voltage was measured across the terminals of a $1\text{K}\Omega$ resistive load. At a distance of 20cm from a 5.5W transmitter (through a 6dB gain square patch antenna), board-1, board-2, and board-3 generated 80mW, 155mW, and 320mW of output DC power respectively, where powers were algebraically summed from each individual antenna.

When the outputs of the individual elements on board-3 were connected in parallel, for a DC output voltage of 5V to be produced, the operating distance was extended by 284%. This showed that while the required chip area was increased by 83% to incorporate the four antennas, the output produced DC power was increased by 300%. This prototype presented an idea that could be utilized to design harvesters by incorporating energy scavenging antennas on a limited chip area.

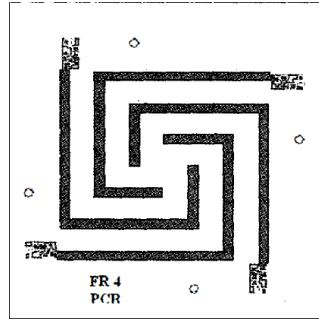


Figure 11. Four square spiral antennas on a single FR4 substrate [18]

In [19], the authors proposed a new compact and efficient rectenna array with the aim of harvesting very-low ambient RF energy to power a temperature and humidity measurement system along with its display from a typical WiFi router (operating at 2.45GHz) in a (5.79m x 8.53m) office environment. For this reason, their design consisted of miniaturized antennas, efficient rectifier, and a power management circuit.

The authors first started by characterizing the RF signal strength of a Wi-Fi router in the office environment. To accomplish this task, they used a quarter-wavelength monopole antenna which operated in the (2.3~2.5)GHz frequency range and a spectrum analyzer as the receiver. They conducted measurements of Wi-Fi signal strength at various points within the office to take into consideration the fading effects. Measurements showed that the rectenna array must be capable of harvesting power levels below -20dBm efficiently.

The authors used a DC-combining configuration with their rectenna array. In this case, multiple miniaturized antennas were used, with each antenna being connected to its own rectifier. Output DC voltages were then combined and fed to the power management circuitry which operated the sensor load. In order to reduce power losses due to reflections, diodes had to be matched to the antenna as well as the management circuit. This was performed using simulations where the rectifier impedance was

measured for an input power of -40 to -20dBm over the required frequency range of (2.4~2.48)GHz. Based on the results, the network was designed considering a 50 Ω impedance for the source and a (85~105)K Ω resistance for the management unit.

For the antenna, the authors used a high permittivity substrate (Rogers RO6010 with $\epsilon_r = 10.2$ and thickness of 2.54mm) in order to reduce its size. For additional miniaturization, they employed a modified version of the Koch patch antenna. The patch antenna had a size of $0.164\lambda_0 \times 0.162\lambda_0$ and was circularly polarized for reliable harvesting of ambient RF energy. It possessed a bandwidth of 6% with a gain greater than 4.5dBi at bore sight. The authors used a modified version of the single-stage full-wave Greinacher rectifier which employed four zero-bias Schottky diodes (SMS-7630).

In order to reach the goal of harvesting (1.5~3)V at the output of the rectifier, the authors fabricated a 3x3 planar array of the simple Koch patch antenna. The resulting antenna array had a final physical size of 9cm x 9cm. Series connection of the patch-rectifier combinations was used to combine the individual output DC voltages.

The management circuitry consisted of ICs (S882 and AS1310) which were employed to step-up and regulate the voltage fed to the sensor system from the harvesting circuit. Testing was performed in the office environment using the fabricated rectenna array. The device was able to supply 10 μ A of continuous current to the sensor at 1.8V. 5 minutes were needed for the harvesting circuit to initialize. The sensor gave accurate temperature and humidity measurements on its display, while relying on nothing but harvested ambient WiFi energy to operate. The fabricated rectenna array is shown in figure 12.

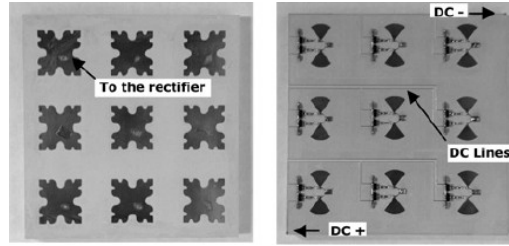


Figure 12. Fabricated 2.45GHz rectenna array [19]

In [20], the authors proposed a methodology that utilized the reciprocity principle, and combined Electromagnetic simulation (EM) with Harmonic Balance (HB) analysis to design an optimized rectenna for low-power RF harvesting applications. For this reason, the parameters of the antenna's Thevenin equivalent circuit in the receiving mode were computed via the EM simulation of the antenna in its transmit mode. These parameters were then incorporated into the HB analysis to optimize the rectenna design.

The authors designed an aperture-coupled dual linearly polarized patch antenna with the help of the HFSS EM simulator. The antenna's radiator and feed were etched on 20-mil-thick Arlon 25N substrate with a 6mm foam layer placed between them to optimize the bandwidth of the antenna. By etching a cross-shaped slot on its surface, a 32.5% antenna size reduction was achieved. The antenna was designed to operate at 2.45GHz frequency, where both linear polarizations could be received through the utilization of two orthogonal coupled slots.

Rectification of the received RF signals was carried out at each polarization by using single-stage voltage doubler circuits. The doublers used SMS-7630 Schottky diodes with series and shunt capacitors having values of 3.3 and 5.6pF respectively. The antenna ports were matched to each rectifier via matching networks (one for each polarization) optimized at 2.45GHz and consisting of shunt and series inductors implemented as high impedance transmission lines. The outputs of both rectifiers were

joined together via a common capacitor and resistive load (R_L) which allowed the rectenna to convert received RF power by the antenna into DC power regardless of the RF signal's polarization relative to that of patch.

The rectenna was fabricated and its conversion efficiency was measured. At 2.43GHz, and for an input power density of $1.5\mu\text{W}/\text{cm}^2$, the maximum conversion efficiency obtained was 38.2% for $6.2\text{K}\Omega R_L$. The maximum conversion efficiency for an input power density of $0.15\mu\text{W}/\text{cm}^2$ was 14.1% obtained at a frequency of 2.42GHz and a $6.2\text{K}\Omega R_L$. At 2.45GHz, the optimum (R_L) value was simulated to be $4.5\text{K}\Omega$. After varying the angle between the input RF signal's polarization and that of the patch from 0° to 360° , it was validated that the designed rectenna could convert RF power to DC regardless of the input signal's polarization.

In [21], the authors derived analytical models and closed-form expressions to design a low-cost, low-power rectenna. The models derived could be used to study the effects of several rectenna parameters over its performance. The rectenna was fabricated for operation at 2.45GHz while assuming an input RF power of 0dBm. A layered design approach was followed for the rectenna to acquire a small area. Measurements were performed in order to validate the proposed analytical models. The authors avoided the use of a matching network between the antenna and rectifier by designing both elements in such a way that they were already matched. For this purpose, a microstrip probe fed patch antenna was designed. By varying the probe position, the input impedance of the antenna could be varied to acquire a matched design. To determine the input impedance of the rectifying circuit, the voltage over and current through the Schottky diode (HSMS-2852) had to be evaluated. The authors followed an approach whereby the linear parts of the diode's equivalent circuit were evaluated in the frequency domain and

the non-linear parts were evaluated in the time domain. By considering the effects of the generated harmonics, the closed-form equations modeling the rectifier were derived.

A radial stub was inserted between the rectifier and DC load to prevent harmonics from being dissipated in the load. A prototype was fabricated and measurements were performed to validate the analytical models of the antenna, rectifier, and filter. For an input power level of 0dBm and a DC load of 470Ω within the frequency band of (2~3)GHz, the analytical models of the rectifier's input impedance were in good agreement with the measurements. However, for the output DC voltage to be accurately predicted, it was found that at least 2 harmonics should be considered.

A layered design approach was used to acquire a small area for the rectenna. Hence, the backside of the antenna was used for the rectifying circuit. The ground of the antenna was used as a ground plane for the rectifier as well. The analytical models were used to achieve matching between the antenna and rectifier with radial stubs. The feed's position was chosen in such a way that the patch had a high output impedance in order for the conversion efficiency to be increased. The rectenna gave a maximum conversion efficiency of 40% at a frequency of 2.45GHz, with a 470Ω load and 0dBm input power. The schematic of the designed rectenna is shown in figure 13.

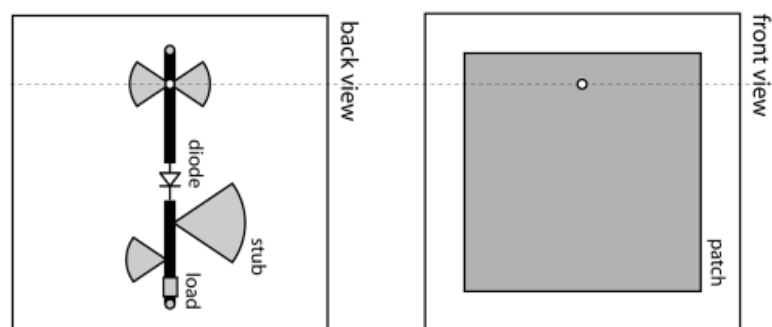


Figure 13. Schematic of the layered 2.45GHz rectenna [21]

C. Summary

This chapter introduced the subject of RF energy harvesting by presenting a number of rectifiers proposed by different researchers for operation under different conditions of frequency and available RF power. The surveyed designs were grouped into two sections according to the achieved PCE. It could be noticed that high rectification efficiency (~80%) is usually accomplished at relatively high power levels (58mWatt in [4]). Also, it is concluded that factors such as impedance matching, diode harmonics, resistive load, RF choking etc... all significantly influence the PCE of a rectifying circuit. Finally, it was noticed that all the presented rectifiers used Schottky barrier diodes for operation at microwave frequencies. Consequently, due to the crucial role they play in any RF rectifying device, the next chapter sheds light upon the physical and electrical properties of commercial Schottky diodes. It should be noted however, that CMOS based RF rectifiers have also been reported in the literature. CMOS provides advantages over SMD based circuits especially in terms of compactness and sensitivity to ultra-low power levels. But due to the additional complexity involved in designing such circuits as well as availability reasons, CMOS was not used throughout this research. However, interested readers are referred to [26] – [38].

CHAPTER III

CHARACTERISTICS OF RF SCHOTTKY DIODES

A. Objectives

The factors that make an RF Schottky diode capable of rectifying microwave signals are studied in this chapter. For this reason, a brief review of the PN junction is first carried out. Afterwards, the main modifications implemented over the PN junction to give rise to Schottky diodes which reliably operate at high microwave frequencies are presented. Due to their significant effect on the performance of any rectifier, the electrical properties of these devices are also discussed.

B. The PN Junction

A PN junction is formed by bringing into contact an N-type semiconductor (heavily doped by free electrons) and a P-type semiconductor (heavily doped by positively charged holes). This is illustrated in figure 14, where electrons are represented by blue negative signs and holes by red positive ones. Because particles of the same charge repel, electrons and holes near the interface are subjected to repulsive forces that cause them to diffuse into the opposite material. Each hole leaves behind a negatively charged ion in the P-type material, whereas diffusing electrons leave behind positively charged ions in the N-type material. As diffusion continues, more ions gather near the interface leading to the formation of an electric field as demonstrated in figure 15.

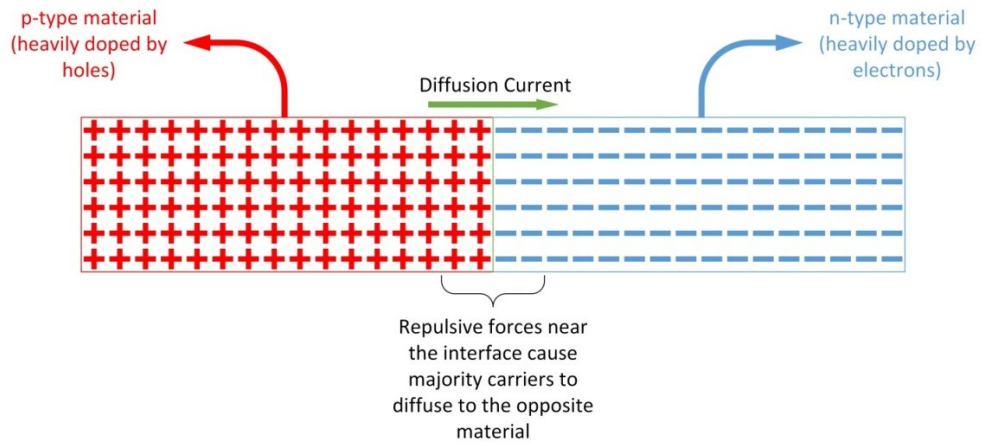


Figure 14. Diffusion current across the interface of a PN junction

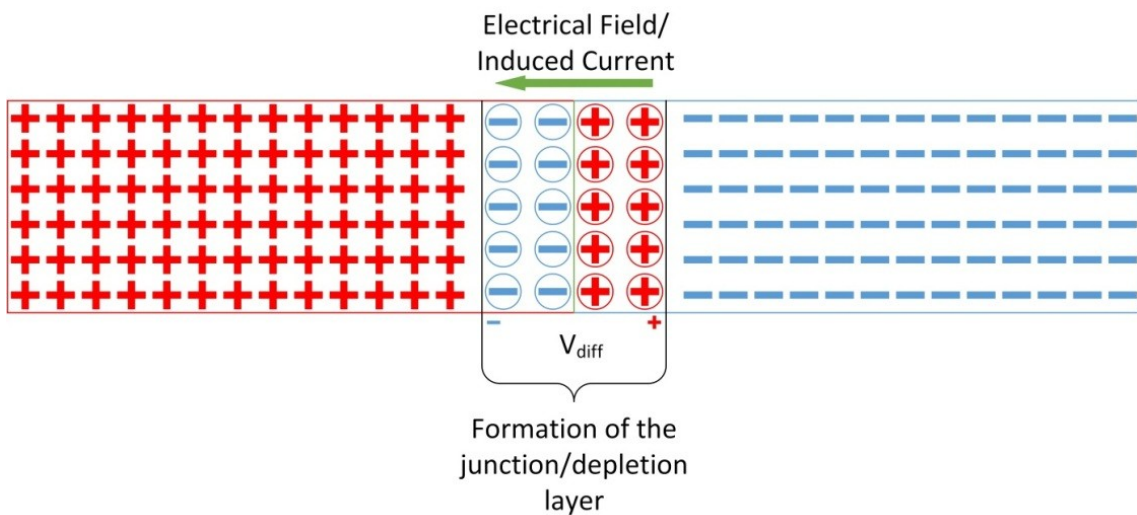


Figure 15. Formation of the depletion layer across the PN interface

Upon reaching equilibrium, a depletion layer void of mobile charges is formed with a width (d_s) and potential difference (V_{diff}). Since the depletion layer is made up of oppositely charged ions separated by a distance (d_s) within a semiconductor material of specific dielectric constant, this region is said to have the effect of a parallel plate capacitor.

Referring to figure 16, if $V_A > 0$, an electric field, which opposes the naturally induced one at equilibrium, is applied across the junction. In this case, the junction gets

narrower. Its capacitance is said to increase, whereas its resistance decreases. However, if $V_A < 0$, the external electric field assists the naturally induced one and ideally no charges can flow across the diode. In this case, the junction widens and its capacitance decreases, whereas its resistance increases. This effect of variable resistance and capacitance, which is based on the level of applied external bias, makes the diode a nonlinear device.

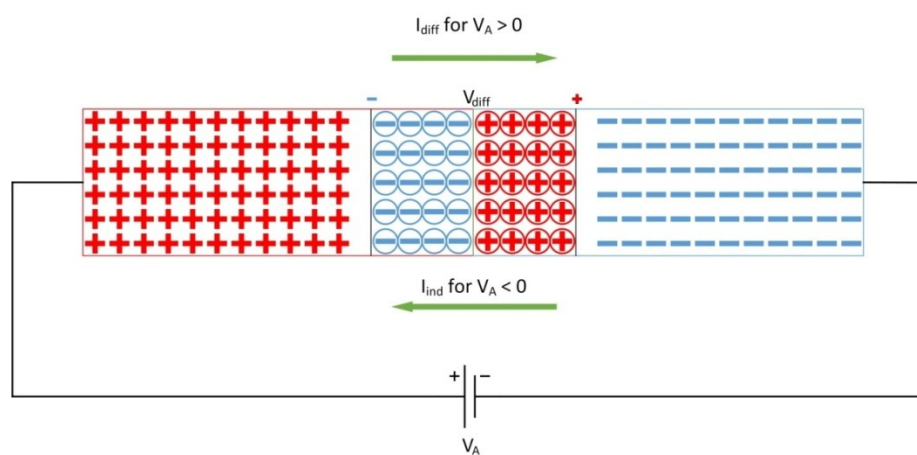


Figure 16. External voltage V_A applied to bias the PN junction

Referring to figure 16 and assuming that $V_A > V_{diff}$, the diode is in forward bias and the diffusion current flows across the junction. However, due to the minority carriers (electrons in the P-type and holes in the N-type) gathering at the edges of the two semiconductors, as illustrated in figure 17, a diffusion capacitance arises and limits the switching behavior of the diode. In this case, the total capacitance of the diode is that of the junction (C_J) in addition to that of diffusion (C_d). Now, assume that the external voltage source is removed. Ideally, we expect the diode to stop conducting current. Practically however, the induced electric field causes the minority carriers at the edges to diffuse into the opposite materials. This is similar to a discharging scenario,

which causes current to flow across the junction for a certain time period known as the transient-off time. The higher the concentration of minority carriers is, the higher the transient-off time is. As a result, the diode's switching behavior is degraded causing its maximum frequency of operation to be lowered. As a practical example, a typical Silicon PN junction diode has a (C_d) of about 194nF when forward-biased by a 1V DC source. This high (C_d) limits its maximum operational frequency to around 50MHz. Hence, for a diode to operate reliably at microwave frequencies, its transient-off time should be reduced. One type of RF diodes is known as "Schottky Diodes". These are majority carrier components with superior switching properties that make them capable of rectifying microwave signals.

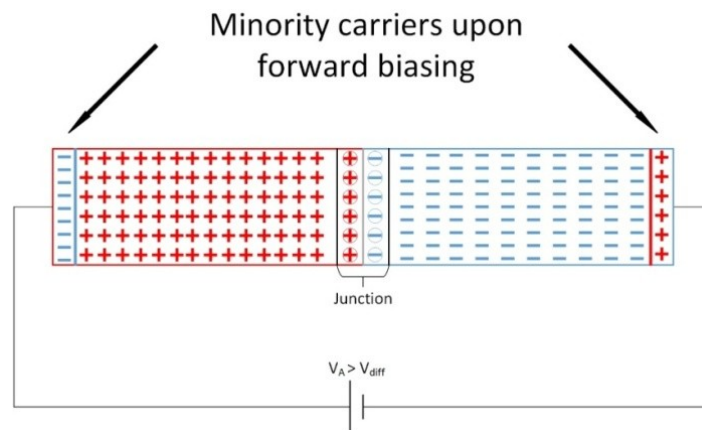


Figure 17. Formation of diffusion capacitance upon forward biasing the junction

C. Schottky Diodes: Physical and Electrical Characteristics

Unlike PN junctions, Schottky contacts are formed when a metallic electrode (Aluminum, Gold etc...) gets in contact with a semiconductor material (usually N-type). As with the PN junction, diffusion current rises upon initial contact where electrons diffuse from the semiconductor into the metal leaving behind positively charged ions.

At equilibrium, an induced electric field which opposes the direction of diffusion arises and stops the flow of current across the junction. A depletion layer is formed with a specific width (d_s) that varies with external biasing and causes the resistance and capacitance of the diode to vary as well. Due to the significant reduction in the concentration of minority carriers, the diffusion capacitance is eliminated and the switching behavior of the diode is improved in order to operate at microwave frequencies.

Because of their low capacitance, RF diodes find wide applications in a variety of RF components like mixers, detectors, oscillators, attenuators, and amplifiers. While RF Schottky diodes are mainly used as rectifiers, the metal-semiconductor junction can be used to construct RF diodes that act as variable resistors (attenuators) and high frequency switches such as the case of PIN diodes. The variation of the junction's capacitance with respect to the applied biasing voltage can be used to construct voltage controlled tuning circuits where the diode acts as a variable capacitor (varactors) [22].

Figure 18 shows the physical construction of a typical Schottky diode. The n-type layer is weakly doped whereas the substrate is heavily doped with free electrons. The Silicon dioxide (SiO_2) dielectric layer separates the semiconductor material from the metal.

Figure 19 shows the equivalent electrical model of the Schottky diode. (C_J) and (R_J) model the bias-dependent junction whereas (R_s) models the diode's series resistance. (C_g) and (L_s) model the parasitics formed due to the metallic contacts [22].

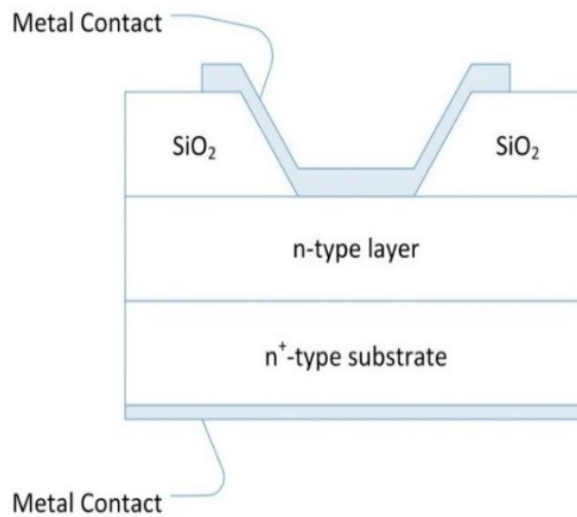


Figure 18. Physical construction of a typical Schottky diode [22]

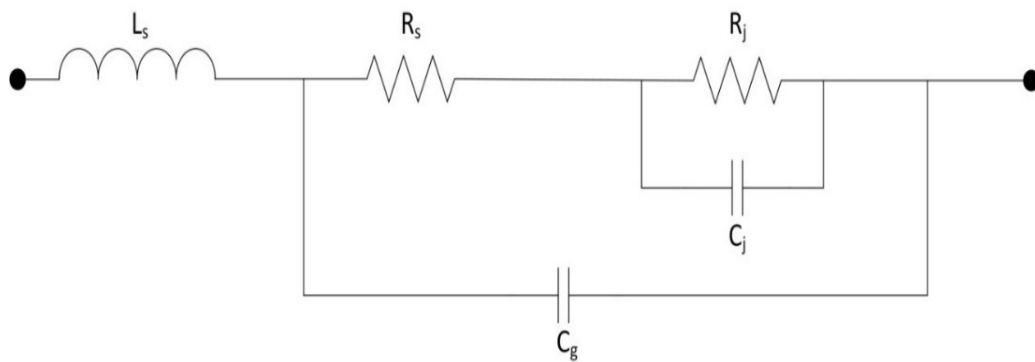


Figure 19. Electrical model of a typical Schottky diode [22]

Table 1 shows some of the common electrical parameters of Schottky diodes which should be taken into consideration when designing RF rectifiers.

Table 1. Common Parameters of Schottky Diodes [22]

Parameter	Significance
I_s (A)	Saturation current: Defines diode junction resistance at zero-bias
R_s (Ω)	Diode series resistance: Defines Ohmic losses in the semiconductor

(Table 1 continued)

Parameter	Significance
C_{J0} (pF)	Zero bias junction capacitance: Affects the switching behavior of the diode
V_{bi} (V)	Built-in potential: The minimum forward voltage needed for the diode to conduct current
V_{br} (V)	Breakdown potential: The maximum reverse voltage above which the diode breaks down
I_{bv} (A)	Current at breakdown: Reverse current that flows through the diode when it breaks down

In table 1, the term saturation current (I_s) is used with Schottky diodes as part of their SPICE model. To better understand how this term affects the performance of Schottky diodes, the current-voltage characteristics equation (1) is used as illustrated below.

$$I_D = I_s \left[e^{\left(\frac{qV_D - qI_D R_s}{nkT}\right)} - 1 \right]$$

$$\frac{I_D + I_s}{I_s} = e^{\left(\frac{qV_D - qI_D R_s}{nkT}\right)}$$

$$\ln\left(\frac{I_D + I_s}{I_s}\right) = \left(\frac{qV_D - qI_D R_s}{nkT}\right)$$

$$\boxed{V_D = \frac{nkT}{q} \ln\left(\frac{I_D + I_s}{I_s}\right) + I_D R_s} \quad (1)$$

In equation (1), (V_D) refers to the voltage drop across the diode's terminals. (I_D) is the current flowing through the diode as a result of (V_D). (nkT/q) is a constant term. (R_s) and (I_s) are the diode's series resistance and saturation current respectively. The equation of (V_D) was solved for a range of (I_D) values and the current-voltage characteristics of two commercial Schottky diodes from Skyworks [41] are plotted as shown in figure 20.

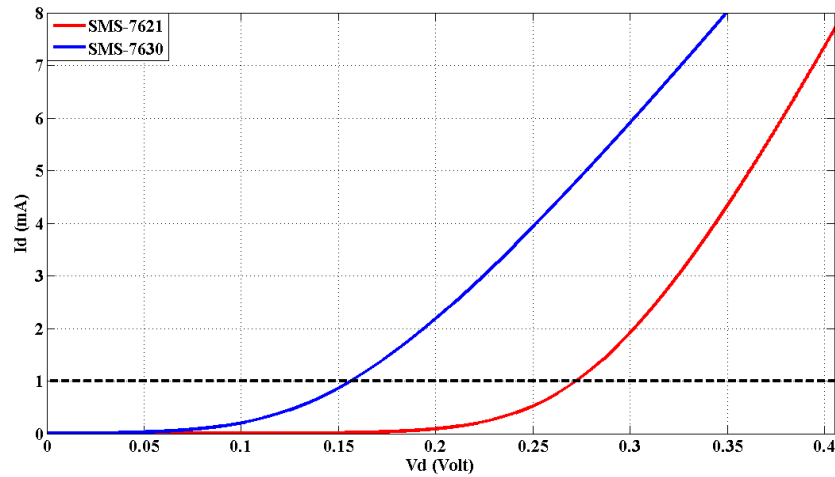


Figure 20. Current-voltage characteristics of two commercial Schottky diodes

As shown in figure 20, for a forward current of 1mA to flow through each diode, a minimum forward voltage (V_{bi}) of around 160mV is required in the case of the SMS-7630 (zero-bias) diode whereas a forward voltage of at least 270mV is needed for the case of the SMS-7621 (low-barrier) diode. While the zero-bias diode has a series resistance of around 20Ω , it is 12Ω for the case of the low-barrier diode. This is consistent with the curves since the red graph has a higher slope ($1/R_s$) than the blue one. Hence, the effect of the series resistance is inferred from the slopes of the curves. On the other hand, the saturation current (I_s) has a direct influence on the forward voltage of the diodes. The zero-bias diode, whose I_s is around $5\mu A$, conducts the same

current at a lower forward voltage as compared to the low-barrier diode ($I_s \approx 40\text{nA}$). Hence, diodes with higher saturation currents have lower (V_{bi}) values but higher (R_s) characteristics, and therefore, are more suitable for low power operations. Accordingly, a decrease in the saturation current is usually reflected as a higher (V_{bi}) value and at the same time a lower series resistance.

D. Summary

In this chapter, the physical and electrical characteristics of RF Schottky diodes are presented. Simply stated, Schottky diodes behave in a similar way to that of the PN junction. However, the main difference is that Schottky diodes are majority carrier devices with a significantly improved transient-off time that allows them to operate at higher frequencies. For Schottky diodes, the voltage-current characteristics equation is presented for two commercially available components. Based on the attained results, it was deduced that higher saturation currents yield lower built-in potential and higher series resistance values.

CHAPTER IV

THEORETICAL ANALYSIS OF RECTIFICATION

A. Objectives

In this chapter, a theoretical analysis for a typical RF-DC converter is carried out. Output power equations, up to the third harmonic, are derived for two different cases based on the amplitude level of the RF excitation signal. The aim of this chapter is to gain insight into how the performance of the rectifier changes with respect to diode parameters, input RF power, and load resistance. Conclusions derived from this analysis are later used to design rectifiers with improved efficiency performance.

B. Assumptions

The considered rectifier configuration for this analysis includes a shunt Schottky diode connected in reverse as shown in figure 21.

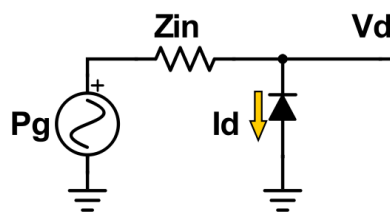


Figure 21. Shunt Schottky diode connected in reverse

To model the Schottky diode, a linear piecewise model is considered. For this configuration, the diode current-voltage characteristics are as shown in figure 22 [40]. In this figure, (V_{bi}) represents the minimum forward voltage that should exist across the terminals of the diode to conduct. Hence, the region characterized by ($V_d > V_{bi}$) is

referred to as the “Forward Bias” region. (V_{br}) represents the maximum reverse voltage beyond which reverse current flows through the diode. Consequently, the region characterized by ($V_d < -V_{br}$) is referred to as the “Breakdown” region. The $-V_{br} \leq V_d \leq V_{bi}$ region is called the “Reverse Bias” region, where the diode conducts no current.

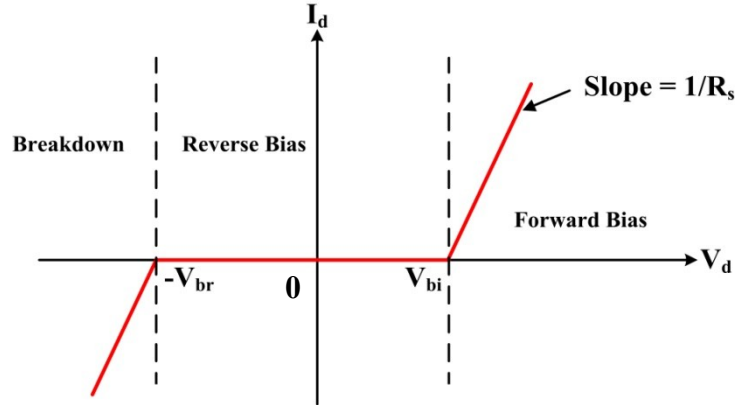


Figure 22. Assumed current-voltage characteristics of the Schottky diode

In order to keep the analysis simple, it is assumed that perfect matching conditions exist between the source and the diode. Hence, no RF power is lost due to reflections. The voltage supplied by the generator is assumed to exhibit sinusoidal variation with time according to equation (2).

$$v_{in} = V_p \cos(2\pi f_0 t) \quad (2)$$

In equation (2), (V_p) denotes the peak voltage of the RF signal supplied by the generator. It can be expressed as in (3) where (P_g) refers to the maximum power available from the generator.

$$V_p = \sqrt{8P_g R(Z_{in})} \quad (3)$$

C. Study Cases

1. Scenario I: $V_p < V_{br}$

In this case, the diode in the circuit of figure 21 can be replaced with an equivalent DC voltage source (V_{bi}) in series with the internal resistance (R_s). This is illustrated in the figure 23 where the junction resistance (R_J) is assumed to be ideal.

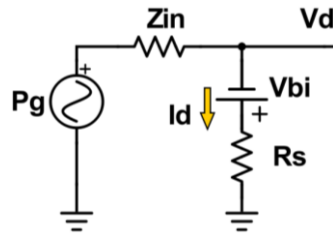


Figure 23. Diode model when $V_p < V_{br}$

In figure 24, (t_1) denotes the time point at which the diode enters the forward biasing region. On the other hand, (t_2) denotes the point at which the diode exits this region and goes back into the cut-off mode. The operating regions are summarized in table 2. (V_p) and (V_{bi}) in figure 24 are respectively chosen to be 1V and 170mV for illustrative purposes.

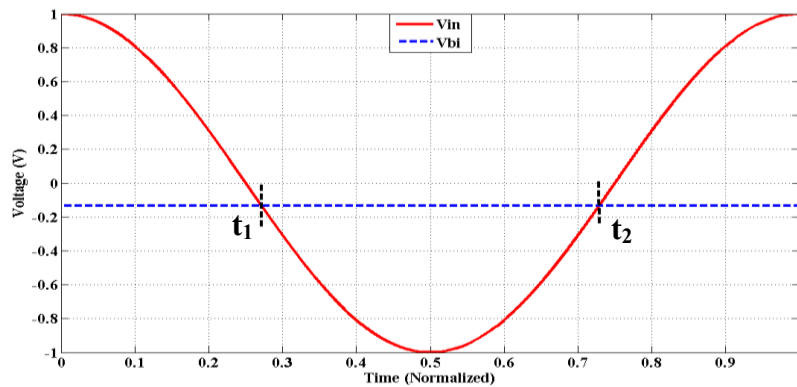


Figure 24. Time points for the case of $V_p < V_{br}$

Table 2. Operating regions for the case of $V_p < V_{br}$

Time	Region	Status of (R_J)	(v_d) , (i_d)
$0 \leq t < t_1$	Cut-off	Infinite (open switch)	$v_{dr} = v_{in}$ $i_{dr} = 0$
$t_1 \leq t \leq t_2$	Forward bias	Zero (closed switch)	$v_{df} = i_{df}R_s - V_{bi}$ $i_{df} = \frac{v_{in} + V_{bi}}{R_s + Z_{in}}$
$t_2 < t \leq T$	Cut-off	Infinite (open switch)	$v_{dr} = v_{in}$ $i_{dr} = 0$

The values of (t_1) and (t_2) can be derived as follows:

$$v_{in}(t_1) = -V_{bi}$$

$$V_p \cos(2\pi f_0 t_1) = -V_{bi}$$

$$t_1 = \frac{T \cdot \cos^{-1}\left(\frac{-V_{bi}}{V_p}\right)}{2\pi} \quad (4)$$

Hence, $t_2 = T - t_1$ due to the symmetry in the curves of figure 24. The equations in table 2 are plotted over a single period of the input signal (v_{in}). A special case of ($V_{bi} = 170\text{mV}$, $R_s = 20\Omega$, $Z_{in} = 50\Omega$) are assumed to generate the diode voltage and current curves. The results are shown in figure 25.

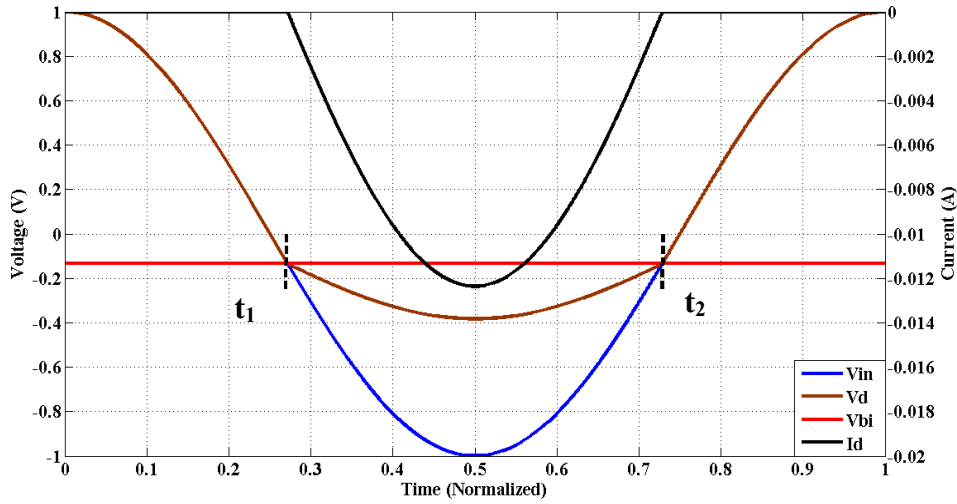


Figure 25. Diode voltage and current waveforms for $V_p < V_{br}$

As illustrated in figure 25, the diode voltage (v_d) is clipped during the negative cycle of (v_{in}). This allows harmonics of the fundamental frequency (f_0) to be generated by the diode. Since (v_d) and (i_d) are periodic, Fourier series can be used to derive equations for the harmonic content of both waveforms. According to Fourier series, a time periodic signal ($f(t)$) of period (T) can be represented in terms of its harmonics as:

$$f(t) = \frac{a_0}{2} + \sum_{n=1}^{\infty} [a_n \cos(2\pi n f_0 t) + b_n \sin(2\pi n f_0 t)] \quad (5)$$

In equation (5), (n) denotes the order of the harmonic where:

$$a_0 = \frac{2}{T} \int_0^T f(t) dt \quad (6)$$

$$a_n = \frac{2}{T} \int_0^T f(t) \cos(2\pi n f_0 t) \quad (7)$$

$$b_n = \frac{2}{T} \int_0^T f(t) \sin(2\pi n f_0 t) \quad (8)$$

Applying equation (6) allows us to find an approximate solution for the DC voltage generated by the diode. This is done as follows:

$$V_{DC} = \frac{a_0}{2} = \frac{1}{T} \int_0^T v_d(t) dt = \frac{1}{T} * \left(\int_0^{t_1} v_{dr} dt + \int_{t_1}^{t_2} v_{df} dt + \int_{t_2}^T v_{dr} dt \right)$$

$$V_{DC} = \frac{Z_{in} * \left[V_p \sin \left(\cos^{-1} \left(\frac{V_{bi}}{V_p} \right) \right) - V_{bi} \cos^{-1} \left(\frac{V_{bi}}{V_p} \right) \right]}{\pi (R_s + Z_{in})} \quad (9)$$

Similarly, the DC current flowing through the diode can be derived as:

$$I_{DC} = \frac{1}{T} \int_0^T i_d(t) dt = \frac{1}{T} * \left(\int_{t_1}^{t_2} i_{df} dt \right)$$

$$I_{DC} = \frac{V_{bi} \cos^{-1} \left(\frac{V_{bi}}{V_p} \right) - V_p \sqrt{1 - \left(\frac{V_{bi}}{V_p} \right)^2}}{\pi (R_s + Z_{in})} \quad (10)$$

We notice from the equations of (V_{DC}) and (I_{DC}) the following:

$$\frac{V_{DC}}{I_{DC}} = -Z_{in} \quad (11)$$

This allows representing the circuit of figure 21 by its equivalent model in figure 26, where the RF and DC components of (v_d) and (i_d) are isolated through the incorporation of a DC blocking capacitor and an RF choke. For the analysis to remain valid, the DC load resistance (R_L) should be equal to (Z_{in}) where (Z_{in}) is the internal impedance of the generator and is assumed to be 50Ω.

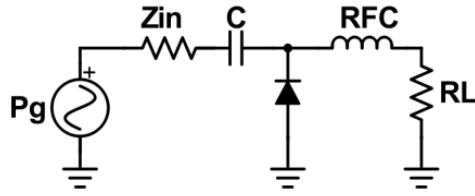


Figure 26. Equivalent circuit of the rectifier after adding R_L

In order to make sure that the above steps along with the derived equations are accurate enough to make conclusions, ADS [44] simulations are carried out. For fair comparison purposes, only the diode parameters, which are considered in the above derivations, are included in the simulations. However, the other ones, such as the zero-bias junction capacitance, are idealized in the SPICE model of the diode. Although the choice of frequency should not affect the amplitudes of the voltage and current harmonics, a fundamental frequency of 1GHz is used to validate scenario I. The value of the fundamental frequency was chosen to be compatible with the diode's switching speed. However, the junction capacitance (C_J) causes the impedance of the diode to vary versus the operating frequency. This requires impedance matching, at the frequency of interest, to make sure that no power is reflected back to the generator. The parameters (R_s), (V_{bi}), and (Z_{in}) are chosen to be 20Ω , 170mV , and 50Ω respectively. These characteristics are inherent to zero-bias Schottky diodes (such as the SMS-7630 diode of Skyworks).

Figure 27 shows a comparison between the derived and simulated DC power of the diode. As can be observed, a good agreement is revealed between the superposed plots. The power level of the fundamental and higher order harmonics can also be computed through the previously derived equations.

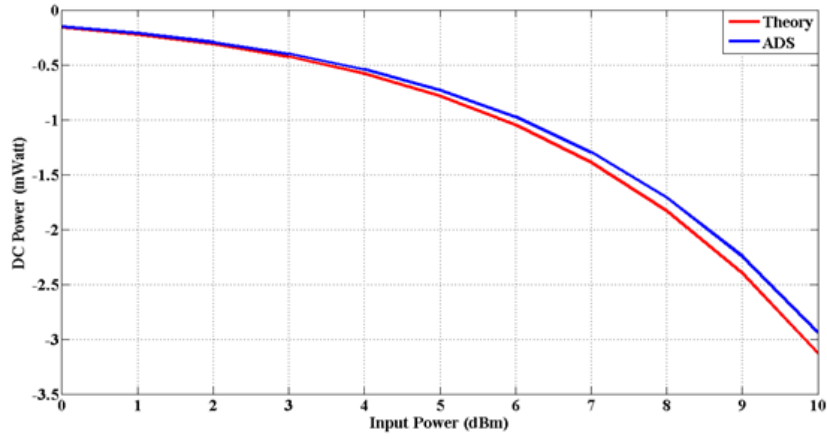


Figure 27. DC power generated by the diode for $V_p < V_{br}$

Again, using Fourier series we can write:

$$a_{1V} = \frac{2}{T} * \int_0^T v_d(t) \cos(2\pi f_0 t) dt = \frac{2}{T} * \left[\int_0^{t_1} v_{dr} \cos(2\pi f_0 t) dt + \int_{t_1}^{t_2} v_{df} \cos(2\pi f_0 t) dt + \int_{t_2}^T v_{dr} \cos(2\pi f_0 t) dt \right]$$

$$a_{1I} = \frac{2}{T} * \int_0^T i_d(t) \cos(2\pi f_0 t) dt = \frac{2}{T} * \left[\int_{t_1}^{t_2} i_{df} \cos(2\pi f_0 t) dt \right]$$

In the above equations, (a_{1V}) and (a_{1I}) denote the amplitudes of the sinusoidal waveforms with frequency (f_0) across the diode. The time average power consumed by the diode can be computed as:

$$P_1 = \frac{a_{1V} * a_{1I}}{2} \quad (12)$$

Part of this power is lost due to the diode's series resistance and built-in potential whereas the remaining part is converted to DC power and higher order harmonics. Figure 28 compares between the power consumed by the diode at the frequency of (f_0) as calculated by the equations and the SPICE model in ADS. Again,

good agreement exists between the results. Similarly, power at higher order harmonics can also be computed using Fourier series equations for $n \geq 2$. A comparison between the computed and simulated power plots at the 2nd and 3rd harmonics is given in figure 29 and figure 30, respectively. However, it should be noted that for harmonics greater than 3 the error between the theoretical and simulated values increases. This is mainly due to the SPICE model as well as the assumption of perfect impedance matching.

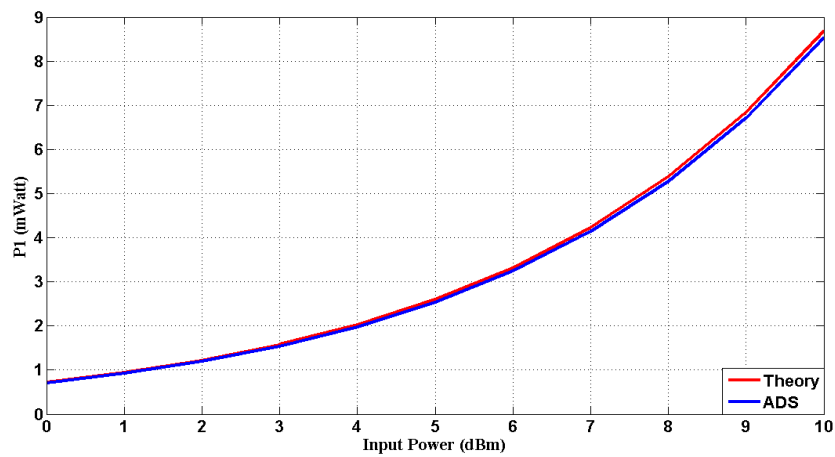


Figure 28. RF power consumed by the diode for $V_p < V_{br}$

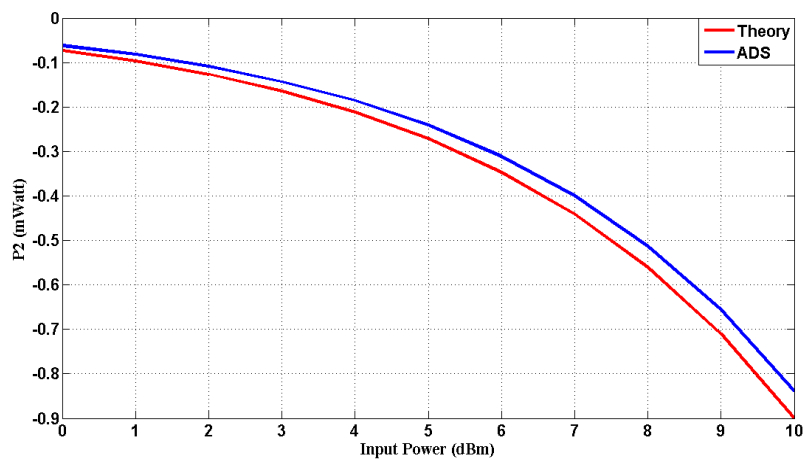


Figure 29. Generated RF power at the second harmonic for $V_p < V_{br}$

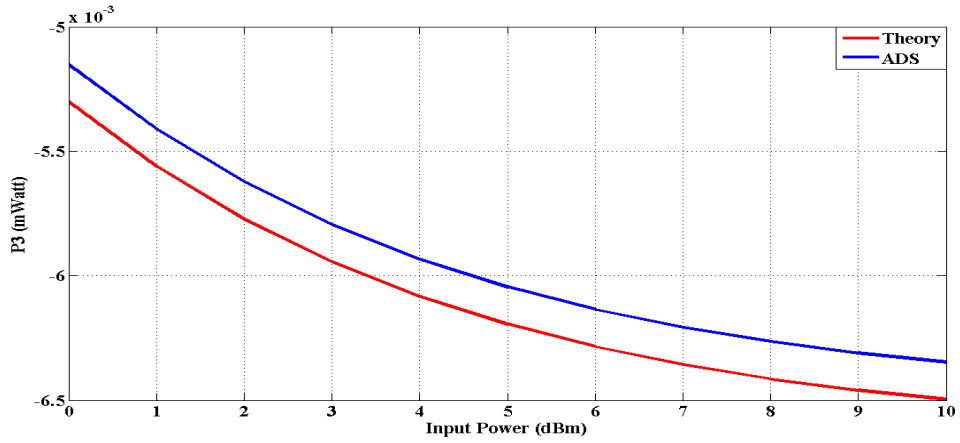


Figure 30. Generated RF power at the third harmonic for $V_p < V_{br}$

From figure 29 and figure 30, we infer that when low power is fed into the diode in such a way that breakdown is avoided, the second and third harmonics both have increasing power levels. However, in this case the third harmonic has much lower power than that of the second.

2. *Scenario II: $V_p \geq V_{br}$*

This section aims at analyzing the harmonics generated by the diode when the input RF signal is large enough such that breakdown occurs. In this case, the breakdown effect has to be accounted for in the diode voltage and current equations. Figure 23 can be used to model the diode during forward bias. During breakdown, the reverse voltage across the diode increases in magnitude beyond (V_{br}). This causes a reverse current (i_{db}) to flow through the junction. This effect is modeled by considering the junction resistance (R_J) to be zero after breakdown. Figure 31 shows the equivalent circuit that is used to model the diode in the breakdown region.

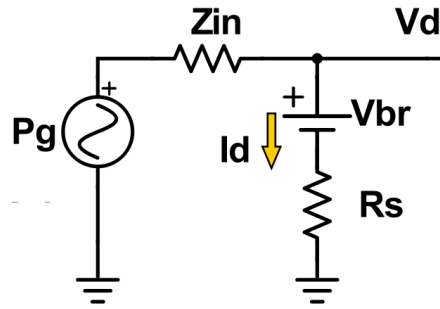


Figure 31. Diode equivalent model during breakdown

Figure 32 shows an example of an RF input signal with a peak voltage of 4V. (V_{bi}) and (V_{br}) are chosen to be 170mV and 3V, respectively. The diode exits the first breakdown region at time (t_1). At (t_2), the diode enters into the forward bias region, which ends at (t_3). The diode again goes into breakdown at (t_4). This behavior is summarized in table 3.

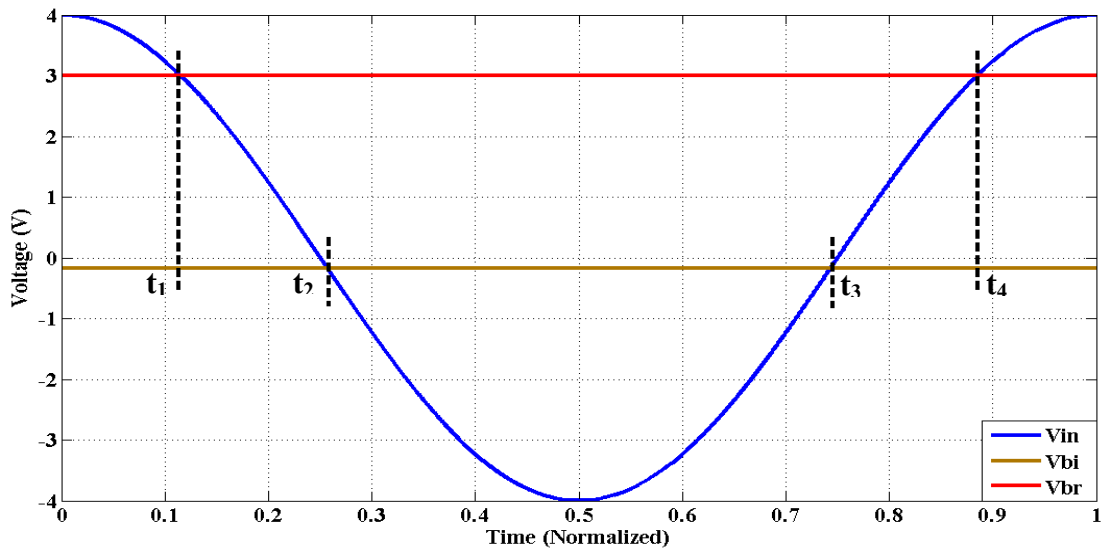


Figure 32. Time points for the case of $V_p \geq V_{br}$

Table 3. Operating regions for the case of $V_p \geq V_{br}$

Time	Region	Status of (R_J)	$(v_d), (i_d)$
$0 \leq t < t_1$	Breakdown	Zero (closed switch)	$v_{ab} = i_{ab}R_s + V_{br}$ $i_{ab} = \frac{v_{in} - V_{br}}{R_s + Z_{in}}$
$t_1 \leq t < t_2$	Cut-off	Infinite (open switch)	$v_{dr} = v_{in}$ $i_{dr} = 0$
$t_2 \leq t \leq t_3$	Forward Bias	Zero (closed switch)	$v_{df} = i_{df}R_s - V_{bi}$ $i_{df} = \frac{v_{in} + V_{bi}}{R_s + Z_{in}}$
$t_3 < t \leq t_4$	Cut-off	Infinite (open switch)	$v_{dr} = v_{in}$ $i_{dr} = 0$
$t_4 < t \leq T$	Breakdown	Zero (closed switch)	$v_{ab} = i_{ab}R_s + V_{br}$ $i_{ab} = \frac{v_{in} - V_{br}}{R_s + Z_{in}}$

The time points in figure 32 can now be derived as follows:

$$v_{in} = V_{br}$$

$$V_p \cos(2\pi f_0 t_1) = V_{br}$$

$$\boxed{t_1 = \frac{T}{2\pi} \cos^{-1}\left(\frac{V_{br}}{V_p}\right)} \quad (13)$$

$$v_{in} = -V_{bi}$$

$$V_p \cos(2\pi f_0 t_2) = -V_{bi}$$

$$t_2 = \frac{T}{2\pi} \cos^{-1} \left(\frac{-V_{bi}}{V_p} \right) \quad (14)$$

$$t_3 = T - t_2 \quad (15)$$

$$t_4 = T - t_1 \quad (16)$$

The derived diode voltage and current equations are plotted in figure 33 for ($R_s = 20\Omega$, $Z_{in} = 50\Omega$, $V_{bi} = 170\text{mV}$, $V_{br} = 3\text{V}$, and $V_p = 4\text{V}$).

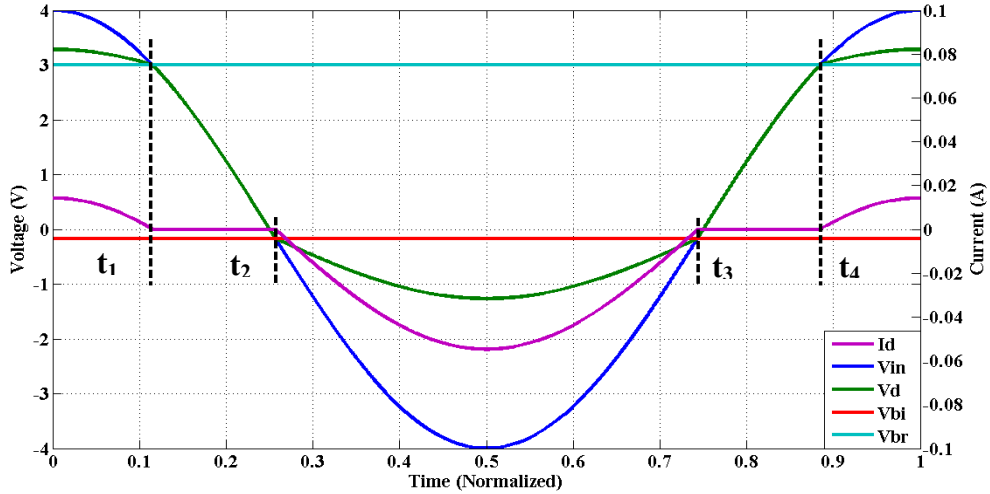


Figure 33. Diode voltage and current waveforms for the case of $V_p \geq V_{br}$

As shown in figure 33, the diode voltage and current waveforms have changed because of the additional breakdown effect. Due to their periodicity, the Fourier series can be used as follows to find their harmonic content.

$$V_{DC} = \frac{a_0}{2} = \frac{1}{T} \int_0^T v_d(t) dt = \frac{1}{T} * \left(\int_0^{t_1} v_{db} dt + \int_{t_1}^{t_2} v_{dr} dt + \int_{t_2}^{t_3} v_{df} dt + \int_{t_3}^{t_4} v_{dr} dt + \int_{t_4}^T v_{db} dt \right)$$

By substituting the equations in table 3 into (V_{DC}), the diode generated DC voltage can be derived. After solving and simplifying the above expression we get:

$$V_{DC} = \frac{Z_{in} * \left[\sqrt{V_P^2 - V_{bi}^2} - \sqrt{V_P^2 - V_{br}^2} - V_{bi} \cos^{-1}\left(\frac{V_{bi}}{V_P}\right) + V_{br} \cos^{-1}\left(\frac{V_{br}}{V_P}\right) \right]}{\pi(R_s + Z_{in})} \quad (17)$$

Similarly, we can find the DC current flowing through the diode as follows:

$$I_{DC} = \frac{1}{T} \int_0^T i_d(t) dt = \frac{1}{T} * \left(\int_0^{t_1} i_{ab} dt + \int_{t_2}^{t_3} i_{df} dt + \int_{t_4}^T i_{ab} dt \right)$$

Again, substitution of the equations in table 3 gives:

$$I_{DC} = \frac{\left[-\sqrt{V_P^2 - V_{bi}^2} + \sqrt{V_P^2 - V_{br}^2} + V_{bi} \cos^{-1}\left(\frac{V_{bi}}{V_P}\right) - V_{br} \cos^{-1}\left(\frac{V_{br}}{V_P}\right) \right]}{\pi(R_s + Z_{in})} \quad (18)$$

As previously computed, the ratio of (V_{DC}) to (I_{DC}) is found to be ($-Z_{in}$). Hence, the equivalent circuit of figure 26 is still valid. In other words, the derivations that are made in both scenarios assume that the DC load resistance connected across the diode has a value of $R_L = Z_{in}$. Since Z_{in} is the internal impedance of the generator, R_L is assumed to be 50Ω .

To validate the derived equations, ADS simulations are carried out for comparison purposes. For this reason, the Schottky diode chosen is considered to have a 170mV (V_{bi}), 20Ω (R_s), and (2V) V_{br} . The generator's impedance ($Z_{in}=R_L$) is 50Ω . The fundamental frequency (f_0) over which the simulations are performed is 1GHz and the power input to the diode is swept from 10 to 13dBm in steps of 0.3dB . The above

assumptions are used to compute the DC power as shown in figure 34. The effects of the junction capacitance in the SPICE model are ignored.

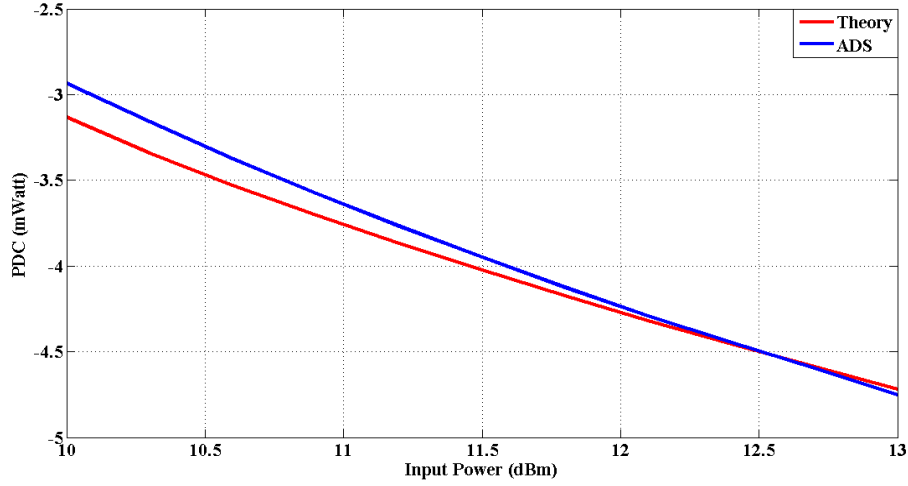


Figure 34. Generated DC power for the case of $V_p \geq V_{br}$

As previously stated, the Fourier series can also be used to compute the power at higher harmonics. This is done by solving the following equations for the first harmonic power. For the second and third order harmonics the same procedure is followed but (n) is replaced with (2) and (3) respectively.

$$a_{1V} = \frac{2}{T} * \int_0^T v_d(t) \cos(2\pi f_0 t) dt$$

$$a_{1V} = \frac{2}{T} * \left[\int_0^{t_1} v_{db} \cos(2\pi f_0 t) dt + \int_{t_1}^{t_2} v_{dr} \cos(2\pi f_0 t) dt + \int_{t_2}^{t_3} v_{df} \cos(2\pi f_0 t) dt \right] \\ + \frac{2}{T} * \left[\int_{t_3}^{t_4} v_{dr} \cos(2\pi f_0 t) dt + \int_{t_4}^T v_{db} \cos(2\pi f_0 t) dt \right]$$

$$a_{1I} = \frac{2}{T} * \int_0^T i_d(t) \cos(2\pi f_0 t) dt$$

$$a_{1I} = \frac{2}{T} * \left[\int_0^{t_1} i_{db} \cos(2\pi f_0 t) dt + \int_{t_2}^{t_3} i_{df} \cos(2\pi f_0 t) dt + \int_{t_4}^T i_{db} \cos(2\pi f_0 t) dt \right]$$

The curves in figure 35 show a comparison between the computed power values at the fundamental frequency and the simulated ones. As can be observed, good agreement exists between both curves.

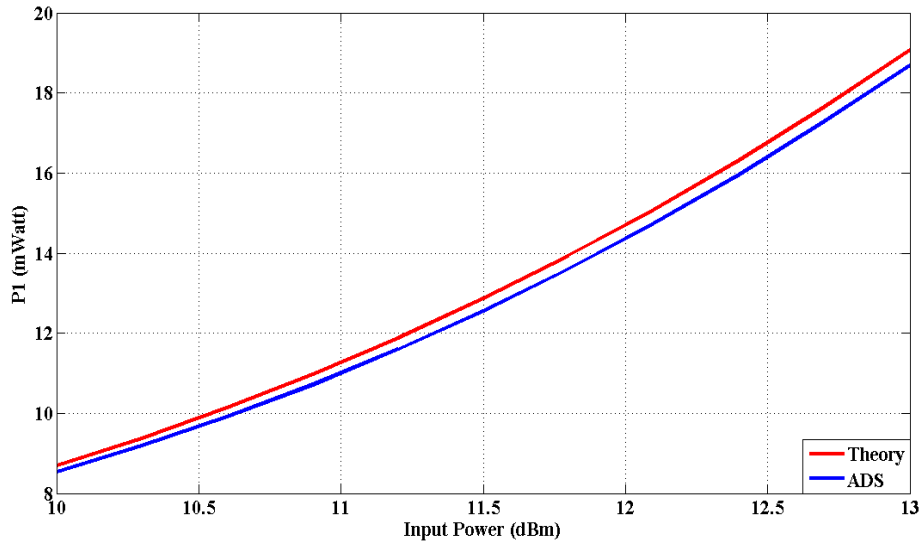


Figure 35. RF power consumed by the diode for the case of $V_p \geq V_{br}$

Figure 36 shows a comparison between the calculated and simulated curves for the diode's generated power at the second harmonic. By comparing those curves with those derived for the same harmonic in case I (figure 29), we conclude that prior to breakdown the generated power at this harmonic level increases exponentially. As breakdown gets surpassed, the power of the generated second harmonic starts decreasing.

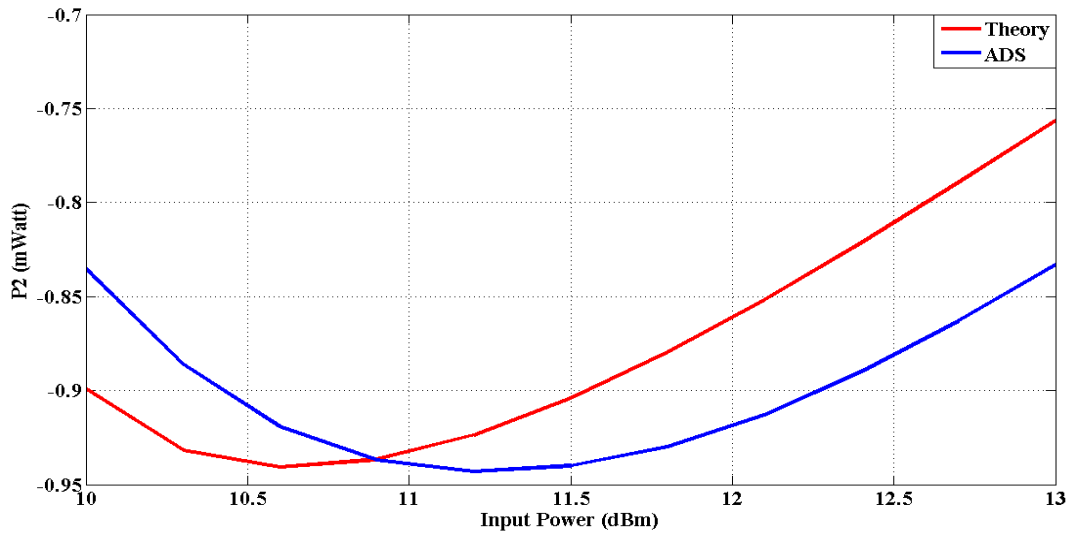


Figure 36. RF power generated at the second harmonic for the case of $V_p \geq V_{br}$

Figure 37 shows a comparison between the computed and simulated power levels of the diode generated third harmonic. As can be observed, contrary to the behavior of the second harmonic, as breakdown gets surpassed, the third harmonic's power keeps increasing.

By comparing figure 37 to figure 30, it becomes clear that the increase in this harmonic's power continues during breakdown in contrast to the power level of the second harmonic. This can be further illustrated by considering the curves in figure 38. These were generated using the derived equations for the power range of 0 to 18dBm. As can be observed, beyond breakdown (~ 10 dBm), the third harmonic power increases in-contrast to the second harmonic. In fact, at some power level (~ 16 dBm in figure 38), the third harmonic power surpasses that of the second harmonic.

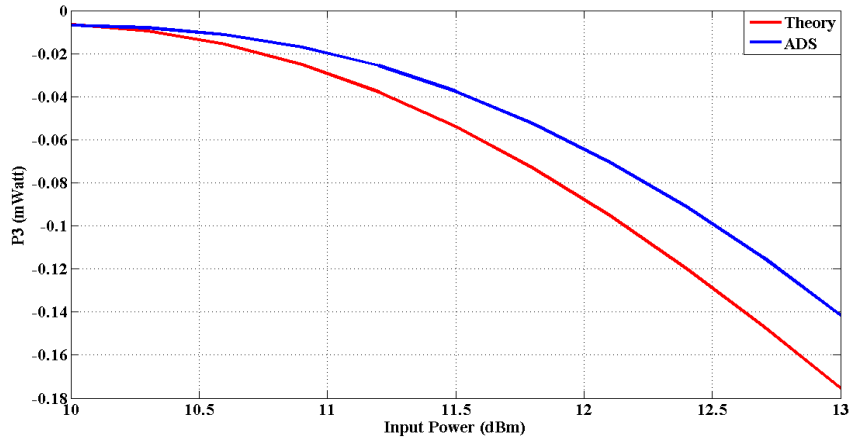


Figure 37. RF generated power at the third harmonic for the case of $V_p > V_{br}$

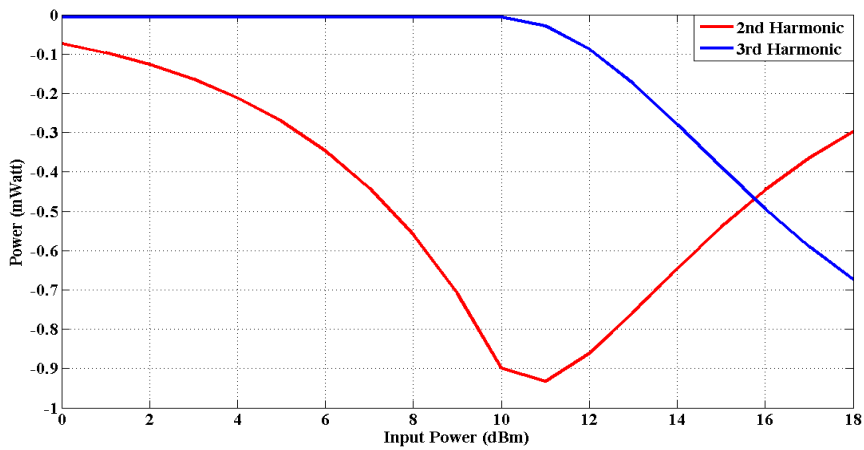


Figure 38. Breakdown effect on the generated second and third harmonic powers

D. Effects of the Diode Parameters

In this part, the aim is to make use of the previously derived and tested diode equations to infer how the different diode parameters affect the output DC power. For this reason, two commercially available Schottky diodes are chosen for comparison. The first is SMS-7621 which is a low-barrier diode and the other is the zero-bias SMS-7630 diode both being from Skyworks. The properties of both diodes are summarized in table 4.

Table 4. Properties of the compared Skyworks diodes

Diode	R_s (Ω)	V_{br} (V)	V_{bi} (mV)	I_s (A)
SMS-7630	20	2	170	$5e-6$
SMS-7621	12	3	260	$4e-8$

The graphs of the generated DC power for each of these diodes as derived by the previously computed equations are shown in figure 39.

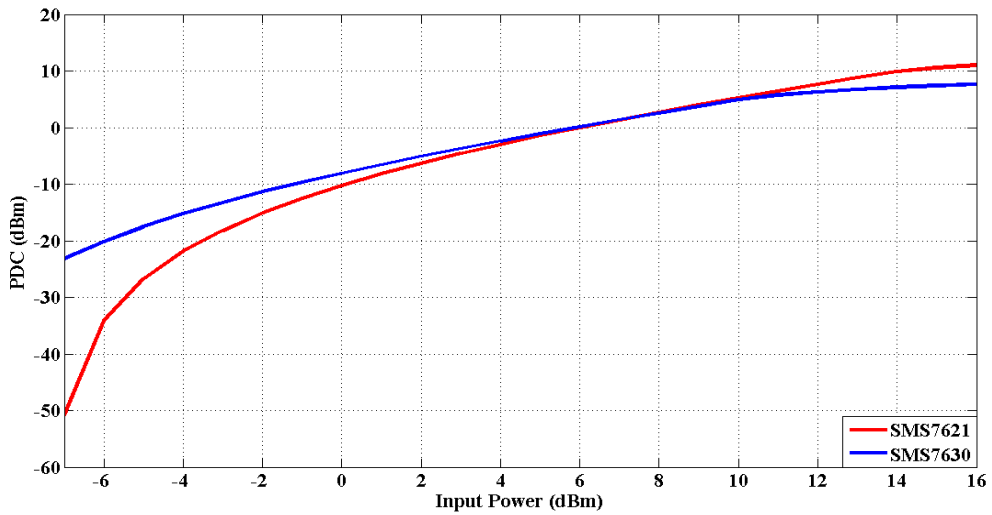


Figure 39. DC power generated by the Skyworks diodes

It can be observed from figure 39 that as the input RF power decreases, the zero-bias diode can generate more DC power due to its lower built-in potential (higher saturation current). This is true even though it has a higher series resistance. It is only when the zero-bias diode reaches breakdown (around 10dBm), that the low-barrier diode starts to generate higher DC power. This is because the DC power generated by the SMS-7630 starts to saturate above 10dBm whereas that of the SMS-7621 diode keeps rising due to its higher breakdown voltage.

E. Effect of the Load Resistance

As stated previously, all the derived equations are valid only under the condition that $R_L = Z_{in} = 50\Omega$. Practically however, the load resistance can be varied to control the output DC voltage. Although in the equations it was assumed that the diode's junction resistance is ideal (short or open), it practically has a large value under reverse bias but it is not infinite. Similarly, under forward bias it has a small value (typically in the range of several Ohms) but it is not zero.

Because the generated DC voltage at the output load reverse biases the diode, its video resistance (DC resistance) would be large. Hence, the DC voltage generated due to the RF signal excitation is divided between the load and (R_J) as shown in figure 40.

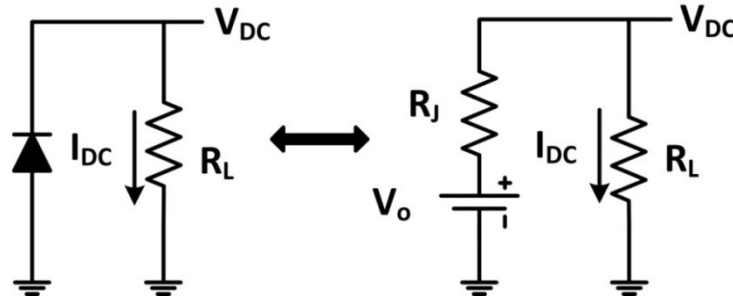


Figure 40. Effect of R_L over the output DC voltage

In figure 40, (V_o) stands for the maximum output DC voltage that the diode can generate at a specific input RF power. The output DC voltage (V_{DC}) can hence be expressed as:

$$\boxed{V_{DC} = \frac{V_o * R_L}{R_L + R_J}} \quad (19)$$

For $R_L \gg R_J$, (V_{DC}) can be expressed as:

$$\boxed{V_{DC} = V_o} \quad (20)$$

Hence, as R_L is increased, the output DC voltage increases until it saturates at V_o . However, there is an effect over the breakdown performance of the diode. Because (V_{DC}) is positive, increasing it causes the diode voltage curve (v_d) to get closer to the breakdown voltage level (figure 33). This is because (V_{DC}) gets superimposed over the RF signals across the diode terminals. For this reason, increasing (R_L) is usually done to enhance the power conversion efficiency of the diode at low power levels. This is because of the additional DC voltage collected at the load without going into breakdown. This explains why lower values of (R_L) are usually needed to enhance the efficiency at higher power levels. Because the DC output voltage decreases across the diode terminals, its diode voltage curve (v_d) moves further away from the breakdown level. The complexity involved in determining the best value of the load resistance for optimal efficiency curves makes it necessary to rely on nonlinear simulations using ADS along with practical measurements.

F. Summary

In this chapter, equations were derived to predict the performance of a typical rectifier using a reverse shunt-connected Schottky diode. The analysis was performed for the case of small input signals which do not cause the diode to breakdown and large input signals which lead to this phenomenon. From the derived equations it was concluded that the lower the available RF power, the higher should be the saturation current of any used Schottky diodes. In other words, lower built-in potential values are

needed for better efficiencies even if this condition is practically accompanied by higher series resistances. Also, the equations derived made it possible to gain insight into the diode generated harmonics. It was deduced that below breakdown, the third harmonic has typically much lower power than the second harmonic. When breakdown is reached, the second harmonic power starts decreasing whereas the third harmonic power increases exponentially until at some input RF power it surpasses that of the second harmonic. This means that when breakdown is reached, the efficiency of the rectifier is expected to drop due to the rise in the total harmonic power. This is practically explained by the saturation of the output generated DC voltage across (R_L). In the next chapter, two methods are studied to overcome the breakdown effect which leads to degradation in the efficiency of RF rectifiers.

CHAPTER V

EFFICIENT RF HARVESTING OVER WIDER POWER RANGE

A. Objectives

From chapter II it is noticed that the rectifiers designed in different research papers usually achieve a peak PCE at a specific optimal input RF power. Deviations from the optimal power level cause the efficiency to drop. In applications where changes in input RF power are expected, this behavior negatively affects the performance of the system being fed by DC power. Therefore, in this chapter, the information previously presented on the characteristics of Schottky diodes and their rectification capabilities are used to widen the RF input power range over which efficient RF-DC conversion is achieved. For acceptable RF energy harvesting, a minimum (PCE) of 50% is required. As revealed in chapter IV, the built-in potential (V_{bi}) and breakdown voltage (V_{br}) of commercial Schottky diodes influence their rectification behavior. For instance, when the input RF power to a Schottky diode is high enough to cause breakdown, the output DC power for a specific load saturates. This in turn causes the PCE curve to degrade rapidly. As a result, two methods are studied herein to overcome the negative effects associated with diode breakdown.

B. Method I – Controlling the Flow of Input RF Power

In chapter III, it was noted that the width of a Schottky diode's junction varies according to the applied bias. This causes the resistance and capacitance of the junction to vary as well. From this, it can be concluded that the RF power fed into the diode causes a change in the latter's impedance. Hence, for increasing RF power levels, the

reactive (capacitive) impedance of the diode is expected to decrease in magnitude whereas the resistive part of its impedance increases. In contrast, lowering the power level causes the capacitive impedance of the diode to increase in magnitude whereas its resistive part decreases. In this method, the objective is to make use of this variable impedance behavior of Schottky diodes in such a way that the flow of input RF power to the rectifier gets alternated between two different branches where different diodes are placed. When the RF power increases beyond a certain level, its path is directed to the branch where diodes with high breakdown potential exist. For lower power levels, the RF signal is directed towards the branch where zero-bias detector diodes exist. This allows rectification to take place efficiently by the zero-bias diodes when low power levels are available. On the other hand, when high power levels exist, instead of degrading the PCE of the rectifier due to the low (V_{br}) of zero-bias diodes, the RF power is fed into diodes with higher (V_{br}) [23]. This concept is illustrated in Figure 41.

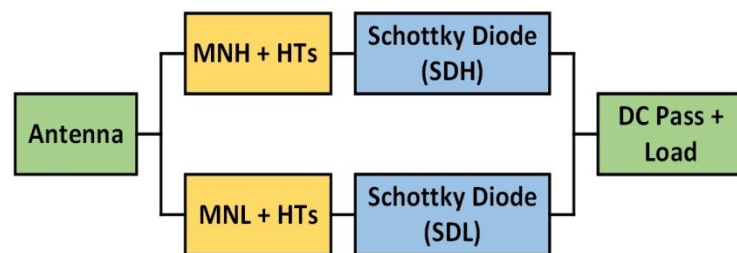


Figure 41. Block diagram of the rectenna proposed in method I

Referring to figure 41, the upper branch of the diagram constitutes the “high power rectification path” whereby (SDH) refers to Schottky diodes with high built-in potential (V_{bi}) and breakdown voltage (V_{br}). It is matched to the antenna through a matching network denoted by (MNH). On the other hand, the lower branch constitutes the “low power rectification path” whereby (SDL) refers to zero-bias Schottky diodes

with lower (V_{bi}) and (V_{br}). It is matched to the antenna through the (MNL) matching network. Harmonic Terminations (HTs) are used to confine the second and third order harmonics generated due to the non-linear behavior of the diodes. Each path is first designed individually where the corresponding matching network is optimized to match each Schottky diode over a specific RF input power range.

Theoretically speaking, when the input RF power is high such that the (SDL) diodes breakdown, the lower path is highly mismatched and hence power is rejected. On the other hand, the upper branch is matched and power is fed into the (SDH) diodes to produce DC power at the load. Conversely, when the input power is low such that breakdown of the (SDL) diodes is avoided, the high power rectifier is highly mismatched and the RF power is fed into the lower rectifier to convert it to DC. This behavior is illustrated in figure 42 where the dotted blocks illustrate the branch which rejects the RF power due to the impedance mismatch. In this figure, the arrows illustrate the theoretical path chosen by the RF power.

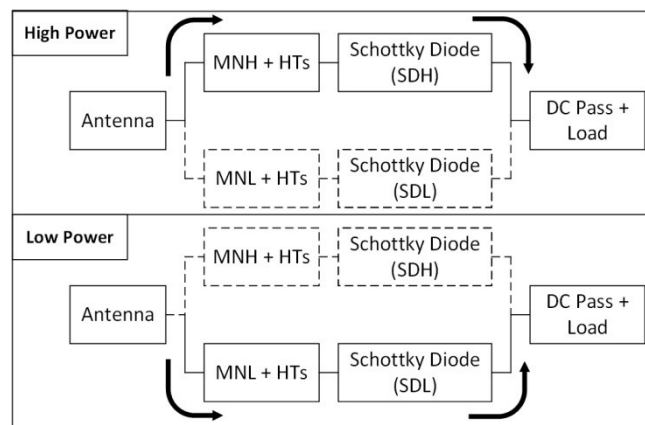


Figure 42. Controlling the RF power flow based on method I

This method was tested using ADS simulations where Harmonic Balance (HB) and Large Signal S-Parameter (LSSP) controllers are used, while taking into

consideration harmonics up to the third order. The ADS schematic and simulation results are provided below, where the source impedance is 50Ω and operating frequency is 2.1GHz.

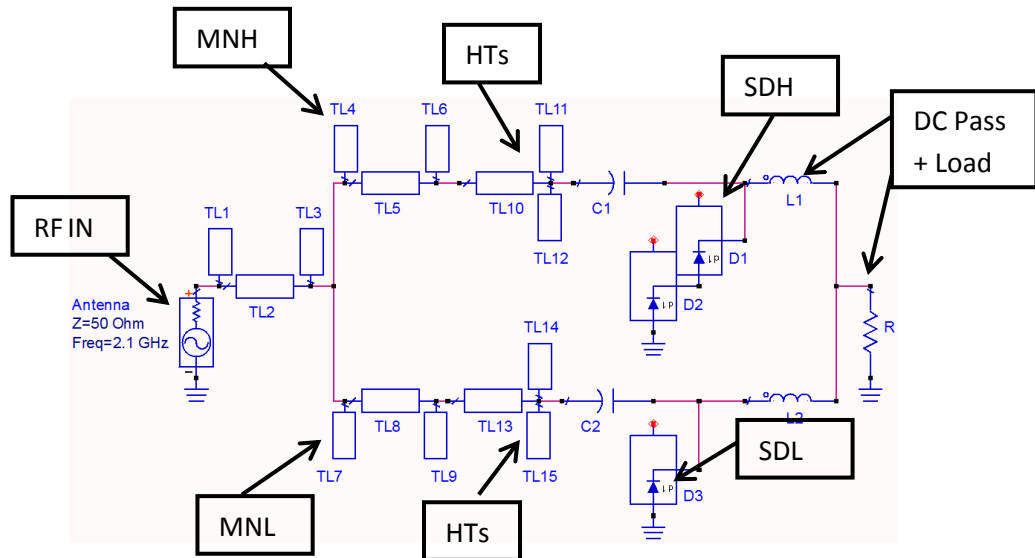


Figure 43. Schematic of the rectifier proposed in method I

As can be observed in figure 43, two series (HSMS-2860) [42] low-barrier diodes are used for (SDH) whereas a single zero-bias (HSMS-2850) [43] diode is used for (SDL). The reason for using a series diode combination for (SDH) is to increase the overall breakdown potential and to have more control over the impedance of the upper branch. This is because single HSMS-2860 and HSMS-2850 diodes have close reactive impedance values due to their same zero-bias junction capacitance. The simulation results are shown in figures 44 and 45.

As can be inferred from figure 44, the rectifier is matched over the power range extending from -12 to around 7dBm with the reflection coefficient being less than -10dB.

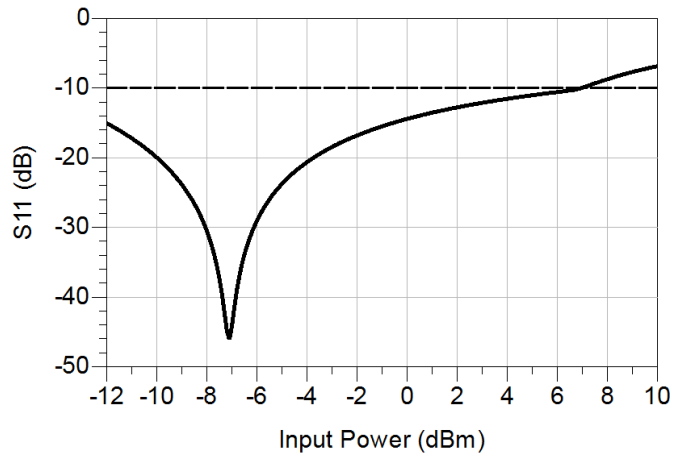


Figure 44. Input reflection coefficient of the rectifier in method I

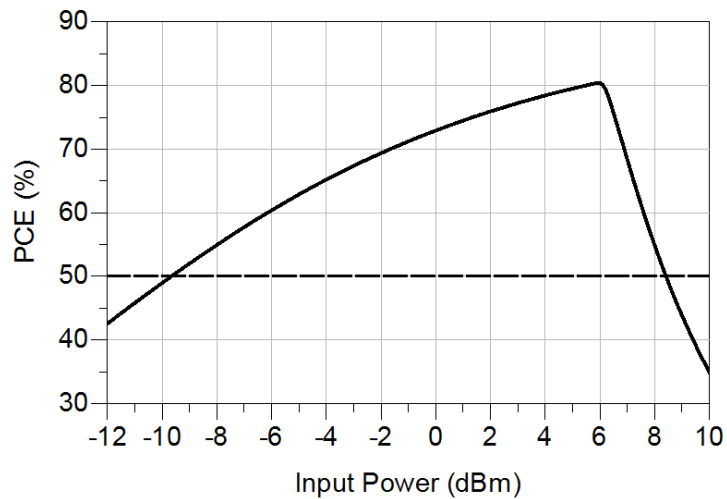


Figure 45. PCE curve of the rectifier in method I

From figure 45, it is clear that the rectifier has PCE values greater than 50% over the -10dBm-8.5dBm power span . A peak efficiency of 81% is achieved for an input power level of 6dBm.

While the rectifier proposed in this method achieved acceptable PCE results, the simulations later appeared to be unrealistic due to the following reasons:

1. The lumped elements (L1, C1, L2, C2) used for DC blocking and RF chocking are ideal. Without accurate models of these components the efficiency results cannot be trusted. This is due to the fact that those

elements incur additional losses, which definitely affect the efficiency values

2. Using diode combinations might cause considerable differences between measured and simulated results. As previously stated, series diodes must be used for the high power branch in order to have more control over the input impedances of the branches. This could have been alternatively done using parallel HSMS-2850 diodes on the low power branch and a single HSMS-2860 diode on the high power one. However, based on DC measurements, it is found that ADS treats those diode combinations in a less accurate way than the practical case. For instance, ADS considers parallel identical junctions to have half series resistance. Nonetheless, practical measurements, performed over HSMS-2850 diode combinations, show that the series resistance decreases but it does not get halved

For these reasons, confidence was low in the simulation results and the design was not fabricated for testing. The experience learned from the errors in this design is then used to come up with a new method that would enhance the PCE range of a typical rectifier. In the new design, the following constraints are considered:

1. The design should be optimized while making use of single diode junctions. Series and parallel junctions should be avoided
2. Accurate models for the used lumped elements should be considered during the simulations. Ideal lumped components provided by the ADS library should be avoided in order to get realistic efficiency curves. Accordingly, ADS Murata library is used for all new designs. This library provides

realistic models of Murata inductors and capacitors for accurate simulation purposes

C. Method II – Splitting of the Input RF Power

In this part, an alternative method to expand the efficient power range of a typical rectifier is proposed. The method is based on the idea of splitting the input RF power between two identical rectifiers in order to delay the breakdown effect of the used diodes. This concept is illustrated in figure 46.

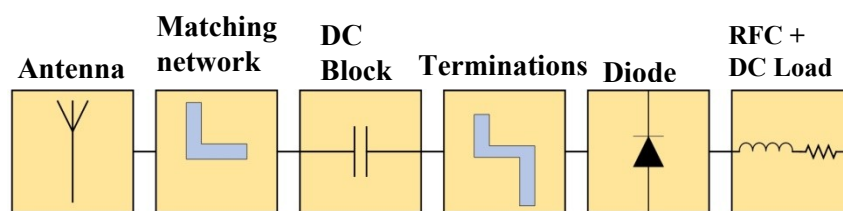


Figure 46. Block diagram of a single diode typical RF rectifier

Figure 46 shows a block diagram of a typical RF rectifier with a single shunt reverse-connected diode. The antenna is used to represent the source of RF input power. Practically however, it can also be replaced by an RF signal generator. The circuit consists of the following components:

1. Matching network: Responsible for converting the impedance of the diode to 50Ω which is that of the antenna/generator
2. DC block: This is a Murata capacitor used to prevent the DC power generated by the diode from returning back to the generator
3. Harmonic terminations: Used to lower the power dissipation within the diode and increase the PCE
4. RFC: Used to prevent the RF power from leaking into the resistive load

5. DC load: The resistance over which the DC voltage generated by the diode is collected. Its value plays a role in controlling the efficiency curve of the rectifier

Figure 47 shows a typical PCE curve for the rectifier of figure 46. At a certain input power level (P_L), the PCE reaches 50%. While increasing the input RF power, the PCE keeps increasing till breakdown is reached. At this point, due to the saturation in the output DC power, the PCE starts its rapid degradation till it reaches 50% again at a certain power level (P_H).

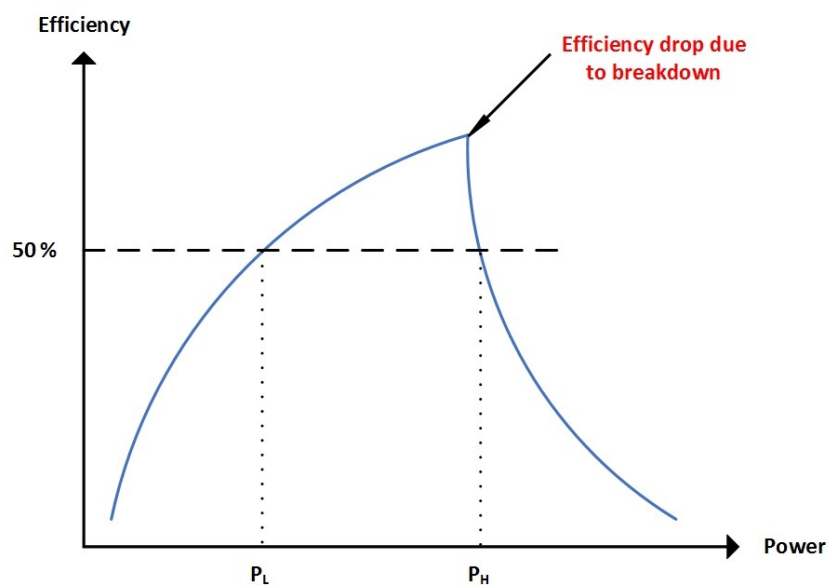


Figure 47. Typical PCE curve for a single diode rectifier

Now, what happens if two identical rectifiers such as the one described in figure 46 are used with the input RF power being equally split through a Wilkinson power divider? To answer this question figure 48 is used.

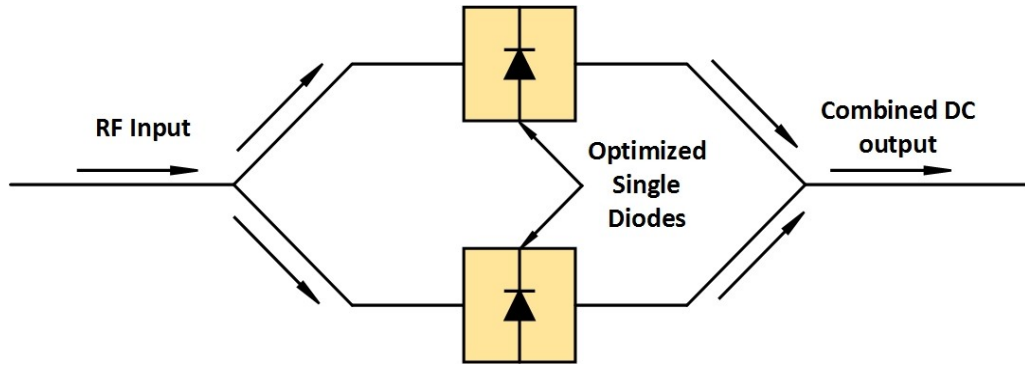


Figure 48. Splitting of input RF power between two identical rectifiers

Consider the input to the power divider to be in the range $(2P_L - 2P_H)$ where (P_L) and (P_H) are linear powers. In this case, upon equal splitting, each rectifier will be fed by RF power in the range $(P_L - P_H)$. Consider also that each rectifier has a PCE curve that is optimized as that shown in figure 47. Hence, for an input power of $2P_L$, each rectifier should theoretically produce DC power of $0.5*(P_L)$. Since both rectifiers are identical and are being fed by the same RF power due to the equal splitting, the output DC power should combine to give (P_L) . Hence, the overall efficiency for $(2P_L)$ input power is 50%. Similarly, for an input of $(2P_H)$, the overall PCE is 50%. Consequently, while a single diode rectifier had a 50% PCE range of $(P_H - P_L)$, the proposed rectifier has a theoretically doubled 50% PCE range of $(2P_H - 2P_L)$.

D. Summary

In this chapter, the aim was to come up with new methods that can be used to overcome the problem associated with the breakdown potential of commercial Schottky diodes. Since breakdown causes rapid degradation in the PCE, avoiding its occurrence leads to rectifiers that are capable of reliably operating with good efficiencies over wider power ranges. Two methods were discussed in this chapter. The first had a “reconfigurable” approach whereby the impedances of the diodes which vary with the

input RF power are used to control the flow of RF signals between two different rectifying circuits. Zero-bias diodes are used when low RF power is available. As this power increases, the RF signals are directed to another circuit with diodes having higher breakdown voltages. This method was tested using ADS and in conclusion its simulation results were found to be unrealistically good. The other method is more practical and easier to implement. The basic idea behind it is to split the input RF power between two optimized rectifiers in such a way that, on occasions when high power is fed into the circuit, breakdown can still be avoided and the PCE curve's degradation is delayed. In the next chapter, this method is more thoroughly tested by relying on ADS simulations and practical measurements.

CHAPTER VI

A 2.1GHZ RECTIFIER WITH ENHANCED OPERABLE POWER RANGE

A. Objectives

The steps involved in designing a rectifier for operation at 2.1GHz are outlined in this chapter. The aim is to implement method-II illustrated in chapter V in order to expand the power range over which efficient rectification is achieved. The chapter begins by the performed ADS simulations and presents the predicted results. Then, the fabricated rectifier is presented along with details about the conducted measurements. Measurement and simulation results are compared and conclusions are drawn about enhancements that can be added to the design.

B. ADS Simulations and Results

1. *Single Diode Rectifier*

This section starts by simulating the rectification characteristics of a single diode typical rectifier, which according to method II should be later connected to the output branches of a Wilkinson power divider. Figure 49 shows its ADS schematic. The substrate used is Roger's RO3203 with 3.02 dielectric constant, 0.5mm thickness and 0.0016 loss factor. The diode used for this design is SMS-7621 from Skyworks. The properties of this diode were previously presented in table 4. Its SPICE model that is provided by the manufacturer's datasheet is used to model its performance. The dimensions of the used transmission lines along with the electrical properties of the used lumped components are provided in table 5. All transmission lines (TL)s have 1mm width to achieve 50 Ω characteristic impedance.

Table 5. Dimensions and component values of the 2.1GHz single diode rectifier

Component	Dimensions/Values	Component	Dimensions/Values
TL1	10mm	TL9	3mm
TL2	19.3mm	TL10	45.2mm
TL3	2.6mm	TL11/TL12	3mm
TL4	1mm	V1/V2/V2/V3	1mm (W)/0.5mm(D)
TL5/TL6	7.4mm	L1,L2	470nH
TL7	11mm	C1	1 μ F
TL8	1mm	RL	300 Ω

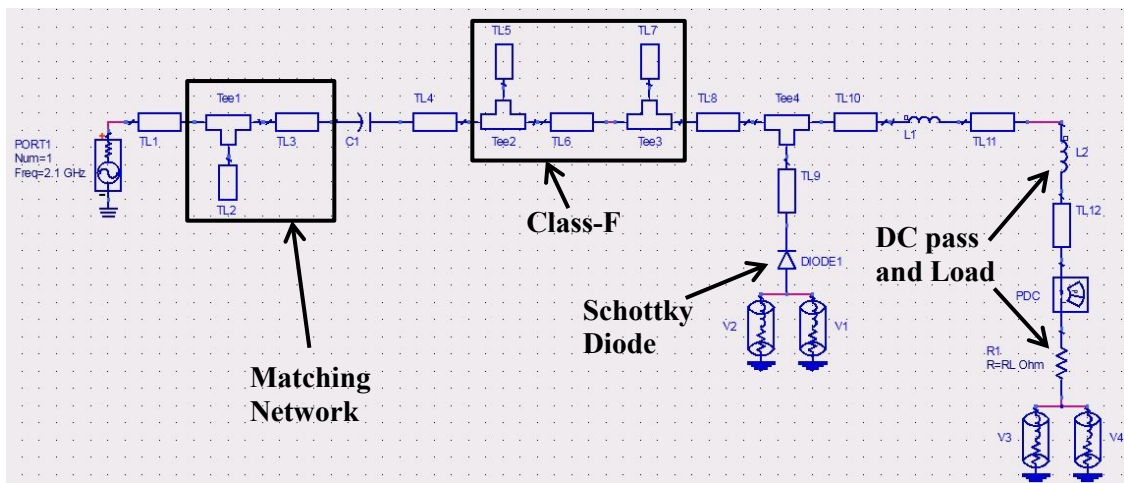


Figure 49. ADS schematic of the single diode 2.1GHz rectifier

The rectifier of figure 49 consists of the following components:

- TL1: Simulates the input feeding line to which an SMA connector is practically soldered
- TL2,TL3: These form the single stub matching network
- TL4: A 1mm line used as a soldering pad for the DC block capacitor
- C1: 1 μ F DC blocking capacitor from Murata

- TL5,TL6: Quarter wavelength (at 6.3GHz) transmission lines to suppress the third harmonic generated by the diode
- TL7: Quarter wavelength (at 4.2GHz) transmission line to suppress the second harmonic generated by the diode
- TL8: 1mm separation line between TL7 and TL9
- TL9: A line over which the diode is soldered
- TL10: Line over which the inductor is soldered
- TL11,TL12: Separation lines between the two inductors
- L1,L2: 470nH RF chokes from Murata
- R_L : A 300 Ω load whose value is chosen using ADS optimization techniques

As previously concluded in chapter IV, when fed by power at (2.1GHz), the diode generates harmonics at DC, 4.2GHz, 6.3GHz, etc... Allowing these harmonics to return to the generator, which is practically translated as re-radiation from the antenna and hence electromagnetic interference, causes the PCE to drop. This becomes more serious as the input RF power levels increase because the power levels of the second and third order harmonics keep increasing as previously illustrated. One way to avoid this efficiency drop is by using resonators to confine those harmonics across the diode. Referring back to figure 49, the combined effect of (TL5, TL6) is to provide an open circuit impedance to block off the third harmonic (6.3GHz). Hence, the power generated at this frequency is confined across the diode. Similarly, TL7 short-circuits the second harmonic (4.2GHz) in order to prevent the backflow of the power generated at this frequency. This type of harmonic terminations is known as Class-F [4] terminations. It is incorporated in order to reduce the overlap between the voltage and current waveforms across the diode. This would in turn reduce the power dissipation within the

diode and hence improve the PCE. Theoretically, class-F terminations are expected to alter the waveforms of the diode in such a way that the diode voltage becomes similar to a square wave, whereas the diode current becomes similar to a half sine signal. Other harmonic termination techniques can be used. However, it all depends on the circuit being designed and the underlying constraints. The simulation results of the rectifier in figure 49 are shown in figures 50 and 51.

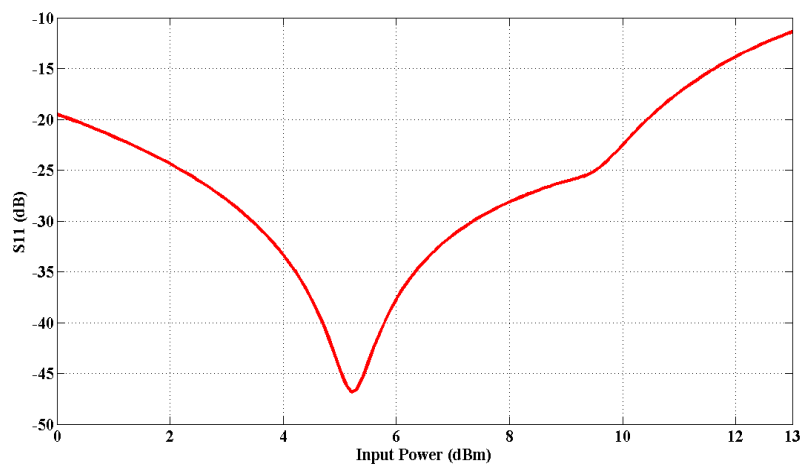


Figure 50. S_{11} of the 2.1GHz single diode rectifier

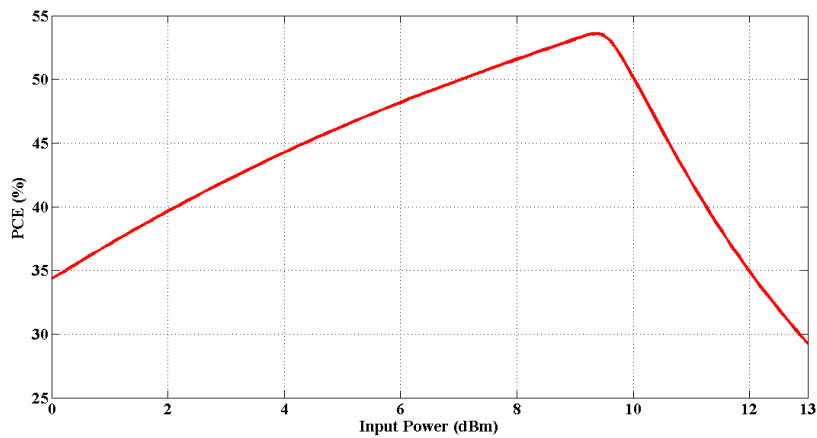


Figure 51. PCE of the 2.1GHz single diode rectifier

As can be observed in figure 50, the single diode rectifier is matched at 2.1GHz over the power range extending from 0 to 13dBm. On the other hand, figure 51 shows that the PCE of the circuit remains greater than 50% for the power range extending from 7dBm to 10dBm. Figure 52 shows that the expected theoretical waveforms across the diode due to the class-F harmonic terminations have been achieved. The voltage waveform has a shape similar to a square wave whereas the current waveform becomes similar to a half-sine wave. These waveforms were simulated for an input power level of 0dBm.

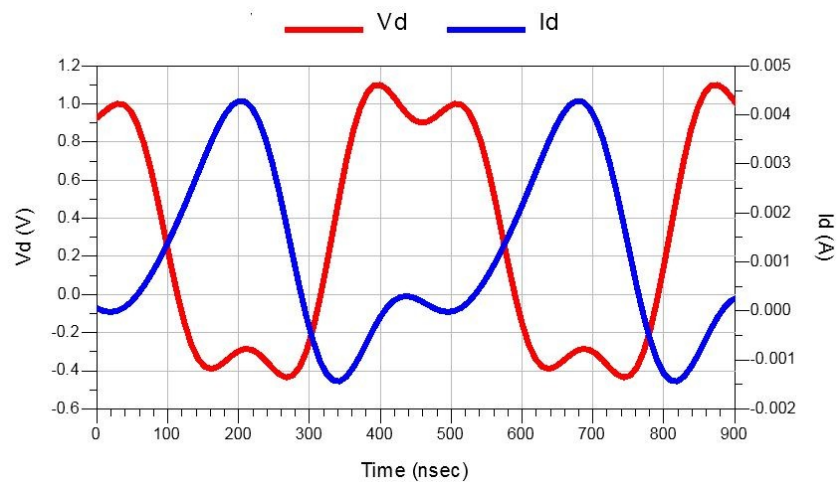


Figure 52. Diode voltage and current waveforms for the rectifier in figure 49

2. *Design of the Wilkinson Power Divider*

Figure 53 shows the design of a typical equal split Wilkinson power divider. The two branches of the divider have a length of $(\lambda_g/4)$ at the frequency of 2.1GHz. The output branches of the divider are matched to 50Ω impedance. The simulated S-parameters of the designed power divider are shown in figure 54.

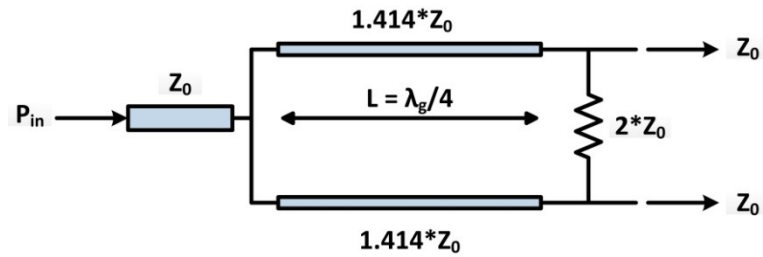


Figure 53. Design of an equal split Wilkinson power divider

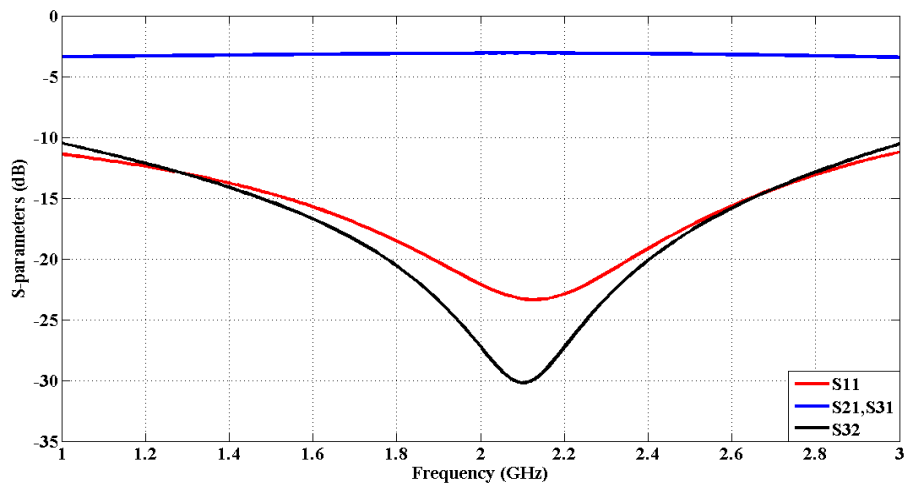


Figure 54. S-parameters of the 2.1GHz Wilkinson power divider

As shown in figure 54, the designed power divider is well matched at the input at 2.1GHz, and power gets equally split between its branches as shown by the S_{21} and S_{31} values which correspond to -3dB at 2.1GHz. In addition, due to the 100Ω resistance inserted between both branches, the output ports are well isolated as shown by the S_{32} curve.

3. *The Complete Rectifier*

Two replicas of the single diode rectifier shown in figure 49 are connected to the output branches of the previously designed Wilkinson power divider. The complete circuit is tuned in terms of impedance matching and optimized in terms of the output

resistive load to achieve the best possible PCE curve. A 150Ω load, whose value is half the one used in the single diode rectifier, is found to give optimal efficiency values. The layout of the complete design is shown in figure 55. The achieved S_{11} and PCE simulation results are given in figures 56 and 57 respectively.

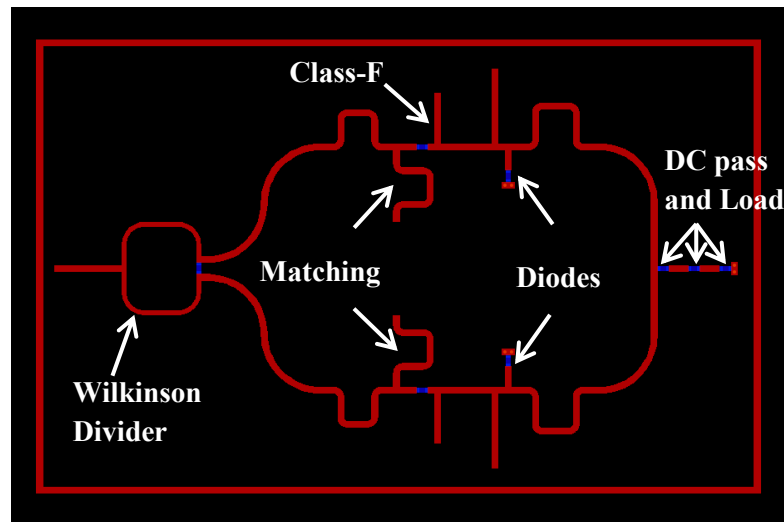


Figure 55. Layout of the complete proposed 2.1GHz rectifier

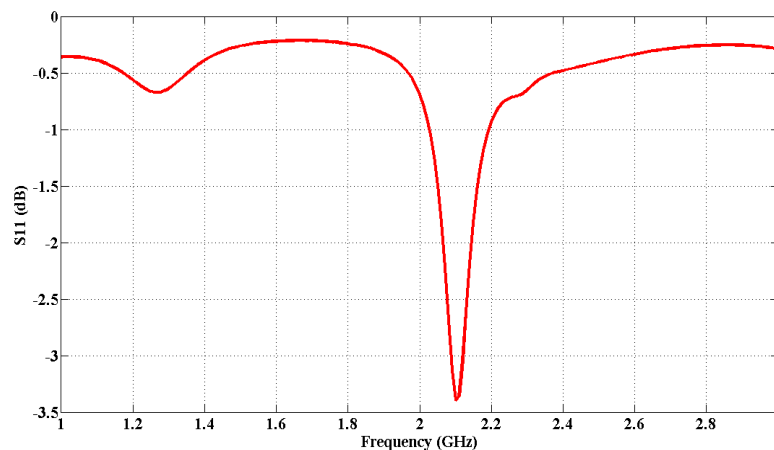


Figure 56. Reflection coefficient of the complete 2.1GHz rectifier at -15dBm

As observed in figure 56, the simulated reflection coefficient curve has a minimum S_{11} value at 2.1GHz which is the design frequency. S_{11} is greater than -10dB

due to the low input power (-15dBm) at which the simulations are performed. At this power level, the impedance of the diode is highly reactive causing mismatch to take place.

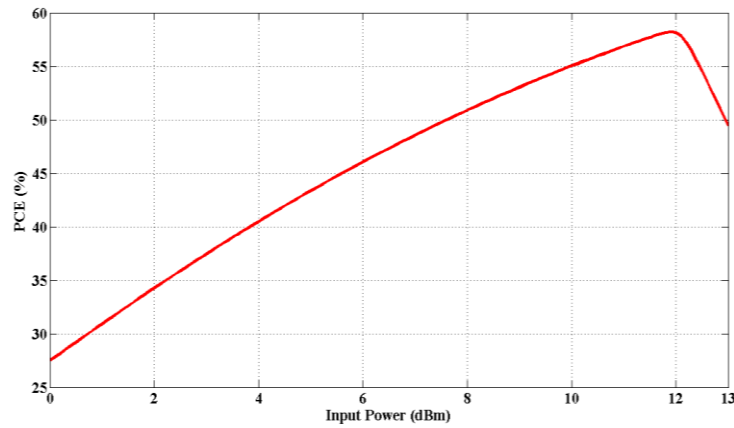


Figure 57. PCE of the complete 2.1GHz rectifier

As shown in figure 57, the efficiency remains greater than 50% over the power range extending from 7.5dBm to 13 dBm. The PCE curves of the single diode rectifier and that of the complete one are given in figure 58 using a linear power scale for better visualization of the improvement.

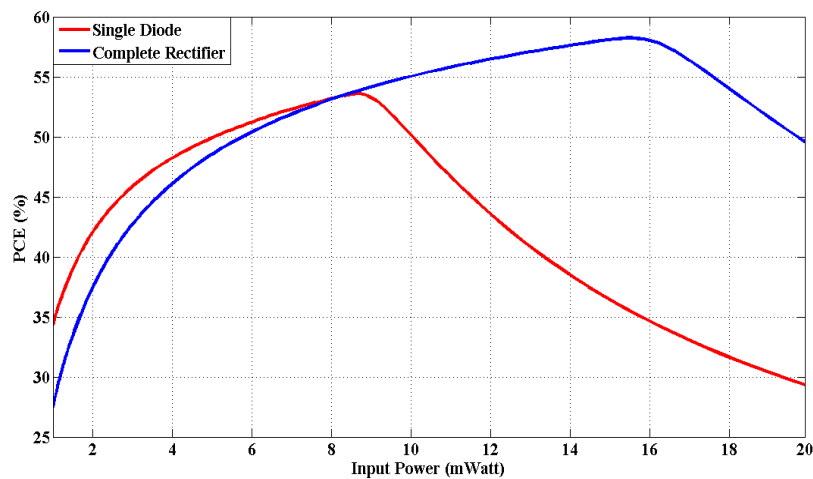


Figure 58. Achieved enhancement over the efficient rectification power range

From figure 58, it can be concluded from the simulations that the proposed 2.1GHz rectifier has a wider efficient power range as compared to that of the single diode circuit. While the latter can efficiently convert RF energy to DC over the power range extending from 5 to 10mWatt, the former can operate efficiently from 6 to 20mWatt which shows more than two times improvement in the efficient power range. In figure 59, the simulated output DC voltage increases with input RF power till it reaches a maximum value of 1.2V.

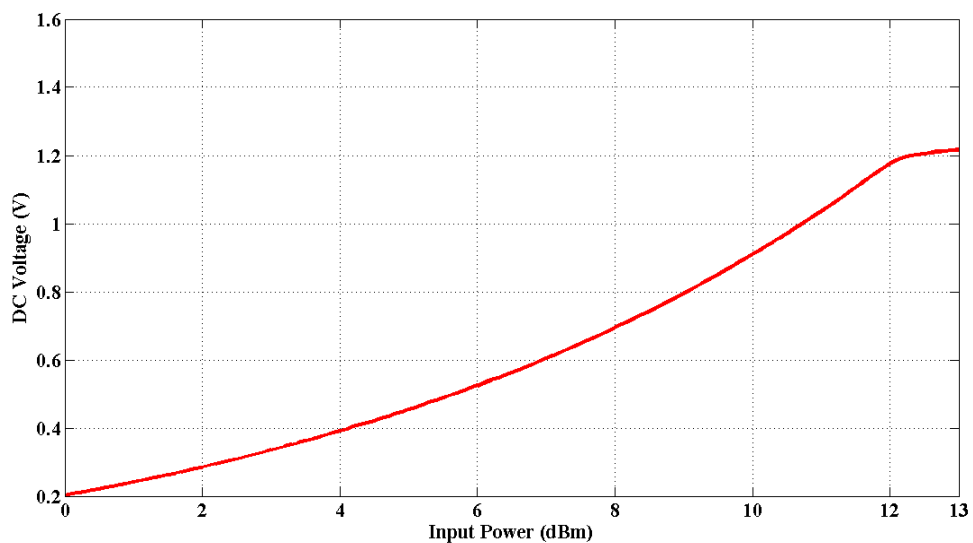


Figure 59. Simulated output DC voltage from the proposed 2.1GHz rectifier

C. Fabrication and Measurement

The layout of figure 55 is fabricated and measurements are conducted to compare its performance with the results attained from ADS simulations. In figure 60, the fabricated rectifier is shown. A power amplifier was used to conduct the measurements in order to feed the rectifier with the necessary amount of RF power. This is mainly because the RF signal generator in the laboratory had a maximum output power level of 14dBm. Due to discrepancies between the measured and simulated

results, it was found that input power greater than 14dBm was required to accurately characterize the circuit's behavior.

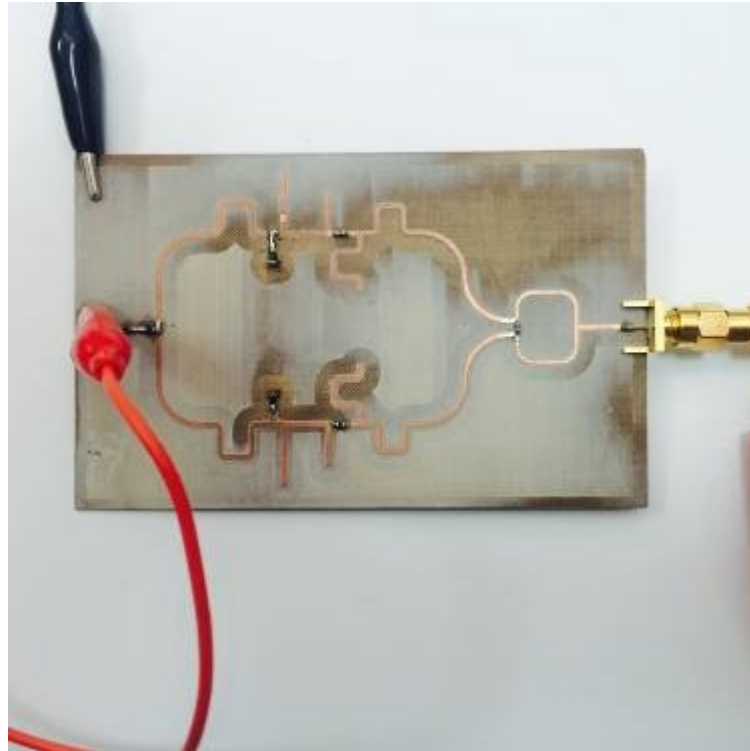


Figure 60. Fabricated 2.1GHz rectifier

For measurement purposes, the following devices are used:

- Agilent E8257D: Analog signal generator capable of generating RF power up to 20GHz frequency and 14dBm power. It has a 50 Ω output port
- Agilent E5071B: Vector network analyzer with operational frequency up to 8.5GHz. It is used to measure the S-parameters of the circuit. Its output port is matched to 50 Ω
- Agilent N1912A: RF power meter and sensor. It is capable of accurately measuring RF power levels up to 23dBm till 18GHz. It is matched to 50 Ω impedance

- Agilent E3631A: DC power source which supplies variable DC voltage up to 25V and has a fixed 6V DC source. It also has a current limit control that allows better protection in case of short circuits. It is used to provide the DC bias required for the power amplifier
- ZXP-3011: RF amplifier from mini-circuits. It is operable at 2.1GHz and has a gain of around 10dB. It has an output 1dB compression point of typically 21dBm

As shown in figure 61, the power amplifier draws 74mA current at 12V DC. It feeds the rectifier whose DC output voltage across the 150 Ω load resistance is measured via the voltmeter. In figure 62, an output DC voltage of 2.91V is revealed at the 150 Ω DC load when 10dBm power from the generator (20dBm after amplification) is supplied to the rectifier.

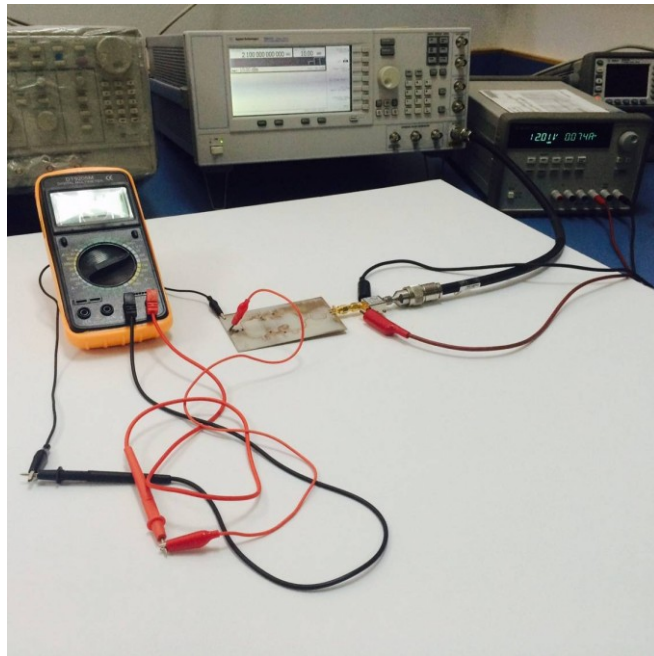


Figure 61. Measurement setup for characterizing the 2.1GHz rectifier

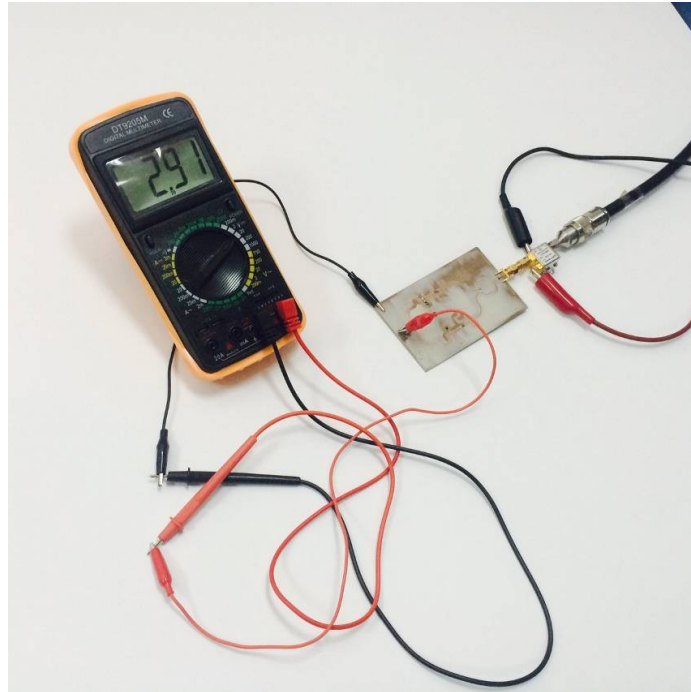


Figure 62. DC voltage (2.91V) measured from the rectifier at 20dBm input power

Figure 63 shows an LED lit through the DC voltage produced by the rectifier. Because the LED has practically a high resistance, connecting it in parallel to the 150Ω load should produce a slight loading effect. When fully on (brightest light) the output DC voltage at 20dBm input reduces from 2.91V to 1.95V.

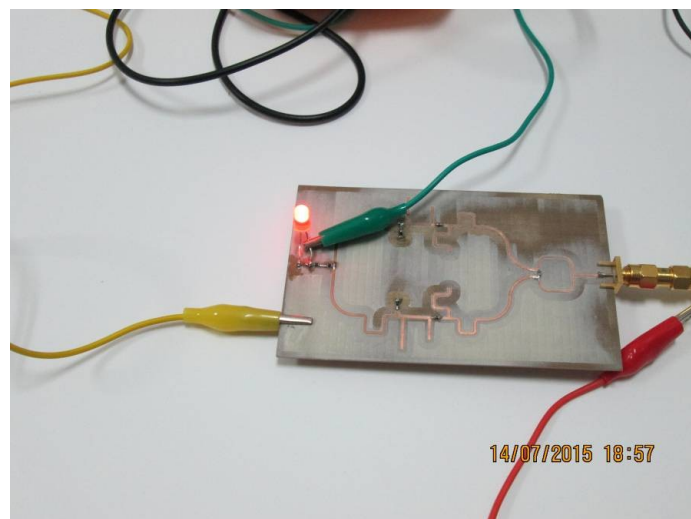


Figure 63. Lighting an LED using the output DC voltage by the 2.1GHz rectifier

This is enough to keep the LED on; however the decrease in DC output voltage means that the overall DC resistance at the output has decreased below 150Ω due to the connection of the LED. This effect is shown in figure 64.

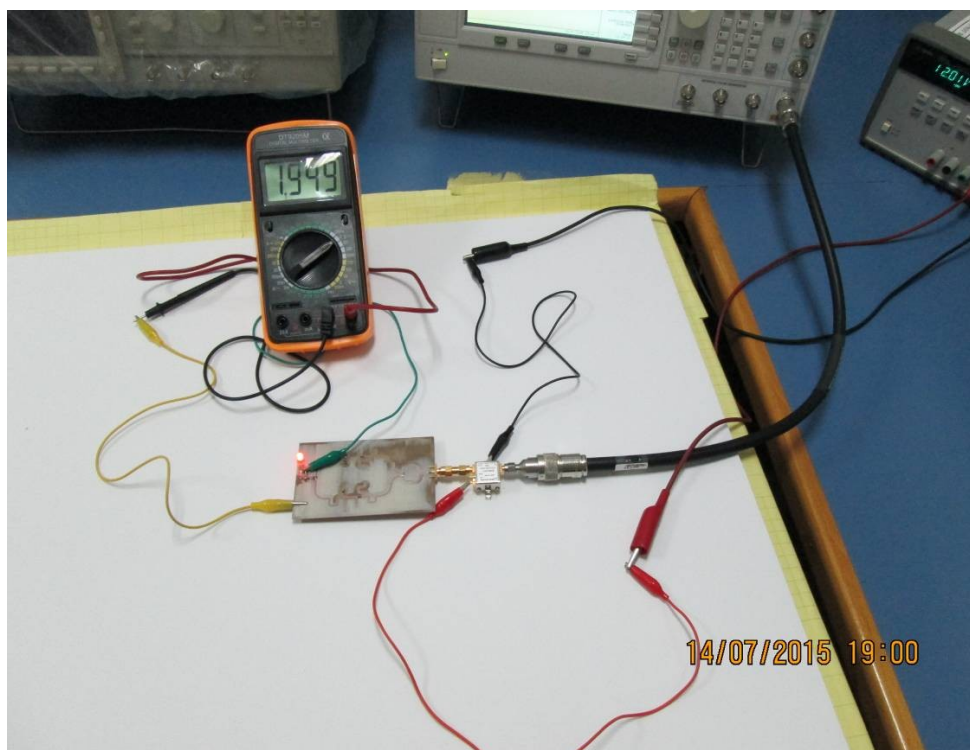


Figure 64. Reduction of the output DC voltage due to the connection of the LED

Figure 65 shows a comparison between the measured and simulated reflection coefficients of the 2.1GHz rectifier. As can be observed, both curves overlap with their minimal point being at 2.1GHz, the design frequency. Again, mismatch exists since the data are taken at low RF power where the diodes' impedances are highly reactive.

In figure 66, good agreement between the measured and simulated DC voltage exists. However, this match between both results is obtained after slightly tuning the SPICE model of the used diodes [24], [39]. This is the main cause of the small differences that exist between simulations and measurements especially near the

breakdown voltage. Upon tuning the SPICE model, the simulated and measured efficiency curves are superposed as shown in figure 67.

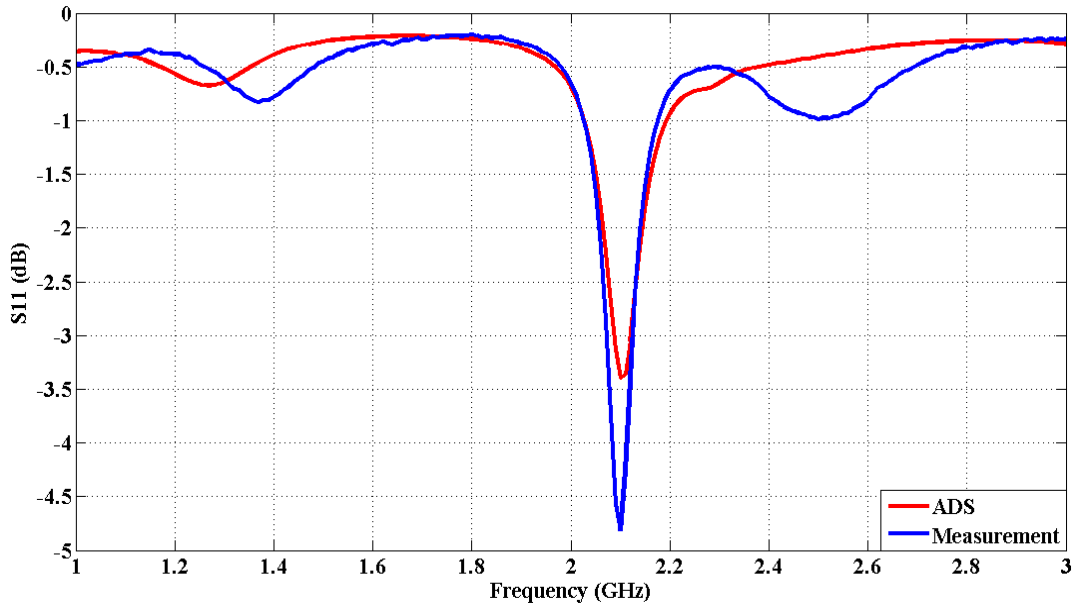


Figure 65. Reflection coefficient of the 2.1GHz rectifier at -15dBm

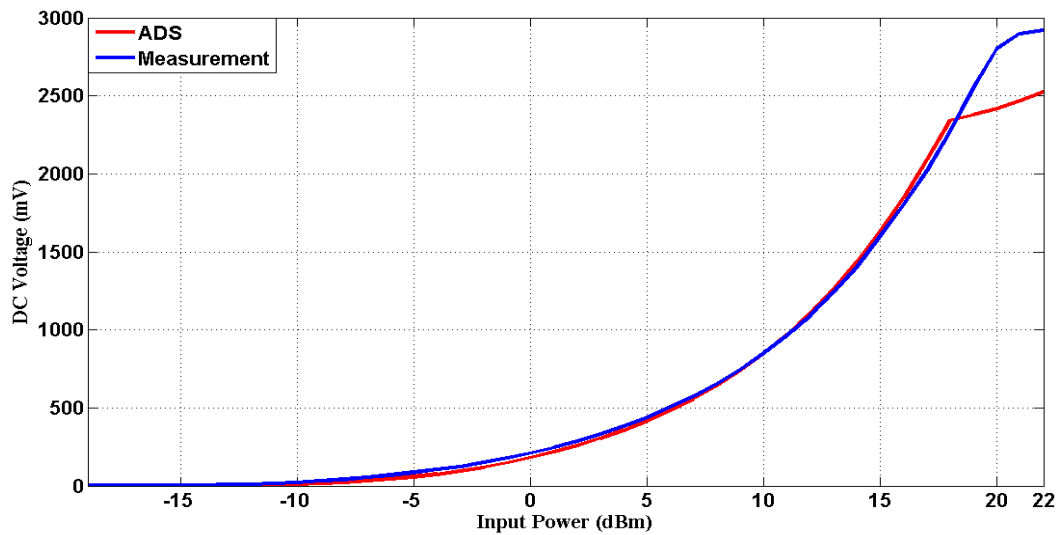


Figure 66. Measured output DC voltage of the 2.1GHz rectifier

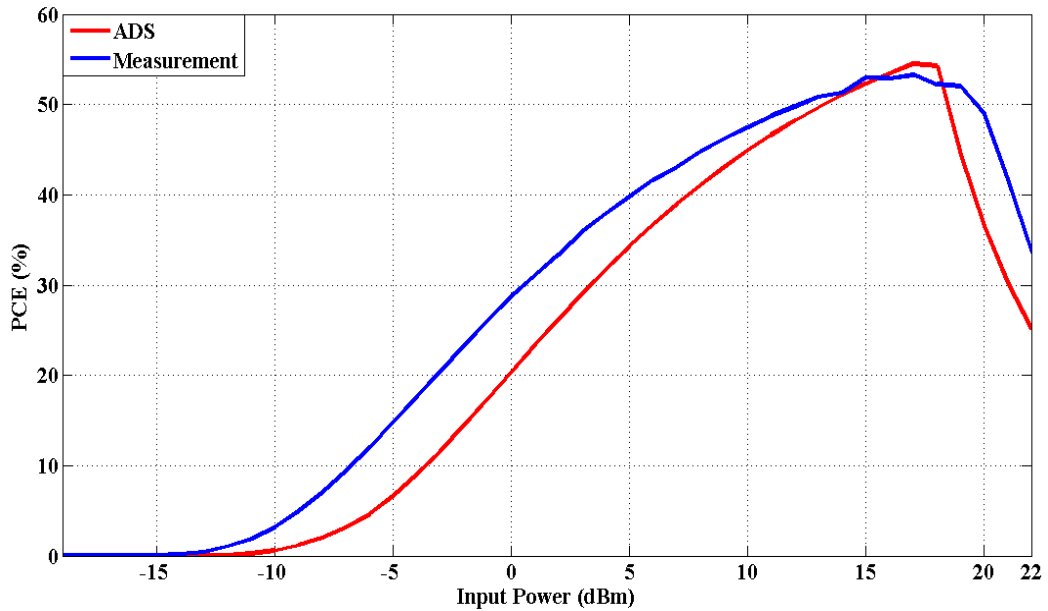


Figure 67. Measured PCE of the 2.1GHz rectifier

As can be observed in figure 67, the PCE is measured to be above 50% for the input power range of 12dBm to around 20dBm (15.8 to 100mWatt). Since such power levels are rarely available as far as ambient RF power harvesting is concerned, a new rectifier has to be designed that takes into consideration this practical constraint. For this reason, changes over the 2.1GHz rectifier should target the used diodes as well as the structure of the circuit in such a way that better efficiency can be obtained at lower power levels.

D. Summary

In this chapter, a 2.1GHz rectifier was designed, simulated and fabricated. Its measured results showed that it is capable of efficiently rectifying RF waves over a wide range of input powers. However, since its efficient operation is biased towards relatively high power levels (in comparison with those usually available under ambient conditions), further modifications need to be done in such a way that a new design with

improved breakdown performance and better efficiency values at low power levels is realized. In the next chapter, another rectifier is designed with the aim of achieving those objectives.

CHAPTER VII

A 2.4GHZ RECTIFIER WITH ENHANCED OPERABLE POWER RANGE

A. Objectives

The aim of this chapter is to design a new circuit for operation at 2.4GHz. The concept of input power splitting is used to improve its breakdown properties. In this case however, the efficiency curve needs to be “biased” towards lower power levels as compared to those over which acceptable performance was achieved before. In the next section the design is presented along with ADS simulations and predicted performance. This is followed by the details of the results obtained from measurements conducted over the fabricated prototype. The chapter is concluded with a summary of the achieved improvements along with a round-up of the lessons learned from debugging the circuit.

B. Rectifier Design

In the previous chapter, the designed rectifier used SMS-7621 low barrier diodes. This yields efficiency values that are generally too low at low power levels (< 30% at 0dBm for example). In this design, zero-bias detectors are used instead to achieve better efficiencies at such low powers. This decision is consistent with the results of the theoretical analysis carried out in chapter IV from which it was concluded that lower built-in potential values lead to higher output DC voltages at lower input power levels and over the same DC load . SMS-7630 diodes from Skyworks are used in this case. Their electrical parameters are listed in table 4. In addition, an unequal split Wilkinson power divider is designed for the aim of achieving better efficiency results at low power levels, while still making use of the power splitting advantage.

C. ADS Simulations and Results

1. Unequal Split Wilkinson Power Divider

The design of the unequal split Wilkinson divider is influenced by the following factors:

1. The required splitting ratio
2. The characteristic impedances of the branches

In figure 68, it is clear that the output branches of the power divider now have different characteristic impedances. The equations required to design such a divider with a predetermined power splitting ratio are given below [25].

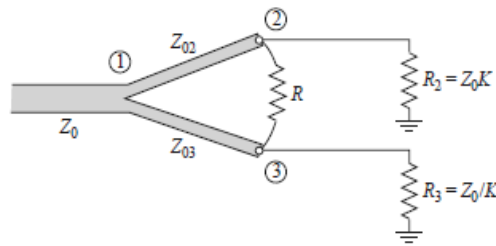


Figure 68. Schematic of an unequal split Wilkinson divider

$$K^2 = \frac{P_3}{P_2} \quad (21)$$

$$Z_{03} = Z_0 \sqrt{\frac{1+K^2}{K^3}} \quad (22)$$

$$Z_{02} = Z_0 \sqrt{K(1+K^2)} \quad (23)$$

$$R = Z_0 \left(K + \frac{1}{K} \right) \quad (24)$$

In the above equations, (K) denotes the ratio of the power split. (P₂) and (P₃) denote the output powers from the upper and lower branches respectively. For a better understanding, the output powers from ports 2 and 3 can be written in terms of the input power (at port 1) as follows:

$$\boxed{\frac{P_2}{P_1} = \frac{1}{1+K^2}} \quad (25)$$

$$\boxed{\frac{P_3}{P_1} = \frac{K^2}{1+K^2}} \quad (26)$$

By varying (K), it is possible to write a MATLAB code which allows the choice of a suitable splitting ratio with Z₀ taken to be 50Ω. In figure 69, as (K) approaches unity, less percentage of the input power flows into port 2. This is vice versa with respect to the power at port 3 which increases with (K). For (K=1), each port receives half of the input power, which denotes the operation of an equal split divider.

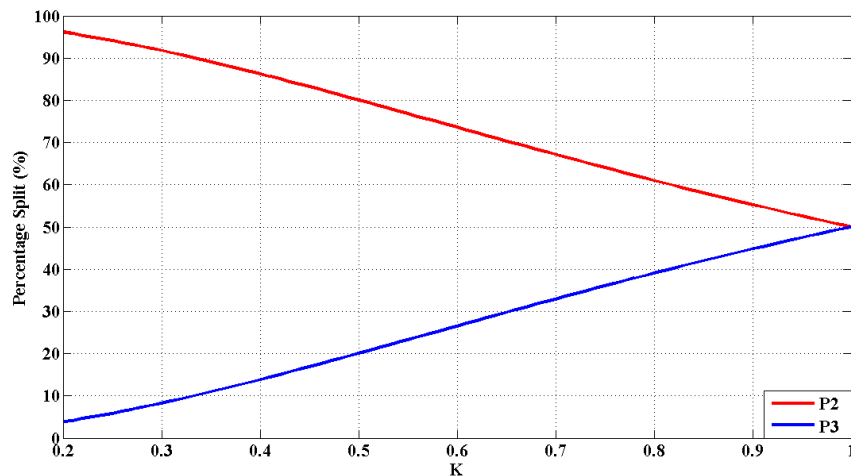


Figure 69. Splitting of input power (P₁) between ports 2 and 3

In figure 70, (Z_{03}) of the lower branch is too high for (K) < 0.55. For the substrate used (RO3202), the width of the lower branch would have to be below 0.1mm to achieve such ratios. Hence, the choice of (K) is limited to values greater than 0.55. For $K=0.8$, 60% of the input RF power is fed into the upper branch whereas the remaining 40% is fed to the lower one. This is a good splitting ratio which allows the investigation of how the efficiency of the rectifier improves. For this value of (K), (Z_{03}) is around 90Ω which is realizable and corresponds to a width of 0.4mm. From figures 71 and 72, it can be concluded that for $K = 0.8$, the isolation resistance should be $\approx 102\Omega$, whereas the output resistances of ports 2 and 3 are 40Ω and 62.5Ω respectively.

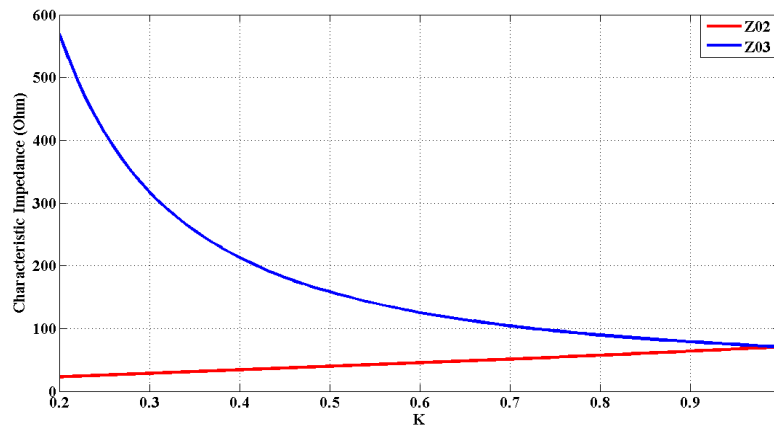


Figure 70. Characteristic impedances of the upper and lower lines

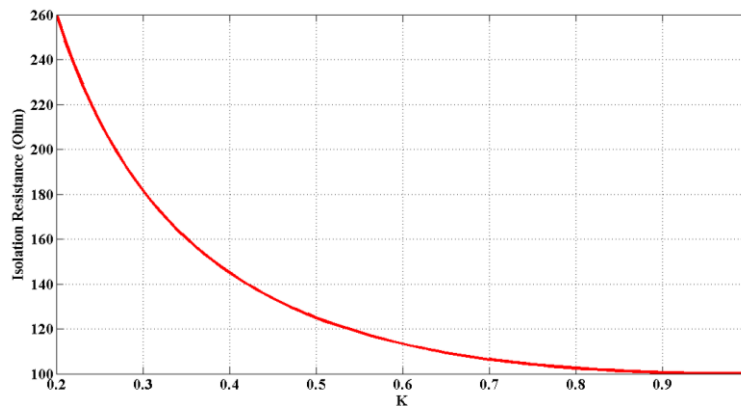


Figure 71. Isolation resistance as a function of (K)

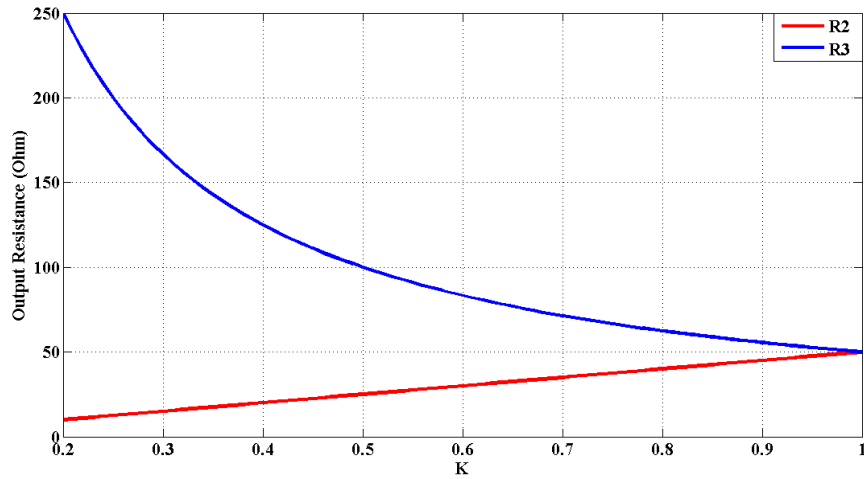


Figure 72. Output resistance as a function of (K)

2. *The Complete Rectifier*

Based on the above analysis, the Wilkinson power divider is designed and optimized using ADS. Each output branch is connected to a rectifier which has two SMS-7630 diodes connected in a parallel configuration. The final layout is shown in figure 73.

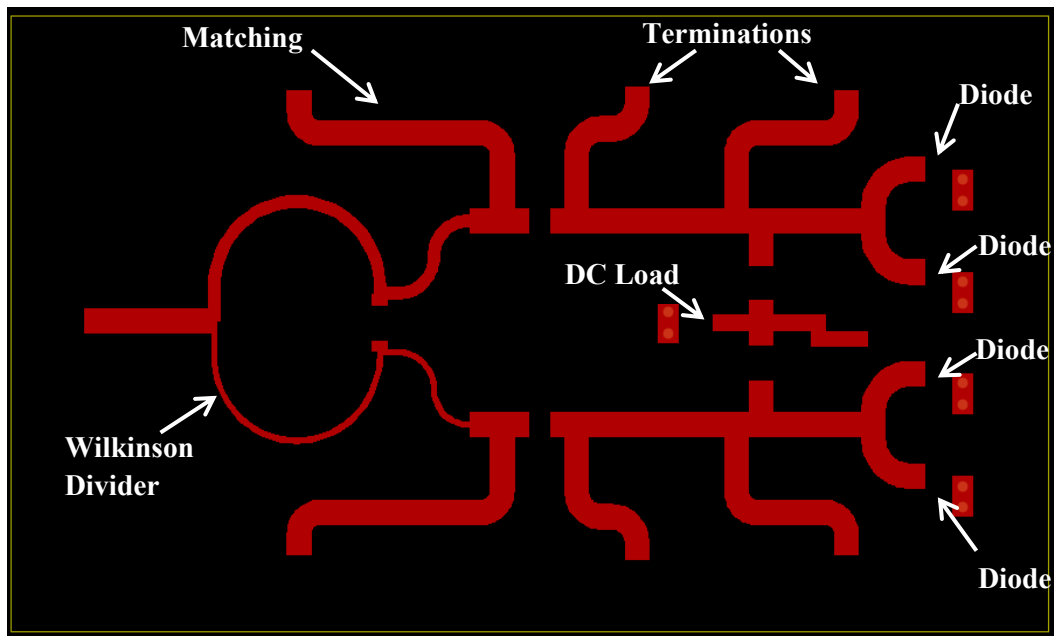


Figure 73. Layout of the designed 2.4GHz rectifier

From figure 73, it can be inferred that the design uses class-F harmonic terminations as the case of the previous 2.1GHz circuit. The matching network in this case uses a series 5.4pF capacitor which acts as a DC block as well to prevent the DC power from finding a path back to the RF generator. In figure 73, four diodes are used, with two connected in parallel per branch. The decision to use such a configuration is explained below.

In chapter IV an equation was derived for the output DC power generated by the shunt diode over a 50Ω load. By solving this equation for an input power range of 0 to 10dBm while using a series resistance of $R_{S1} = 20\Omega$ (that of SMS-7630) and $R_{S2}=10\Omega$ (to simulate parallel junctions), the curves of figure 74 were obtained. It is clear that the effect of lowering the series resistance should theoretically lead to better efficiencies due to the increase in the generated DC power. This is reasonable, since a lower resistance means lower Ohmic losses.

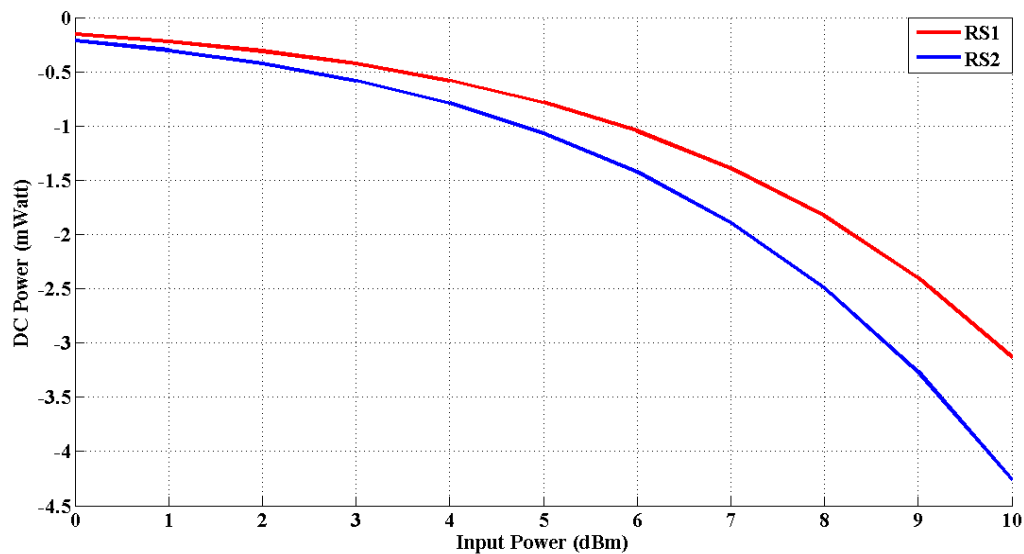


Figure 74. DC power generated over a 50Ω load for 20Ω and 10Ω series resistances

D. Fabrication and Measurement

The fabricated circuit (before soldering any components) is shown in figure 75. In addition, figures 76 and 77 show a comparison between the measured and simulated DC output voltage and PCE curves of the rectifier for a 150Ω load.

Although in figure 76, the results appear to be close, the PCE curves in figure 77 appear to have some mismatch. For instance, at 10dBm, the measured DC voltage is 871mV, whereas the simulated one is 960mV. This 9.3% error in voltage is almost doubled in the efficiency measurement where it becomes 18%. This illustrates the difficulty that one has to deal with when optimizing a rectifier's performance at low powers. Any loss in DC voltage can greatly degrade the efficiency of the circuit.

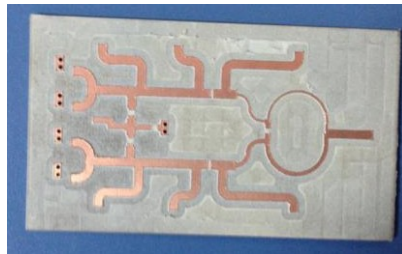


Figure 75. Fabricated 2.4GHz rectifier with unequal split Wilkinson divider

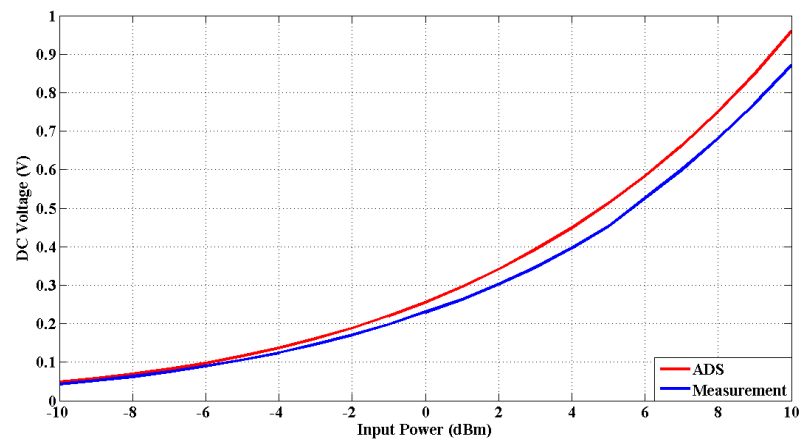


Figure 76. Simulated versus measured output DC voltage

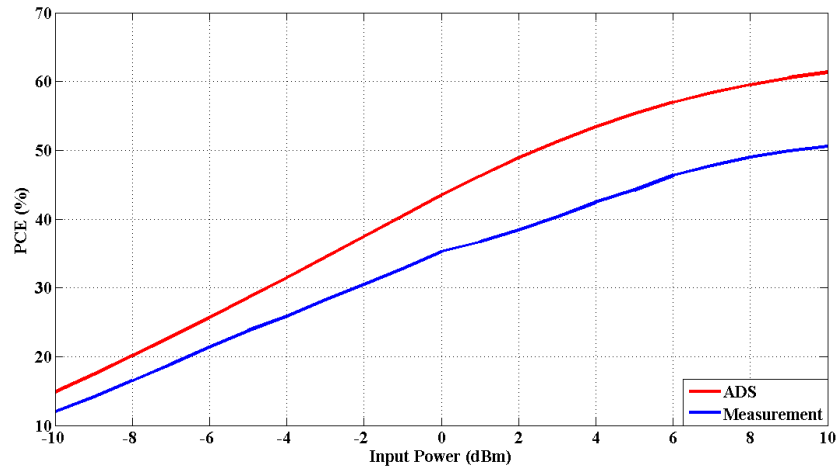


Figure 77. Simulated versus measured PCE

E. Debugging the Circuit

Although the rectifier's measured results are not highly matched with the simulated ones, its performance is better than that of the 2.1GHz rectifier.

The PCE at relatively low powers has been improved. Although SMS-7630 diodes have a low breakdown voltage, the circuit is capable of efficiently rectifying RF signals in the excess of 10dBm. As for the sources of error they are listed below.

1. Assumption of halved series resistance

While theoretically parallel diodes should have a halved series resistance, practically this doesn't turn out to be the case. In fact, the SPICE model of the diode has the drawback of not considering accurate bias-dependent models for (R_S). This is further ensured through DC measurements.

As can be inferred from figure 78, the SPICE model treats parallel junctions as an equivalent single diode having a halved internal resistance. This is why for the same applied DC voltage the forward current is doubled in the case of parallel junctions.

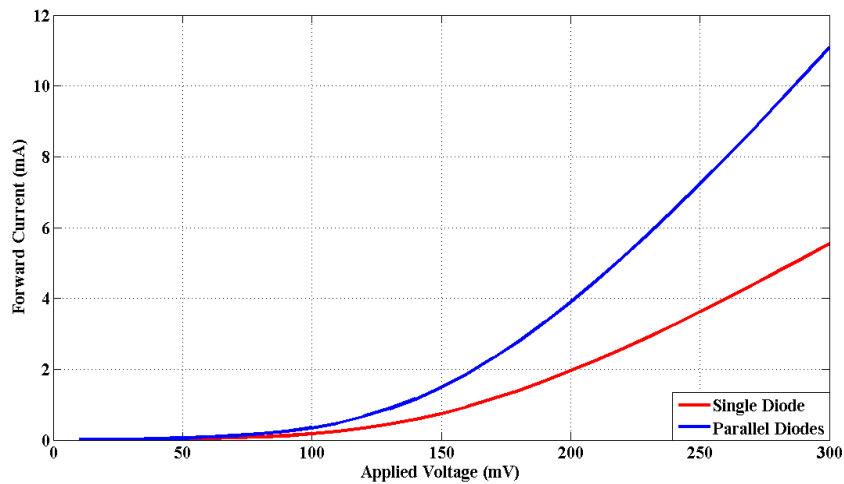


Figure 78. Simulated forward current through single and parallel SMS-7630 diodes

The curves in figure 79 show the discrepancies between the SPICE model and the actual behavior of the junctions. The diodes are first measured at 100mV DC voltage and the results of the forward DC current are compared with those given by the datasheet. After making sure that the results are consistent, the DC voltage is varied in steps of 10mV from 10 to 300mV. While the measured forward DC current increases over all DC voltages in the case of the parallel diodes, its value is not doubled. For low DC voltages, the current in the parallel diodes is greater than that in the single diode by a factor of 2. However, as the DC biasing rises, this factor decreases where it reaches a measured value of around 1.2 at 300mV. Hence, it is concluded that the SPICE model during the simulations exaggerated the effect of the parallel junctions. Due to the assumed 50% drop in the series resistance, the simulated PCE is better than the measured one.

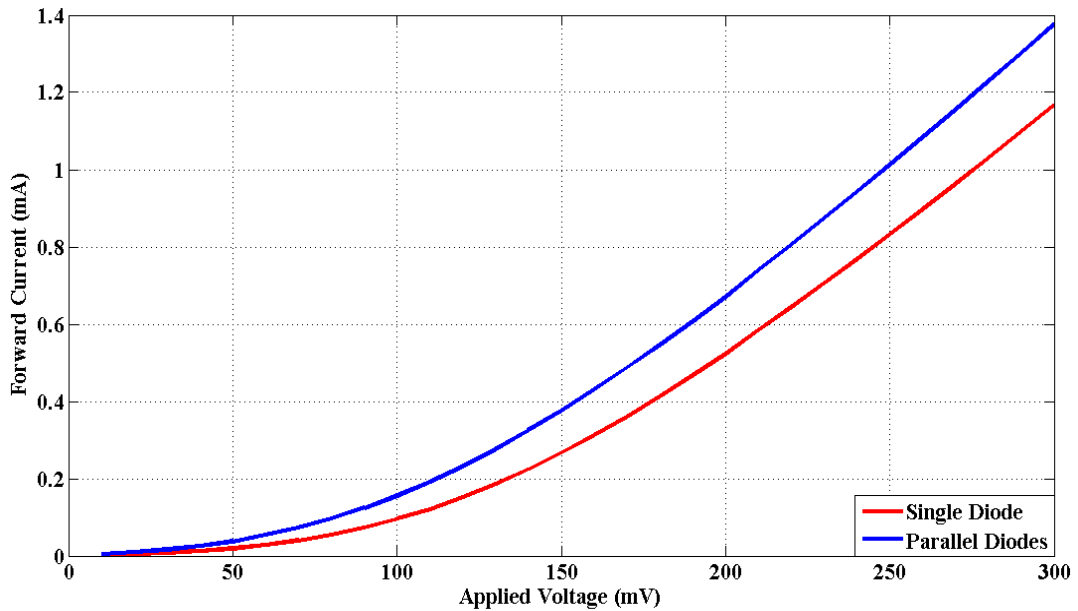


Figure 79. Measured forward current through single and parallel SMS-7630 diodes

2. *Other error sources*

Other error sources include the usage of capacitors as part of the matching network. Since capacitors get affected by many factors including temperature and aging effects, their values provided by the manufacturer are not necessarily precise. In addition, using capacitors in the matching network makes the operation of the circuit sensitive to small variations in the capacitance values. In addition, the RF chokes which are meant to provide open circuit impedance to the RF power coming from the source or generated by the diode are connected to small transmission lines for soldering. However, these 1.5mm lines worsened the RF choking performance. The reason why those lines are shortened as compared to the previous circuit (in which they are chosen to be half-wave length at the fundamental frequency) was to gain more compactness.

F. Summary

In this chapter, a 2.4GHz rectifier was designed using ADS. New ideas were tested with the aim of improving the PCE. The main objective was to check the suitability of combining zero-bias diodes in parallel with the aim of reducing their series resistance to decrease power losses and hence improve the efficiency. Breakdown improvement was done using an unequal split Wilkinson power divider with the aim of further enhancing the efficiency when the input power is low. DC measurements performed over single and parallel diodes showed that the SPICE model halves the series resistance of parallel junctions whereas practical measurements proved that this is only true under small DC biasing conditions. In other words, the series resistance changes with the applied bias and assuming that it is halved is inaccurate. Finally, aiming at achieving circuit compactness should not be accomplished by sacrificing crucial properties of the rectifier. In this circuit, compactness was at the expense of worse RF choking at the DC load. These results are used in the next chapter to design another rectifier with better performance as compared to the one introduced here. Specifically, the aim is to further enhance the efficiency at low power levels while still overcoming the problem of diode breakdown.

CHAPTER VIII

A 1.84GHZ RECTIFIER WITH ENHANCED OPERABLE POWER RANGE

A. Objectives

In this chapter, a 1.84GHz rectifier is designed using ADS by following the same procedure illustrated previously. The aim is to achieve better efficiency values at lower power levels (compared to those of the previous two circuits) while at the same time making use of the power division concept to enhance the power range over which efficient rectification can take place. Again, it should be noted that aiming for better efficiency values at lower powers is a challenging task. This is because the lower the input power, the worse are the effects that factors such as impedance mismatch and incurred losses have over the PCE. For this reason several modifications were carried out and are illustrated in the next section.

B. The Rectifier's Modified Design

Since the 2.1GHz rectifier gave the closest results as compared to the simulated ones by ADS, the rectifier studied in this chapter followed the same structure with some modifications. Apart from the frequency, which in this case is 1.84GHz, the following changes took place with respect to the 2.1GHz circuit:

1. The SMS-7621 low barrier diodes were replaced by SMS-7630 zero-bias ones. The lower built-in potential of these diodes allows them to generate more DC power at low RF levels. Their main disadvantage is their lower breakdown potential. However, splitting of the input RF power should theoretically limit this side effect

2. Class-F terminations were removed and replaced by a different configuration of harmonic terminations
3. The 50Ω transmission lines used to connect the output ports of the Wilkinson power divider to the inputs of the rectifiers were shortened down after being exaggerated in the 2.1GHz circuit where their lengths were chosen to be $(\lambda_g/2)$ at the fundamental frequency. This helped in reducing power losses and also in making the circuit more compact

C. ADS Simulations and Results

1. Single Diode Rectifier

Figure 80 shows a single diode rectifier optimized for performance at 1.84GHz. The diode used is SMS-7630 from Skyworks whose electrical parameters are given in table 4. Table 6 summarizes the dimensions of the used TLs and VIAs as well as the electrical values of the lumped components.

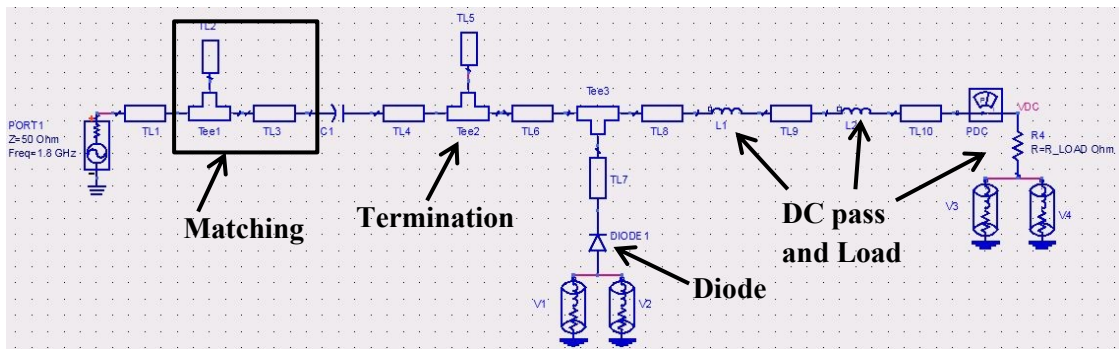


Figure 80. Schematic of the single diode 1.84GHz rectifier

The components that make up the circuit of figure 80 along with their roles are summarized as:

- TL1: A 10mm line over which the input SMA connector is practically soldered
- TL2/TL3: Together these transmission lines make up the open-circuit single stub matching network
- TL4: A 2mm line to which the DC block capacitor is soldered
- TL5: A ($\lambda_g/12$) open circuit stub that provides a short circuit impedance at the third harmonic (5.5GHz)
- TL6: A 2mm line to provide sufficient separation between TL5 and TL7
- TL7: A line to which the diode is soldered. It affects the diode's impedance
- TL8: A ($\lambda_g/2$) line which allows the DC power to pass to the resistive load
- TL9/TL10: Soldering lines for the inductors
- L1/L2: 470nH inductors from Murata which operate as RF chokes
- C1: 1 μ F DC block (Murata). It prevents DC power leakage to the generator
- R_LOAD: 1200 Ω load whose value was chosen for best PCE results using ADS optimization techniques

Table 6. Dimensions and component values of the 1.84GHz single diode rectifier

Component	Dimensions/Values	Component	Dimensions/Values
TL1	10mm	TL8	53.2mm
TL2	31.7mm	TL9/TL10	3mm
TL3	6.2mm	V1/V2/V2/V3	1mm (W)/0.5mm(D)
TL4/TL6	2mm	L1,L2	470nH
TL5	9.2mm	C1	1 μ F
TL7	2.3mm	R_LOAD	1200 Ω

Referring back to figure 80, it can be observed that class-F terminations were not used in this case. This is because the matching network associated with this type of harmonic terminations was rather large (the feed line of the network was $> \lambda_g/4$). Since we are aiming for better efficiencies at lower power values, a larger matching network incurs more losses. Also additional losses will be incurred in the $(\lambda_g/12)$ line which should provide an open circuit at the third harmonic. These factors, coupled with the fact that the power of the generated second and third order harmonics in the case of the SMS-7630 diode is generally lower than that generated by the SMS-7621 diode, required that these terminations be replaced with better ones. Hence, simulations were performed over different harmonic termination types while making sure in each case to re-optimize the impedance matching. It was found that the best PCE curve was obtained when a short-circuit was placed at the third harmonic. The simulation results of the 1.84GHz single diode rectifier are given in figures 81 and 82.

As shown in figure 81, the single diode rectifier is well-matched to 50Ω at 1.84GHz over the input power range extending from -1 to 4dBm. For the same power range, figure 82 gives the PCE of the rectifier. It can be inferred from this figure that the usage of the zero-bias diode along with the attempts made to minimize losses incurred by conductors as well as losses due to impedance mismatching led to far better PCE values at lower power levels as compared to the 2.1GHz single diode rectifier previously shown. While 50% efficiency was reached starting from an input power level of 7dBm (5mWatt) with the 2.1GHz circuit, the same efficiency value was reached starting at around -1dBm (0.8mWatt) with the 1.84GHz circuit. However, the breakdown performance of the 1.84GHz rectifier is worse. While breakdown starts at around 10dBm input power with the 2.1GHz rectifier, it appears at almost 3dBm for the

1.84GHz circuit. However, as previously illustrated, using a power divider that splits the input RF power and feeds two such rectifiers should theoretically enhance the power range over which efficient rectification is maintained.

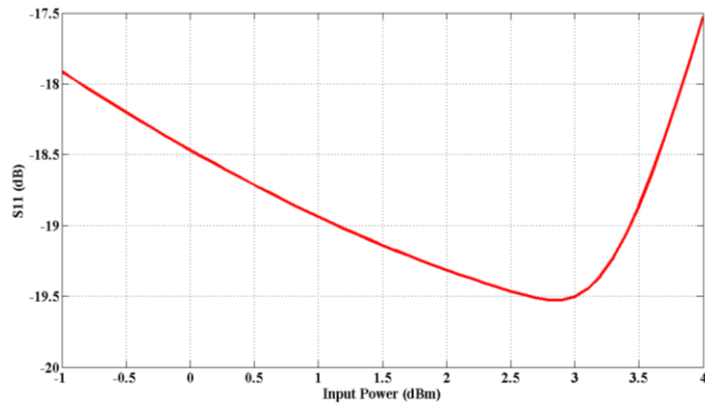


Figure 81. Input reflection coefficient of the single diode 1.84GHz rectifier

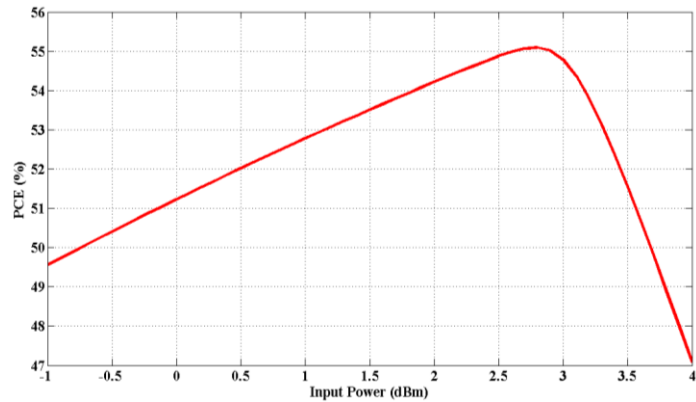


Figure 82. PCE of the 1.84GHz single diode rectifier

2. *The Complete Rectifier*

An equal split Wilkinson power divider operating at 1.84GHz was designed based upon the same theory illustrated before. Its output branches were connected via ($\lambda_g/10$) lines with 50Ω characteristic impedance to the input ports of two 1.84GHz rectifiers designed similar to the circuit shown in figure 80. Figure 83 shows the layout of the complete rectifier upon inserting the 1.84GHz power divider.

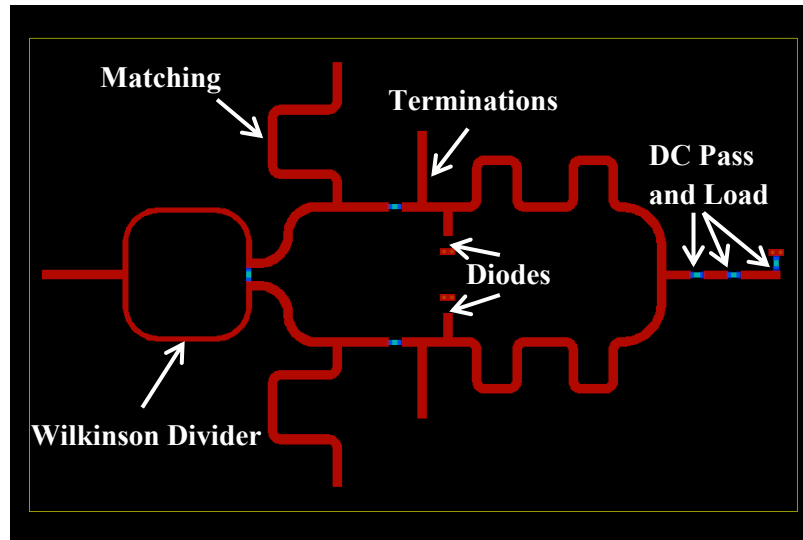


Figure 83. Layout of the 1.84GHz complete rectifier

Although the frequency is lower, which should theoretically lead to a larger size of the overall circuit, removing the Class-F terminations and correcting the connection lines between the power divider and rectifiers yielded an overall circuit that is more compact than the first one (2.1GHz). The best PCE curve was obtained for a DC load of 600Ω.

As shown in figure 84, the complete rectifier is matched to 50Ω at 1.84GHz over the input power range of (-1 to 10) dBm. For the same range, the simulated PCE is shown in figure 85.

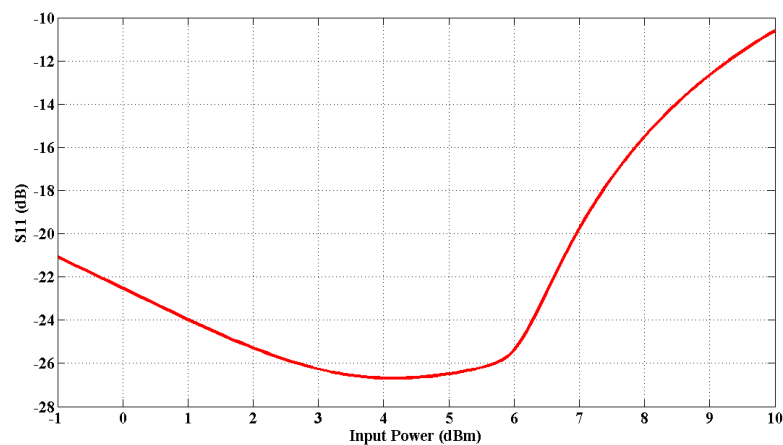


Figure 84. Simulated S₁₁ of the 1.84GHz complete rectifier

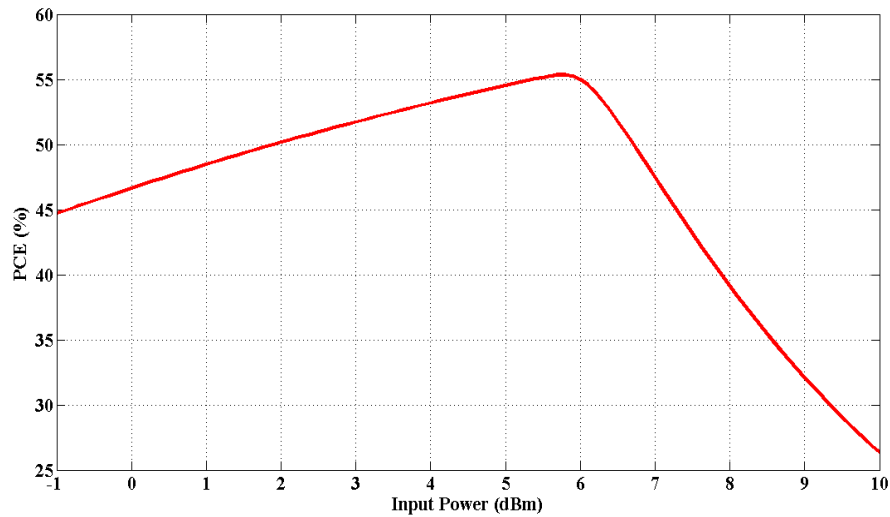


Figure 85. Simulated PCE of the complete rectifier at 1.84GHz

It is clear that the circuit has a better performance at low power levels as compared with that designed at 2.1GHz. Simulated PCE is now maintained above 50% for the input power range extending from 2 to 6.8dBm (1.6 to 4.8mWatt).

Figure 86 shows the simulated output DC voltage of the rectifier at 1.84GHz. It is clear that the output DC voltage starts saturating at 6dBm input power which is consistent with the results of the PCE shown in figure 85 where the efficiency starts degrading around the same power level.

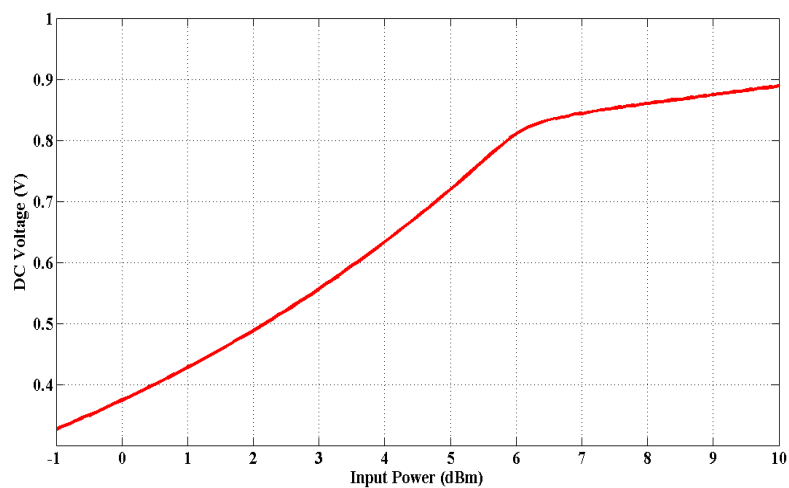


Figure 86. Simulated output DC voltage of the 1.84GHz complete rectifier

Figure 87 provides a comparison between the PCE curves of the single diode circuit and complete rectifier at 1.84GHz using linear powers for better visualization of the achieved improvement. As can be observed, the single diode circuit operates efficiently from 0.8 to 2.4mWatt. On the other hand, after inserting the power divider the circuit operates efficiently from 1.5 to 4.7mWatt. This yields a two times increase in the efficient power range as predicted by the ADS simulations.

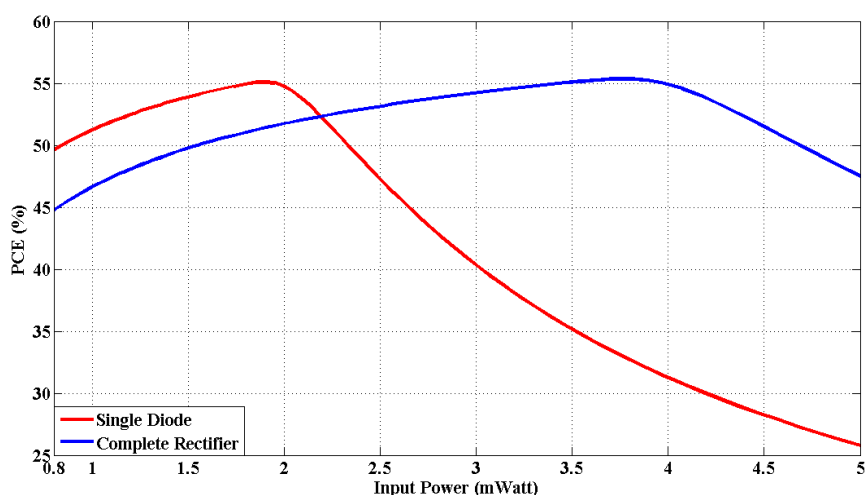


Figure 87. Simulated improvement in efficient power range at 1.84GHz

A comparison between the achieved PCE curves for the 2.1 and 1.84GHz designs as predicted by ADS is shown in figure 88. The zero-bias diodes of the 1.84GHz rectifier allow it to operate efficiently starting from much lower power levels as compared with the 2.1GHz rectifier. However, since the latter has diodes with higher breakdown voltage, the efficient operation was maintained up to higher power levels as compared with the 1.84GHz circuit.

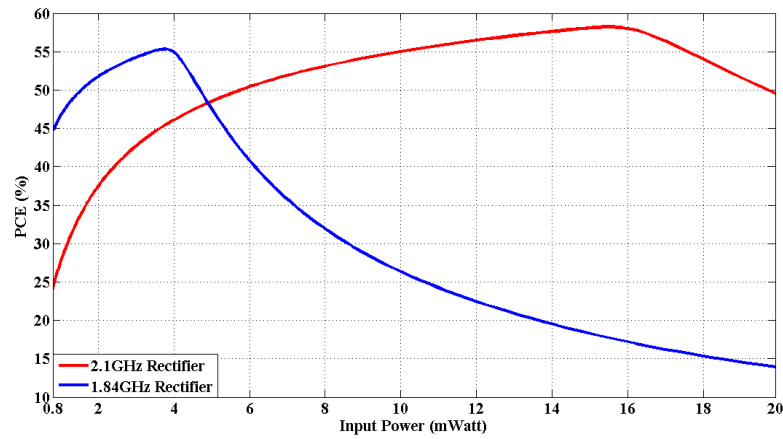


Figure 88. Simulated PCE of the 1.84 and 2.1GHz rectifiers

D. Fabrication and Measurement

The 1.84GHz complete rectifier was fabricated and measured by the same equipment used to characterize the performance of the 2.1GHz circuit. In this case however, the power amplifier was not used. This is because, as predicted by ADS, the 1.84GHz circuit should breakdown at much lower power levels than 14dBm which is the maximum that the signal generator can provide. Figure 89 shows the fabricated prototype. In this circuit, an SMA-to-BNC adapter was used along with BNC-CROC cables to measure the output DC voltage. This configuration made the measurements more stable.

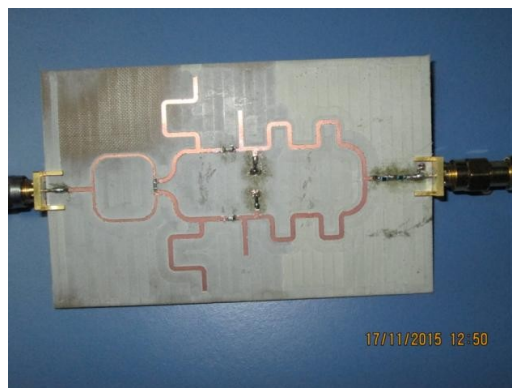


Figure 89. Fabricated 1.84GHz rectifier

Figure 90 shows the measured output DC voltage when a 600Ω load was connected to the output of the circuit. For an input RF power level of 0dBm , the output voltage was found to be 515mV which corresponds to 45% PCE. However, when measurements were first conducted this voltage was 522mV . Due to the continuous connection and removal of the SMA cables, numerous soldering and de-soldering of components, continuity tests performed over the circuit, etc... along with the thin board thickness, the output DC voltage slightly got lower. The circuit was so sensitive that slight movements or applying slight tension to the substrate caused its output DC to fluctuate.



Figure 90. Measured output DC of 515mV at 0dBm input power for a 600Ω load

In figure 91, the measured and simulated S_{11} curves overlap. Although the curves were obtained at an input RF power level of -20dBm , better matching exists as compared with the 2.1GHz rectifier. This is logical because the reactive impedance of the SMS-7630 diodes starts decreasing (in magnitude) at lower power levels due to the lower (V_{bi}) characteristics.

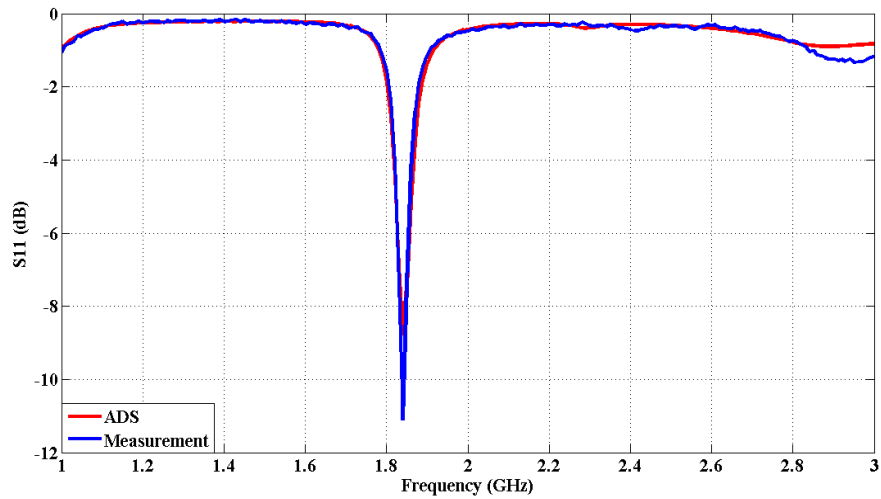


Figure 91. Measured input reflection coefficient of the 1.84GHz circuit

As can be observed in figure 92, the measured output DC voltage over the 600Ω load exceeds the results predicted by ADS. Again, as was concluded with the 2.1GHz rectifier, the SPICE model of the diodes has to be tuned to better match the simulation and measurement results. This was done by tweaking the SPICE parameters of the SMS-7630 diodes especially those related to the breakdown characteristics.

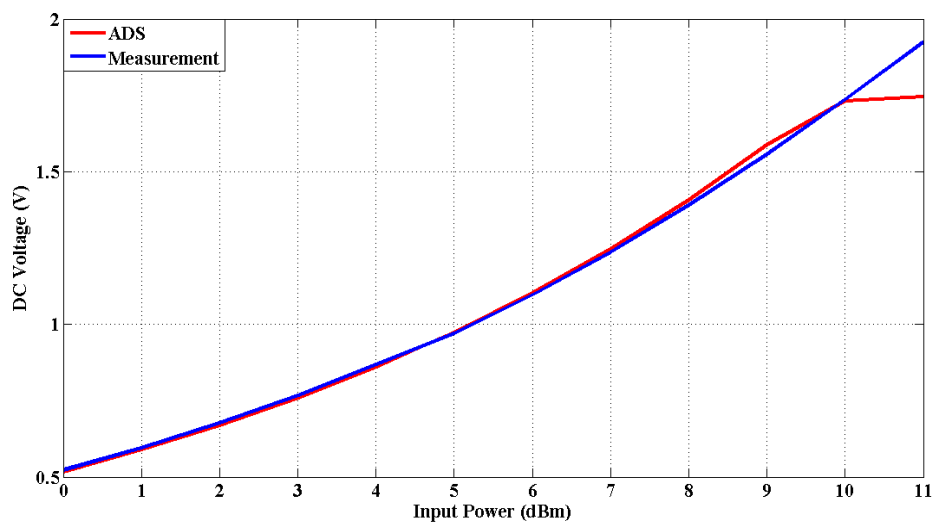


Figure 92. Measured output DC voltage of the 1.84GHz rectifier

Figure 93 shows a comparison between the measured and simulated PCE curves of the 1.84GHz rectifier when an output DC load of 600Ω is used. As can be observed, the efficiency curves show good agreement except near breakdown where the measured efficiency is better than the simulated one. This is mainly because of the discrepancies in the SPICE model of the diodes.

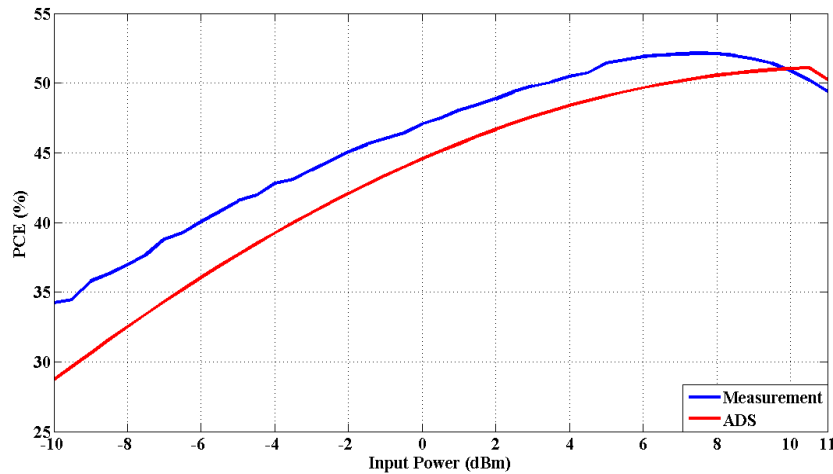


Figure 93. Measured and simulated PCE of the 1.84GHz rectifier

Figure 94 shows a comparison between the performances of three fabricated rectifiers for the input power range of -10 to 10dBm. As can be observed, the measured PCE of the 1.84GHz rectifier is much better than that of the other two circuits. However, as power increases beyond 10dBm, the 1.84GHz circuit's efficiency starts degrading whereas, due to its higher breakdown voltage, the PCE of the 2.1GHz rectifier keeps increasing.

On the other hand, while the ADS simulations predicted that breakdown of the 1.84GHz rectifier starts at 6dBm (4mWatt), the actual breakdown point was measured to be greater than 10dBm (10mWatt) as shown in figure 92 where the DC output voltage keeps increasing without saturation up to 11dBm.

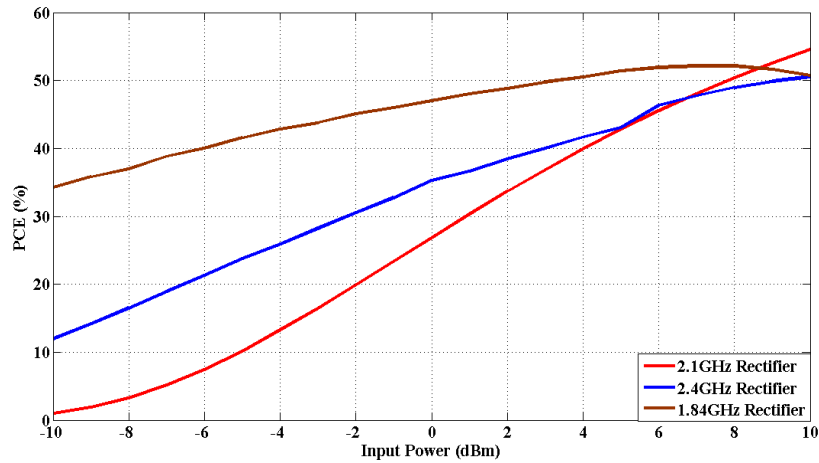


Figure 94. Comparison between the measured PCE curves for the three rectifiers

As previously stated in chapter IV, increasing the load resistance causes an increase in the output DC voltage. Figure 95 shows the measured output DC voltage from the 1.84GHz rectifier when the DC load was 9840Ω. As can be observed, the higher load resistance caused a significant increase in the output DC voltage. In fact, for power levels as low as -10dBm, over 300mV could be measured from the rectifier. For -20dBm input power, around 80mV DC could be obtained. Finally, when the input RF was decreased down to -30dBm (1μWatt), an output DC voltage greater than 10mV could still be detected.

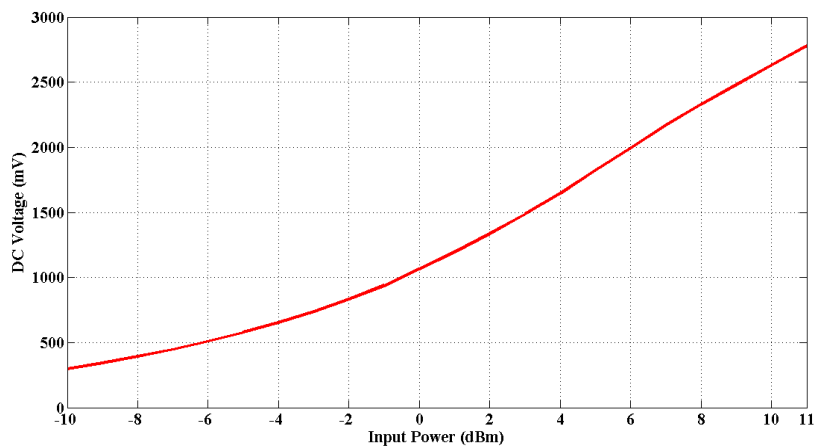


Figure 95. Measured DC voltage from the 1.84GHz rectifier for 9840Ω load

E. Summary

In this chapter, a 1.84GHz rectifier was designed and optimized for operation at low power levels around 3dBm (2mWatt). Equal splitting of the input RF power was used to improve the breakdown performance of the circuit. This allowed it to operate efficiently up to around 10dBm (10mWatt). This final prototype proved to be the best of the three fabricated and measured ones. This is because its efficiency curve is well-biased towards low power levels while at the same time having improved breakdown characteristics. In the next chapter, the 1.84GHz rectifier is combined with a suitable antenna to produce the rectenna device. Tests are performed to check whether RF energy could be transmitted wirelessly to a DC load.

CHAPTER IX

1.84GHZ RECTENNA FOR RF POWER HARVESTING

A. Objectives

In this chapter, the 1.84GHz rectifier is combined with an antenna to form the complete rectenna system. The rectenna is used to practically test the concept of RF energy harvesting. In the next section, details of the used transmitting and receiving antennas are given along with HFSS simulations. Later, the results of measurements conducted over the antennas and complete rectenna are shown.

B. Antenna Design

The two used antennas have board dimensions of 6cm x 6cm. They were fabricated over Rogers RO3206 with 5.8 dielectric constant and 1.28mm thickness. The receiver antenna is shown in figure 96.

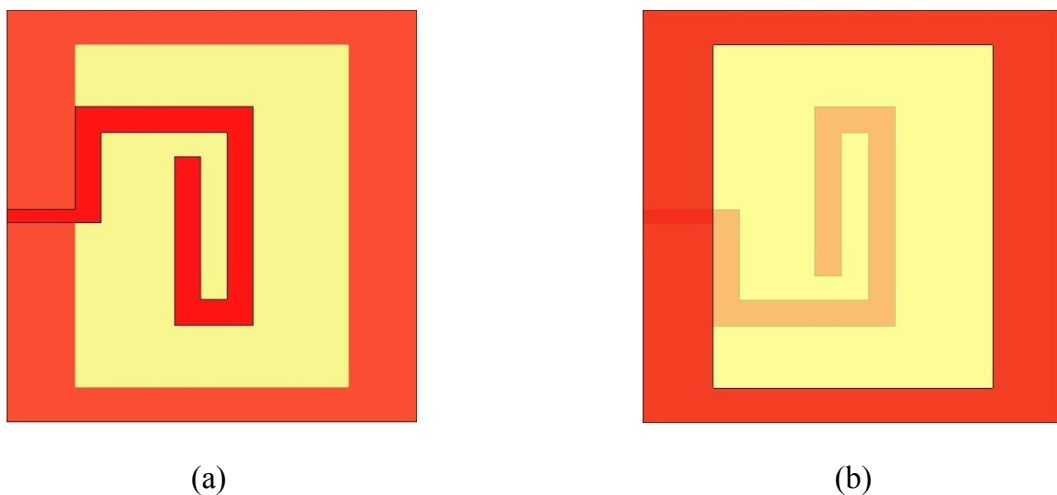


Figure 96. (a) Top layer of antenna-1 (b) Bottom layer of antenna-1

As shown in figure 97, the HFSS simulated S-parameters of antenna-1 match to a great extent the measurement results. At 1.84GHz, antenna-1 is matched with a reflection coefficient of -10.1dB.

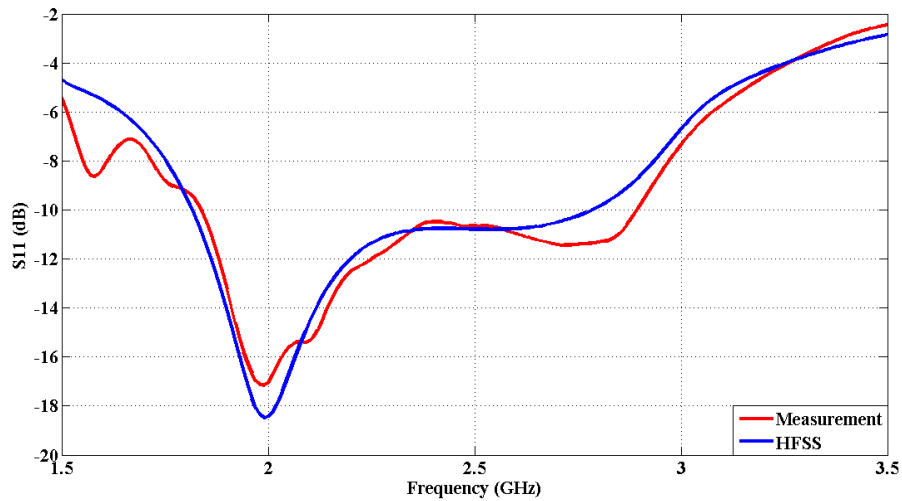


Figure 97. Simulated and measured S-parameters of antenna-1

Figure 98 shows the realized gain of antenna-1 at the frequency of 1.84GHz. As observed, the antenna has a gain of around 3.65dB along the axis normal to its plane. Due to the structure of its ground plane, radiation takes place through the bottom layer.

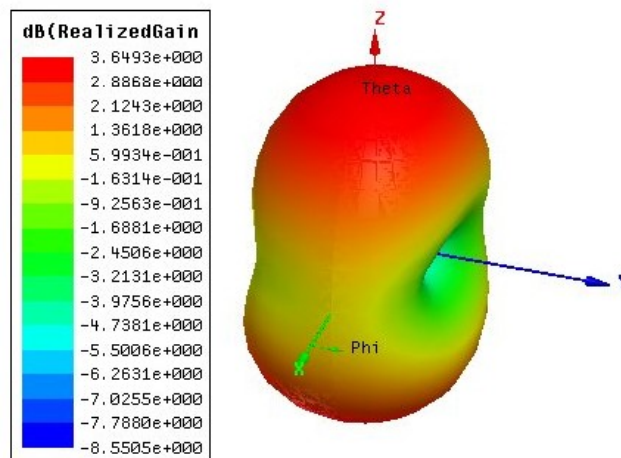


Figure 98. Realized gain of antenna-1 at 1.84GHz

The transmitting antenna is shown in figure 99. Its simulated and measured S-parameters are shown in figure 100. Its realized gain at 1.84GHz is shown in figure 101.

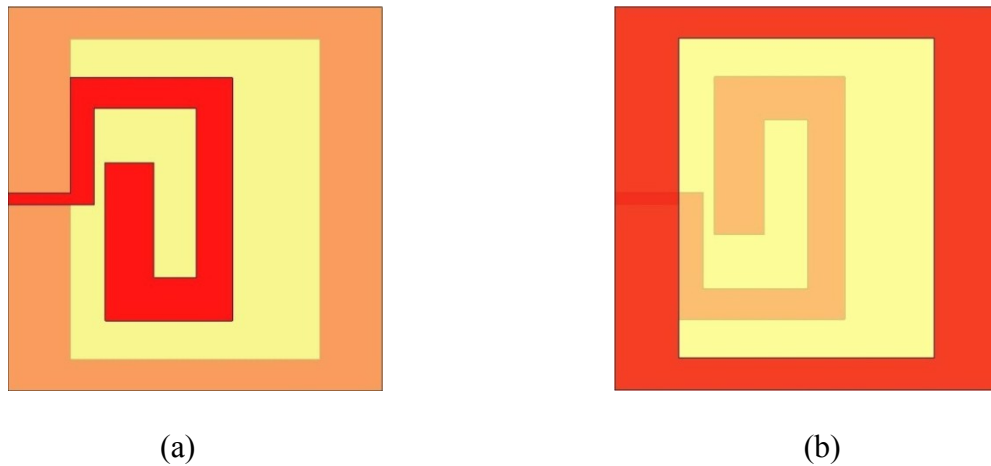


Figure 99. (a) Top layer of antenna-2 (b) Bottom layer of antenna-2

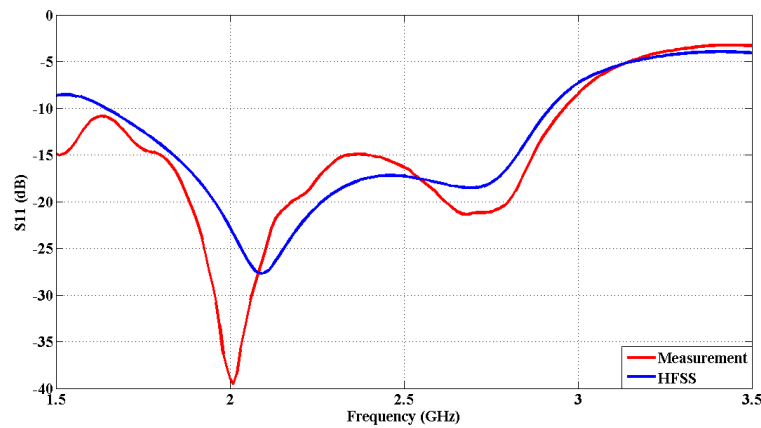


Figure 100. Simulated and measured S-parameters of antenna-2

From figure 100, it is obvious that the measured S_{11} results match the simulated ones. At 1.84GHz, antenna-2 has a -16.5dB reflection coefficient.

In figure 101 the realized gain of antenna-2 at 1.84GHz has a peak value of 4.3dB along the axis normal to its plane. Again, due to its ground structure, radiation takes place through the bottom layer.

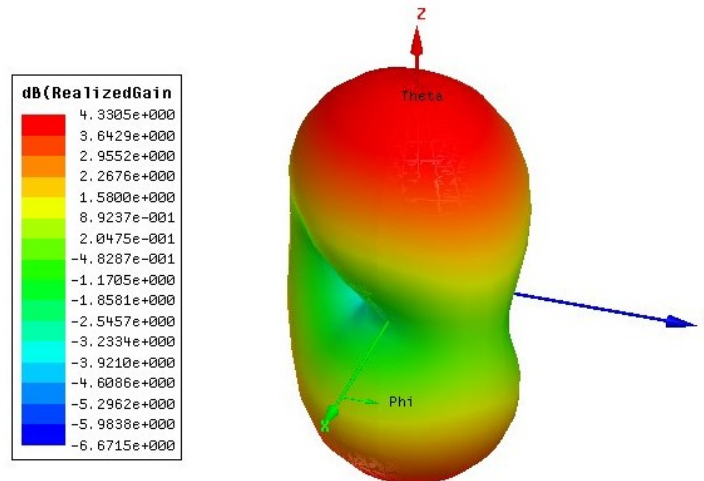


Figure 101. Realized gain of antenna-2 at 1.84GHz

The two antennas were used to wirelessly deliver DC power to an LED. Hence, one was connected to the RF signal generator (antenna-2) whereas the other was connected to the 1.84GHz rectifier (antenna-1). Using the 10dB gain power amplifier between the receiving antenna and the rectifier, the LED could be lit with highest brightness from a distance of 15cm when 10dBm RF power is transmitted. However, using antennas with better gain could achieve the same result from a larger distance or with lower transmitted power. One way to increase the gains of both antennas is to insert a ground plane behind each one at a distance of $(\lambda_g/4)$ which, at 1.84GHz, corresponds to around 1.7cm. This technique was simulated using HFSS for antenna-1 and antenna-2. Figures 102 and 103 show the improvement in the realized gain of both antennas at 1.84GHz after using a ground plane at a distance of 1.7cm behind each antenna. As can be observed, the realized gain of antenna-1 increases from 3.65 to 6.9dB whereas that of antenna-2 increases from 4.3 to 7.7dB. Practically, this translates as a larger distance over which the LED can be wirelessly powered for the same transmitted RF level.

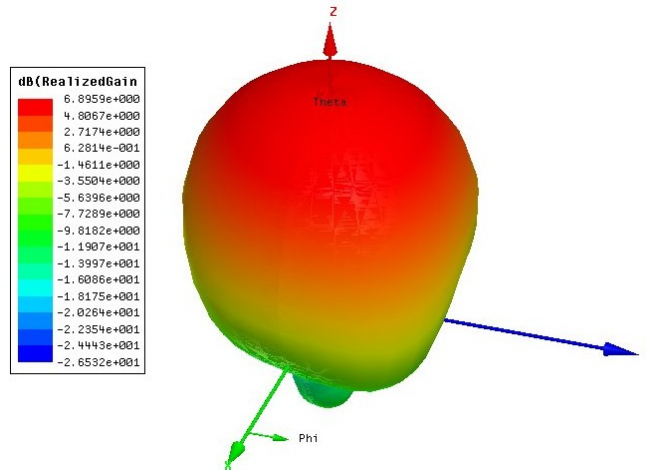


Figure 102. Improved realized gain of antenna-1 after inserting the ground plane

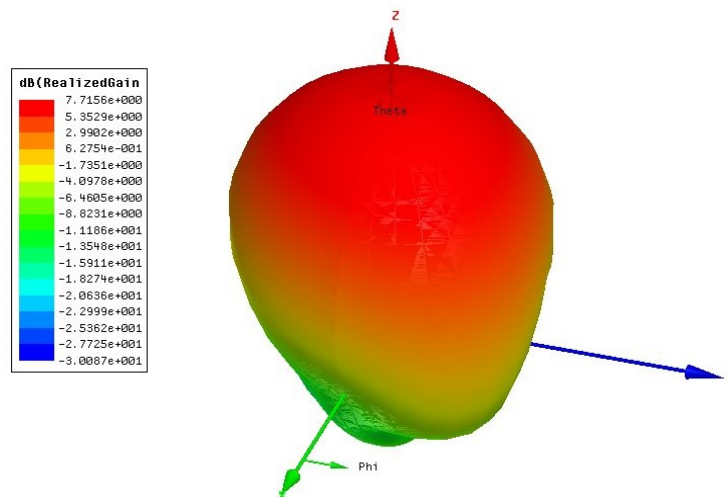


Figure 103. Improved realized gain of antenna-2 after inserting the ground plane

C. Summary

In this chapter, the designed 1.84GHz rectifier was used along with a patch antenna to produce a rectenna system. Without using ground planes to enhance the gains of the transmitting and receiving antennas, an LED could be lit wirelessly over a distance of 15cm when 10dBm of RF power is transmitted and a 10dB gain amplifier is used at the input of the rectifier. For the same conditions, using ground planes with the antennas will surely increase this distance.

CHAPTER X

CONCLUSIONS AND FUTURE WORK

A. Achieved Research Results

The objective of the thesis was to design and test a rectenna with an improved power range over which efficient RF harvesting can take place. For this reason, a brief review of the historical developments in rectenna design and testing was first introduced. After that, in chapter II, a summary of several contemporary rectenna designs available in the literature was presented with the aim of getting familiar with the challenges that exist in this field of study. Chapter III illustrated the differences between PN junction and Schottky contact diodes. The aim was to better understand the physical and electrical properties of Schottky diodes which are key elements to the design of any RF rectifier. Chapter IV then included a theoretical analysis of a typical RF-DC converter to understand how Schottky diodes rectify RF waves. In this chapter, conclusions were made about the relationship between some diode parameters and the expected rectifier efficiency. In addition, it shed light over the degradation that affects the PCE when diode breakdown takes place. Chapter V introduced two methods to limit the effects of diode breakdown. The first method relied on the idea of controlling the flow of input RF power between two different diodes with different properties to avoid breakdown while still operating efficiently at low power levels. This method was tested using ADS simulations and gave good efficiency results which however later appeared to be unrealistic. The second method proposed in this chapter was based on the concept of splitting input RF power between two rectifiers to enhance the efficiency performance. Chapter VI then presented the first designed prototype which used SMS-

7621 diodes and implemented the power division method. It was simulated using ADS, fabricated and measured. It gave good results in terms of efficiency improvement. Chapter VII presented another rectifier which used the same method for efficiency improvement with modifications over the power splitting ratio and circuit's size. It was designed and simulated using ADS for operation at 2.4GHz. However, after fabrication and measurement the circuit appeared to have some flaws, although it gave better PCE results at low power levels as compared to the first rectifier. Chapter VIII presented the third rectifier that was fabricated after making use of the experience gained by debugging the previous 2.4GHz circuit. It achieved good improvement in terms of efficient operable power range and the best PCE values at low power levels. Finally, in chapter IX two patch antennas were introduced along with their measured and simulated S-parameters. These antennas were used with the 1.84GHz rectifier to construct a rectenna. While using a 10dB amplifier between the receiving antenna and rectifier, the device was able to power wirelessly an LED from a distance of 15cm when the transmitted power was 10dBm. For convenience, a summary of the designed rectifiers along with their measured specifications is provided in table 7.

Table 7. Summary of the measured specifications of the three fabricated rectifiers

No.	Freq.	Efficient Power Range (mWatt)	Dimensions (L x W)	Diodes
1	2.1GHz	(15.8 – 100)	10.5cm x 6.5cm	SMS-7621
2	2.4GHz	(6.3 – 10)	5cm x 2.9cm	SMS-7630
3	1.84GHz	(2 – 12.6)	9.5cm x 5.9cm	SMS-7630

B. Future Work

The research carried out in this thesis can be further commenced in the future on three different levels:

1. Output DC Load

In all the rectifiers designed, the DC load was a fixed resistance. As previously illustrated in chapter IV, increasing the output DC resistance causes the PCE curve to improve at low power levels. However, decreasing this load resistance causes it to improve at higher power levels. One way to further expand the PCE curve is to include an output variable resistance that makes use of the output DC voltage to reconfigure its value in such a way that the PCE curve is optimized. One load that can accomplish this task is a diode. Also, in terms of application, the rectenna was only used to provide DC power wirelessly to an LED. However, many other applications can be thought of. One example might be the connection of a DC-DC converter to boost the output DC voltage at low power levels (such as -10dBm) and use this voltage to wirelessly charge a battery. However, care should be taken so as to optimize the output resistance in such a way that the boosted DC voltage does not drop due to any high DC current that the battery could drain.

2. Rectifier Design

All tested rectifiers used shunt reverse-connected Schottky diodes. It might be useful to consider other configurations such as diode voltage doubler. The availability of SMD packages with internally series-connected Schottky diodes eases this task. In addition, finding replacements to the RF inductors and capacitors soldered onto the

board is necessary. These components are time consuming when it comes to soldering and are prone to errors. For RF choking purposes, a Low Pass Filter (LPF) at a design frequency that is well below that of the fundamental can be used between the diode and the DC load in such a way that only DC power passes through it to the load. Also, for DC blocking, it might be beneficial to test transmission line based methods such as using gaps or inter-digital structures realized using microstrip lines. This would make the design more reliable, less time consuming to measure and debug while at the same time providing more control over its performance.

3. *Prediction and Theoretical Analysis of Performance*

While in chapter IV, the performance of a typical rectifier was analyzed through the assumed linear piece-wise model of the Schottky diode, the analysis can still be further improved by taking into consideration additional parameters. For instance, the effect of the load resistance can be added to the equations to better predict an optimal value of the DC load without having to rely only on simulations. Measurements conducted over Schottky diodes can also be used to better extract parameters to be used in the equations.

REFERENCES

- [1] W. C. Brown, "The History of Power Transmission by Radio Waves," *IEEE Trans. on Microw. Theory and Tech.*, vol. 32, no. 9, pp. 1230-1242, Sep. 1984.
- [2] B. Strassner and K. Chang, "5.8-GHz circularly polarized rectifying antenna for wireless microwave power transmission," *IEEE Trans. on Microw. Theory and Tech.*, vol. 50, no. 8, pp. 1870-1876, Aug 2002.
- [3] G. Monti, L. Corchia and L. Tarricone, "UHF Wearable Rectenna on Textile Materials," *IEEE Trans. on Antennas and Propagation*, vol. 61, no. 7, pp. 3869-3873, July 2013.
- [4] J. Guo, H. Zhang and X. Zhu, "Theoretical Analysis of RF-DC Conversion Efficiency for Class-F Rectifiers," *IEEE Trans. on Microw. Theory and Tech.*, vol. 62, no. 4, pp. 977-985, April 2014.
- [5] H. Takhedmit, B. Merabet, L. Cirio, B. Allard, F. Costa, C. Vollaie and O. Picon, "A 2.45-GHz dual-diode RF-to-dc rectifier for rectenna applications," *European Microwave Conference (EuMC)*, Sep. 2010 , pp. 37-40.
- [6] J.O. McSpadden, L. Fan and K. Chang, "Design and experiments of a high-conversion-efficiency 5.8-GHz rectenna," *IEEE Trans. on Microw. Theory and Tech.*, vol. 46, no. 12, pp. 2053-2060, Dec 1998.
- [7] J.O. McSpadden, T. Yoo and K. Chang, "Theoretical and experimental investigation of a rectenna element for microwave power transmission," *IEEE Trans. on Microw. Theory and Tech.*, vol. 40, no. 12, pp. 2359-2366, Dec 1992.
- [8] T. Yoo and K. Chang, "Theoretical and experimental development of 10 and 35 GHz rectennas," *IEEE Trans. on Microw. Theory and Tech.*, vol. 40, no. 6, pp. 1259-1266, June 1992.
- [9] M. Ali, G. Yang and R. Dougal, "A new circularly polarized rectenna for wireless power transmission and data communication," *IEEE Antennas and Wireless Propagation Letters*, vol. 4, pp.205-208, 2005.

- [10] T. Urgan and L.M. Reindl, "Harvesting Low Ambient RF-Sources for Autonomous Measurement Systems," IEEE Instrumentation and Measurement Technology Conference Proceedings, May 2008, pp. 62-65.
- [11] T.M. Chiam, L.C. Ong, M.F. Karim and Y. Guo, "5.8GHz circularly polarized rectennas using schottky diode and LTC5535 rectifier for RF energy harvesting," APMC Microwave Conference, Dec. 2009, pp. 32-35.
- [12] A. Buonanno, M. D'Urso and D. Pavone, "An ultra wide-band system for RF Energy harvesting," Proceedings of the 5th European Conference on Antennas and Propagation (EUCAP), April 2011, pp. 388-389.
- [13] S. Keyrouz, H.J. Visser and A.G. Tjhuis, "Ambient RF energy harvesting from DTV stations," Antennas and Propagation Conference (LAPC), Nov. 2012, pp. 1-4.
- [14] J. Zhang, Y. Huang and P. Cao, "Harvesting RF energy with rectenna arrays," 6th European Conference on Antennas and Propagation (EUCAP), March 2012, pp. 365-367.
- [15] A. Noguchi and H. Arai, "Small loop rectenna for RF energy harvesting," Microwave Conference Proceedings (APMC), Nov. 2013, pp. 86-88.
- [16] N. Zhu, K. Chang, M. Tuo, P. Jin, H. Xin and R.W. Ziolkowski, "Design of a high-efficiency rectenna for 1.575 GHz wireless low power transmission," IEEE Radio and Wireless Symposium (RWS), Jan. 2011, pp. 90-93.
- [17] U. Olgun, C.C. Chen and J.L. Volakis, "Investigation of Rectenna Array Configurations for Enhanced RF Power Harvesting," IEEE Antennas and Wireless Propagation Letters, vol. 10, pp. 262-265, 2011.
- [18] M. Mi, M.H. Mickle, C. Capelli and H. Swift, "RF energy harvesting with multiple antennas in the same space," IEEE Antennas and Propagation Magazine, vol. 47, no. 5, pp. 100-106, Oct. 2005.
- [19] U. Olgun, C.C. Chen and J.L. Volakis, "Design of an efficient ambient WiFi energy harvesting system," IET Microwaves, Antennas & Propagation, vol. 6, no. 11, pp. 1200-1206, August 2012.

- [20] A. Georgiadis, G. Vera and A. Collado, "Rectenna design and optimization using reciprocity theory and harmonic balance analysis for electromagnetic (EM) energy harvesting," *IEEE Antennas and Wireless Propagation Letters*, vol. 9, pp. 444-446, 2010.
- [21] J. Akkermans, M.C. van Beurden, G. Doodeman and H.J. Visser, "Analytical models for low-power rectenna design," *IEEE Antennas and Wireless Propagation Letters*, vol. 4, pp. 187-190, 2005.
- [22] R. Ludwig and P. Bretchko, *RF Circuit Design*, Upper Saddle River, NJ: Prentice Hall, 2000.
- [23] M. Abdallah, J. Costantine, A.H. Ramadan, Y. Tawk, F. Ayoub, C.G. Christodoulou, K.Y. Kabalan, "Wide power range RF energy harvesting circuit," *IEEE International Symposium on Antennas and Propagation & USNC/URSI National Radio Science Meeting*, Vancouver, Canada, July 19-24, 2015.
- [24] Motorola. (November 2001). "Rectifier Applications Handbook," [Online].
- [25] David M. Pozar, *Microwave Engineering*, 4th ed., John Wiley & Sons, 2012.
- [26] Jabbar, H., Song, Y.S., Jeong, T.T., "RF energy harvesting system and circuits for charging of mobile devices," *IEEE Transactions on Consumer Electronics*, vol. 56, no. 1, pp. 247-253, February 2010.
- [27] dela Cruz, S., de los Reyes, M.G., Alvarez, A, de Leon, M.T., Roque, C.R., "Design and implementation of passive RF-DC converters for RF power harvesting systems," *TENCON IEEE Region 10 Conference*, pp. 1503-1508, 21-24 Nov. 2010.
- [28] Jun Wu Zhang, Xiang Yu Zhang, Zhuang Liang Chen, Kye-Yak See, Cher Ming Tan, Shou-Shun Chen, "On-chip RF energy harvesting circuit for image sensor," *13th International Symposium on Integrated Circuits (ISIC)*, pp. 420-423, 12-14 Dec. 2011.
- [29] Chouhan, S.S., Halonen, K., "A modified cross coupled rectifier based charge pump for energy harvesting using RF to DC conversion," *European Conference on Circuit Theory and Design (ECCTD)*, pp. 1-4, 8-12 Sept. 2013.

- [30] Hameed, Z., Moez, K., "Fully-integrated passive threshold-compensated PMOS rectifier for RF energy harvesting," IEEE 56th International Midwest Symposium on Circuits and Systems (MWSCAS), pp. 129-132, 4-7 Aug. 2013.
- [31] Joonhyung Lim, Hanjin Cho, Koonshik Cho, Tahjoon Park, "High sensitive RF-DC rectifier and ultra low power DC sensing circuit for waking up wireless system," APMC 2009 Microwave Conference, pp. 237-240, 7-10 Dec. 2009.
- [32] Gao-Ching Lin, Min-Wei Lee, Yu-Cheng Hsu, "An AC-DC rectifier for RF energy harvesting system," Microwave Conference Proceedings (APMC), pp. 1052-1054, 4-7 Dec. 2012.
- [33] Kotani, K., Ito, Takashi, "High efficiency CMOS rectifier circuit with self-V_{th}-cancellation and power regulation functions for UHF RFIDs," ASSCC Solid-State Circuits Conference, pp. 119-122, 12-14 Nov. 2007.
- [34] Kotani, K., Sasaki, A, Ito, Takashi, "High-Efficiency Differential-Drive CMOS Rectifier for UHF RFIDs," IEEE Journal of Solid-State Circuits, vol. 44, no. 11, pp. 3011-3018, Nov. 2009.
- [35] Umeda, T., Yoshida, H., Sekine, S., Fujita, Y., Suzuki, T., Otaka, S., "A 950-MHz rectifier circuit for sensor network tags with 10-m distance," IEEE Journal of Solid-State Circuits, vol. 41, no. 1, pp. 35-41, Jan. 2006.
- [36] Karolak, D., Taris, T., Deval, Y., Begueret, J.-B., Mariano, A, "Design comparison of low-power rectifiers dedicated to RF energy harvesting," 19th IEEE International Conference on Electronics, Circuits and Systems (ICECS), pp. 524-527, 9-12 Dec. 2012.
- [37] Shameli, A, Safarian, A, Rofougaran, A, Rofougaran, M., De Flaviis, F., "Power Harvester Design for Passive UHF RFID Tag Using a Voltage Boosting Technique," IEEE Transactions on Microwave Theory and Techniques, vol. 55, no. 6, pp. 1089-1097, June 2007.
- [38] Salter, T., Metze, G., Goldsman, N., "Parasitic aware optimization of an RF power scavenging circuit with applications to Smartdust sensor networks," IEEE RWS Radio and Wireless Symposium, pp. 332-335, 18-22 Jan. 2009.

- [39] K. Niotaki, A. Collado, A. Georgiadis, S. Kim, M.M. Tentzeris, "Solar/Electromagnetic Energy Harvesting and Wireless Power Transmission," Proceedings of the IEEE , vol. 102, no. 11, pp. 1712-1722, Nov. 2014.
- [40] E. Falkenstein, M. Roberg, Z. Popovic, "Low-Power wireless power delivery," IEEE Trans. Microw. Theory Tech., vol. 60, no. 7, pp. 2277-2286, July 2012.
- [41] Skyworks Solutions, Inc. (2015, Aug. 7). "Surface Mount Mixer and Detector Schottky Diodes," [Online]. Available: http://www.skyworksinc.com/uploads/documents/Surface_Mount_Schottky_Diodes_200041AB.pdf [Jan. 12, 2016].
- [42] Avago Technologies. "Surface Mount Microwave Schottky Detector Diodes," [Online]. Available: <http://www.avagotech.com/docs/AV02-1388EN> [Jan. 12, 2016].
- [43] Avago Technologies. "Surface Mount Microwave Schottky Detector Diodes," [Online]. Available: <http://www.avagotech.com/docs/AV02-1377EN> [Jan. 12, 2016].
- [44] Advanced Design System, ADS 2009, Keysight Technologies, Santa Rosa, CA.
- [45] High Frequency Structural Simulator, Ansys, Inc., Canonsburg, PA.